ARL-TR-9815 • Oct 2023

DEVCOM ARMY RESEARCH LABORATORY

A Large Deformation Multiphase Continuum Mechanics Model for Shock Loading of Lung Parenchyma: Investigating the Effects of Fluid Viscous Stress

by Zachariah T Irwin, Richard A Regueiro, and John D Clayton

NOTICES

Disclaimers

The findings in this report are not to be construed as an official Department of the Army position unless so designated by other authorized documents.

Citation of manufacturer's or trade names does not constitute an official endorsement or approval of the use thereof.

Destroy this report when it is no longer needed. Do not return it to the originator.

ARL-TR-9815 ● OCT 2023

A Large Deformation Multiphase Continuum Mechanics Model for Shock Loading of Lung Parenchyma: Investigating the Effects of Fluid Viscous Stress

by Zachariah T Irwin
University of Colorado Boulder

Richard A Regueiro and John D Clayton
DEVCOM Army Research Laboratory

REPORT DOCUMENTATION PAGE

Form Approved
OMB No. 0704-0188

1. REPORT DATE *(DD-MM-YYYY)*
October 2023

2. REPORT TYPE
Technical Report

3. DATES COVERED (From - To)
May 2023–September 2023

4. TITLE AND SUBTITLE
A Large Deformation Multiphase Continuum Mechanics Model for Shock Loading of Lung Parenchyma: Investigating the Effects of Fluid Viscous Stress

5a. CONTRACT NUMBER

5b. GRANT NUMBER

5c. PROGRAM ELEMENT NUMBER

6. AUTHOR(S)
Zachariah T Irwin, Richard A Regueiro, and John D Clayton

5d. PROJECT NUMBER

5e. TASK NUMBER

5f. WORK UNIT NUMBER

7. PERFORMING ORGANIZATION NAME(S) AND ADDRESS(ES)
DEVCOM Army Research Laboratory
ATTN: FCDD-RLA-TB
Aberdeen Proving Ground, MD 21005-5066

8. PERFORMING ORGANIZATION REPORT NUMBER
ARL-TR-9815

9. SPONSORING/MONITORING AGENCY NAME(S) AND ADDRESS(ES)

10. SPONSOR/MONITOR'S ACRONYM(S)

11. SPONSOR/MONITOR'S REPORT NUMBER(S)

12. DISTRIBUTION/AVAILABILITY STATEMENT
Approved for public release; distribution is unlimited.

13. SUPPLEMENTARY NOTES
primary author's email: <john.d.clayton1.civ@army.mil>.

14. ABSTRACT
A finite-strain theory of a biphasic mixture, with coupled pore fluid flow and solid skeleton deformation, of a soft porous material has been developed for high-strain-rate dynamic loading. The constitutive model is nonlinear elastic and accounts for the compressibility of the pore air. The formulation does not require equivalency of acceleration of pore fluid to that of solid skeleton, but rather allows them to be different. Through implementation of the concept of solid extra stress, the theory is able to distinguish among solid skeleton, pore fluid (air), and total pressures, and similarly among stress tensors for each constituent. Herein, we depart from prior work, which assumed a nearly inviscid pore fluid, and account for the pore fluid's viscous effects on its stress.

15. SUBJECT TERMS
poromechanics, theory of porous media, nonlinear elasticity, viscous stress, soft tissue mechanics, shock waves, Terminal Effects

16. SECURITY CLASSIFICATION OF:			**17. LIMITATION OF ABSTRACT**	**18. NUMBER OF PAGES**	**19a. NAME OF RESPONSIBLE PERSON**
a. REPORT	**b. ABSTRACT**	**c. THIS PAGE**			John D Clayton
Unclassified	Unclassified	Unclassified	UU	93	**19b. TELEPHONE NUMBER (Include area code)** 410-278-6146

Contents

List of Figures

List of Tables

Acknowledgments

The authors acknowledge support from the Army Research Directorate of the US Army Combat Capabilities Development Command (DEVCOM) Army Research Laboratory (ARL). R Regueiro acknowledges support from a Joint Faculty Appointment at ARL. Z Irwin acknowledges the Department of Defense SMART scholarship program for doctoral students and helpful discussions with R Becker of ARL on shock viscosity applied to higher-order elements and D Mukherjee and C Teeraratkul of the University of Colorado Boulder on fluid dynamics in the framework of the Theory of Porous Media. This work utilized resources from the University of Colorado Boulder Research Computing Group, which is supported by the National Science Foundation (awards ACI-1532235 and ACI-1532236), the University of Colorado Boulder, and Colorado State University. This work was supported in part by high-performance computer time and resources from the DoD High Performance Computing Modernization Program.

1. Introduction

1.1 Background

The lung parenchyma is a highly heterogeneous material composed of alveolar air sacs ranging from 100–330 μm in diameter[1] and connective tissues consisting of a complex network of collagen and elastin fibers.[2] At high rates of strain, such as those induced by a shock wave, the fibers in lung parenchyma are prone to rupture[3] and the remaining stress response percolates through the collagen fibril networks as the collagen fibers start to extend to their uncoiled lengths. This increases the stress response of the entire lung parenchyma.[4] The complex roles that collagen and elastin fibers play in the dynamics of the lung parenchyma are discussed by Freed et al.[3] Dynamic influences of the bronchiole tubes, which are stiffer than the parenchyma, on the response of impacted lung are observed in experiments by Brannen et al.[5] The present focus is on the role that 1-D poro-elasto-dynamics plays at the mesoscopic level. Outcomes of the current research are intended to inform macroscopic, single-phase models of the lung for 3-D modeling of much larger domains.[6–11]

Mixture theory was first established at finite strain by Truesdell and Toupin.[12] Subsequent works by Bowen[13–15] and others[16–18] applied this rich continuum theory to porous media. Shock waves in mixtures were studied using analytical methods by Bowen, Chen, and Wright,[19–22] and more recently by Clayton.[23] The Theory of Porous Media (TPM) is an approximation to a more computationally expensive Fluid-Structure Interaction (FSI) model at the pore length scale. In TPM, interactions are smeared across a continuum material point, simplifying not just the governing mathematical equations but the discretization of the geometry itself.

Lung parenchyma is a complex heterogeneous material.[24] Resolution would require representation by a detailed 3-D finite-element (FE) mesh to model the *explicit* FSI. Resolution could be possible via Computational Fluid Dynamics-Computational Solid Mechanics with arbitrary Lagrangian-Eulerian modeling. However, such frameworks would involve costly simulations and mesh generation and bias regarding the structure of the FE mesh.

Shock waves induce large pressure gradients that are thought to directly cause microstructural tearing of the lung parenchyma leading to hemorrhaging.[24–26] Injury

propagations through the lung parenchyma at the ultrastructural (tissue fibers) and microstructural (air sac) levels are not well understood and constitute active research.[3,8] The fine-scale approach initiated by Freed et al.[3] to model the microstructure necessitates a multiscale model of the whole lung tissue, which includes the highly heterogeneous structure of the lung parenchyma. Work is needed to first accurately simulate the deformation of lung parenchyma using a multiphysics approach, before addressing damage and injury pathology at the microscale (i.e., alveolar regime) and linking that to the macroscale (i.e., parenchymal regime). In the current program,[27,28] we incorporate TPM to take into account the different response times of the two constituents in the lung parenchyma subjected to shock loading: solid skeleton (s) (lung parenchyma) and the pore fluid (f) (air) that occupies the pore space.

In prior work,[27,29] we assumed a nearly inviscid stress response of the pore fluid; viscous effects were accounted for via the "hydraulic conductivity" parameter that governs the magnitude of the seepage flow (the difference in velocity between the pore fluid and the solid skeleton). However, total pore fluid Cauchy stress, assuming a locally homogeneous temperature model between the two constituents (i.e., the temperature of the pore fluid is assumed to be equal to that of the solid skeleton at a finite point, even if the temperature of the fluid-solid mixture is allowed to fluctuate), is written as

$$\boldsymbol{\sigma}^{\mathrm{f}} \coloneqq \boldsymbol{\sigma}^{\mathrm{f}}_{E} - n^{\mathrm{f}} p_{\mathrm{f}} \mathbf{1} \,, \tag{1}$$

where $n^{\mathrm{f}} p_{\mathrm{f}} = p^{\mathrm{f}}$ is the partial pressure contribution, and $\boldsymbol{\sigma}^{\mathrm{f}}_{E}$ is the viscous contribution (hereafter referred to as the pore fluid "extra" stress), which is ignored in the nearly inviscid assumption. Such an assumption may be invalid at high-strain-rates where momentum diffusivity of the pore fluid (air) in lung parenchyma may alter the dynamic response of lung tissue subjected to shock loading. The objective of the present work is to verify whether or not the nearly inviscid pore fluid assumption is valid for our 1-D FE model in various strain-rate regimes. This objective is achieved by comparing numerical simulations between our numerical FE model where the pore fluid extra stress is assumed to be equal to zero to simulations with a modified FE model where it is not.

1.2 Organization

The remainder of this report is organized in the following manner. Section 2 summarizes a brief history of the validity of including the pore fluid extra stress in the framework of TPM. Discussion continues with the associated difficulties with modeling this term in a FE framework, and concludes with the modeling approach employed in the current work. Section 3 presents the modified variational forms of the balance equations from those reported in Irwin et al.,[29,30] wherein we apply the standard Bubnov-Galerkin spatial-discretization procedure for the FE model to solve for the variables of interest: lung parenchyma displacement (and velocity and acceleration), pore fluid pressure and pore fluid displacement (and velocity and acceleration). A review of the numerical time integration schemes from Irwin et al.[29,30] then follows, with modifications for the pore fluid extra stress presented as needed. Section 4 presents a comparison of the Darcy (i.e., nearly inviscid pore fluid flow) and Darcy-Brinkman (i.e., viscous pore fluid flow) numerical simulation results.

2. Theory

2.1 The Fluid Extra Stress Tensor: Background and Challenges

An extensive background of TPM is provided by Bowen,[13–15] Coussy,[17] Ehlers[16] and de Boer,[18] and originally in Truesdell and Toupin.[12] For truncated derivations disclosed in the aforementioned works, refer to Irwin et al.[27] We continue to follow the notation of Holzapfel[31] (for solid mechanics) and de Boer.[18]

We assume that the porous solid continuum body constitutes a control space $\mathcal{B}$ (current configuration of the solid skeleton) and that only liquids or gases in the pores can leave this control space. Rather than modeling the exact microstructure of the porous solid, we assume that the pores are modeled in a statistical sense such that their specific locations are arbitrary. This concept of volume fraction is illustrated in Fig. 1a. The volume fractions n^α are defined such that they relate the "real" differential volumes dv_α of each constituent, or phase, α to the smeared (i.e., homogenized) total differential volume dv:

$$n^\alpha(\boldsymbol{x}, t) = \frac{dv_\alpha(\boldsymbol{x}, t)}{dv(\boldsymbol{x}, t)}\,, \tag{2}$$

where $\boldsymbol{x}$ is the position vector in the current configuration $\mathcal{B}$ (see Fig. 1(b)), and t is current time. Thus, for any mixture, the constituents α occupying some control

volume dv in the control space $\mathcal{B}$ must satisfy

$$\sum_{\alpha} n^{\alpha}(\boldsymbol{x},t) = 1\ , \quad \sum_{\alpha} dv_{\alpha}(\boldsymbol{x},t) = dv(\boldsymbol{x},t)\ . \tag{3}$$

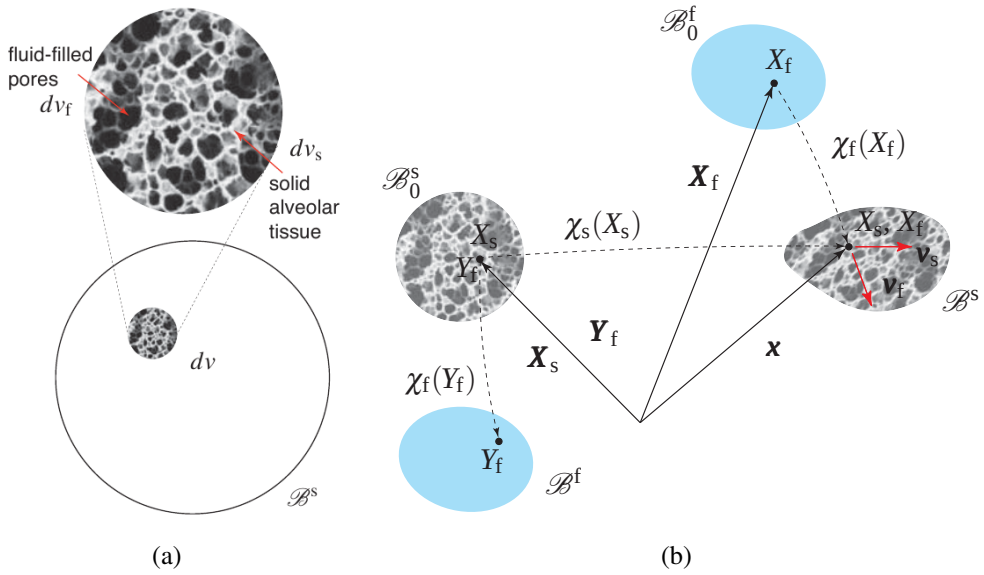

Fig. 1 Concept of volume fraction for biphasic (solid(s)-fluid(f)) mixture theory (a), showing solid skeleton composed of alveolar tissue. Note that in the theory of porous media, it is assumed that the control space is that of the solid phase $\mathcal{B} := \mathcal{B}^{\mathrm{s}}$, also known as "solid skeleton." Kinematics (b) of a biphasic (solid-fluid) mixture theory.

We furthermore assume that the constituents are immiscible (following the principle of phase separation[16]) such that we can relate the partial mass density ρ^{α}, that is, the mass density of constituent α occupying the total differential volume dv containing multiple constituents, to the real mass density $\rho^{\alpha\mathrm{R}}$, the mass density of constituent α occupying the differential volume dv_{α} containing only constituent α, as follows:

$$\begin{aligned} m_{\alpha}(\boldsymbol{x},t) &= \int_{\mathcal{B}^{\alpha}} \rho^{\alpha\mathrm{R}}(\boldsymbol{x},t) dv_{\alpha}(\boldsymbol{x},t) \\ &= \int_{\mathcal{B}} \rho^{\alpha\mathrm{R}}(\boldsymbol{x},t) n^{\alpha}(\boldsymbol{x},t) dv(\boldsymbol{x},t) = \int_{\mathcal{B}} \rho^{\alpha}(\boldsymbol{x},t) dv(\boldsymbol{x},t)\ , \end{aligned} \tag{4}$$

where m_{α} is the mass of constituent α in the control space $\mathcal{B}$. Hereafter we assume that variables written in the current configuration $\mathcal{B}$ are dependent on position $\boldsymbol{x}$ at time t so as to simplify the notation. Similarly, variables written in the reference

configuration $\mathcal{B}_0$ are dependent on position $\boldsymbol{X}$ at time t.

For a materially incompressible solid (s) phase and compressible fluid (f) phase, the balance of mass of the mixture expressed in the reference configuration $\mathcal{B}_0$ is written as[27]

$$\frac{J_{\mathrm{s}} n^{\mathrm{f}}}{K_{\mathrm{f}}^{\eta}} D_t^{\mathrm{s}} p_{\mathrm{f}} + D_t^{\mathrm{s}} J_{\mathrm{s}} + \frac{J_{\mathrm{s}}}{K_{\mathrm{f}}^{\eta}} \operatorname{GRAD}_{\mathrm{s}}(p_{\mathrm{f}}) \cdot \boldsymbol{F}_{\mathrm{s}}^{-1} \cdot (n^{\mathrm{f}} \tilde{\boldsymbol{v}}_{\mathrm{f}}) + J_{\mathrm{s}} \operatorname{GRAD}_{\mathrm{s}}(n^{\mathrm{f}} \tilde{\boldsymbol{v}}_{\mathrm{f}}) : \boldsymbol{F}_{\mathrm{s}}^{-T} = \frac{J_{\mathrm{s}} \hat{\rho}^{\mathrm{f}}}{\rho^{\mathrm{fR}}} , \tag{5}$$

where J_{s} denotes the Jacobian of deformation $\boldsymbol{F}_{\mathrm{s}}$ of the solid (s) phase, K_{f}^{η} is the isentropic bulk modulus of the fluid (f) phase, p_{f} is the pore fluid pressure, $\tilde{\boldsymbol{v}}_{\mathrm{f}}$ is the difference in velocities of the fluid (f) and solid (s) phase, that is, $\tilde{\boldsymbol{v}}_{\mathrm{f}} := \boldsymbol{v}_{\mathrm{f}} - \boldsymbol{v}_{\mathrm{s}}$, and $\hat{\rho}^{\mathrm{f}}$ is the mass supply to the fluid phase from the other phase(s), which we typically assume to be negligible. In present work, the $(n^{\mathrm{f}} \tilde{\boldsymbol{v}}_{\mathrm{f}})$ term is modeled using an appropriate constitutive law, for example, Darcy's law:

$$n^{\mathrm{f}} \tilde{\boldsymbol{v}}_{\mathrm{f}} = -\hat{k} \Big(\operatorname{grad} p_{\mathrm{f}} + \rho^{\mathrm{fR}} (\boldsymbol{a}_{\mathrm{f}} - \boldsymbol{g}) \Big) . \tag{6}$$

However, when the pore fluid extra stress $\boldsymbol{\sigma}_E^{\mathrm{f}}$ is to be accounted for, we use the extension of Eq. 6, the Darcy-Brinkman equation:

$$n^{\mathrm{f}} \tilde{\boldsymbol{v}}_{\mathrm{f}} = -\hat{k} \Big(\operatorname{grad} p_{\mathrm{f}} + \rho^{\mathrm{fR}} (\boldsymbol{a}_{\mathrm{f}} - \boldsymbol{g}) - \frac{1}{n^{\mathrm{f}}} \operatorname{div} \boldsymbol{\sigma}_E^{\mathrm{f}} \Big) . \tag{7}$$

Furthermore, it can be shown that the balance of momenta of the mixture and the fluid phase under the assumptions laid out in Irwin et al.[27] (namely: locally homogeneous temperatures, negligible mass supplies of solid and fluid phases, materially incompressible solid phase and compressible fluid phase and gravity as the only active body force), may be written as follows:

$$\begin{aligned} &\operatorname{DIV}_{\mathrm{s}} \boldsymbol{P}_{\mathrm{s}} + \rho_{0(\mathrm{s})} \boldsymbol{g} = \rho_{0(\mathrm{s})}^{\mathrm{s}} \boldsymbol{a}_{\mathrm{s}} + \rho_{0(\mathrm{s})}^{\mathrm{f}} \boldsymbol{a}_{\mathrm{f}} , \quad \boldsymbol{P}_{\mathrm{s}} = \boldsymbol{P}_{E(\mathrm{s})}^{\mathrm{s}} + \boldsymbol{P}_{E(\mathrm{s})}^{\mathrm{f}} - J_{\mathrm{s}} p_{\mathrm{f}} \boldsymbol{F}_{\mathrm{s}}^{-T} , \\ &\rho_{0(\mathrm{s})}^{\mathrm{f}} \boldsymbol{a}_{\mathrm{f}} + J_{\mathrm{s}} n^{\mathrm{f}} \operatorname{GRAD}_{\mathrm{s}} p_{\mathrm{f}} \cdot \boldsymbol{F}_{\mathrm{s}}^{-1} - \operatorname{DIV}_{\mathrm{s}} \boldsymbol{P}_{E(\mathrm{s})}^{\mathrm{f}} + J_{\mathrm{s}} \frac{(n^{\mathrm{f}})^2}{\hat{k}} (\boldsymbol{v}_{\mathrm{f}} - \boldsymbol{v}_{\mathrm{s}}) - \rho_{0(\mathrm{s})}^{\mathrm{f}} \boldsymbol{g} = \boldsymbol{0} . \end{aligned} \tag{8}$$

$\boldsymbol{P}_{\mathrm{s}}$ denotes the mixture first Piola-Kirchhoff stress, $\boldsymbol{P}_E^{\alpha}$ denotes the extra stress

of phase α (i.e., material stress described by an appropriate constitutive model), $\boldsymbol{a}_\alpha$ is the acceleration of phase α and $\hat{k}$ is the deformation dependent hydraulic conductivity:

$$\hat{k} := \frac{\varkappa}{\eta_{\mathrm{f}}} \frac{\mathcal{F}\left(n^{\mathrm{f}}\right)}{\mathcal{F}\left(n_0^{\mathrm{f}}\right)} \,, \tag{9}$$

where η_{f} is the pore fluid shear viscosity (assumed constant), $\varkappa$ is the intrinsic permeability of the solid skeleton (assumed constant), and $\mathcal{F}$ is a nonlinear function of porosity n^{f} accounting for change in hydraulic permeability due to change in porosity (e.g., the Kozeny-Carman relation):

$$\mathcal{F}\left(n^{\mathrm{f}}\right) := \frac{\left(n^{\mathrm{f}}\right)^3}{1-\left(n^{\mathrm{f}}\right)^2} \,. \tag{10}$$

In prior work,[27–30] it was assumed that the pore fluid first Piola-Kirchhoff extra stress

$$\boldsymbol{P}^{\mathrm{f}}_{E(\mathrm{s})} := J_{\mathrm{s}} \boldsymbol{\sigma}^{\mathrm{f}}_E \boldsymbol{F}_{\mathrm{s}}^{-T} \approx \boldsymbol{0} \,. \tag{11}$$

In the present work, this assumption is not made, and a Newtonian fluid law is assumed,[31] such that

$$\boldsymbol{\sigma}^{\mathrm{f}}_E := n^{\mathrm{f}} \kappa_{\mathrm{f}} \operatorname{tr}(\boldsymbol{d}_{\mathrm{f}}) \boldsymbol{1} + 2\eta_{\mathrm{f}} \boldsymbol{d}_{\mathrm{f}} \,, \tag{12}$$

where κ_{f} denotes the constant bulk viscosity of the compressible pore fluid and

$$\boldsymbol{d}_{\mathrm{f}} := \frac{1}{2}(\mathrm{grad}\boldsymbol{v}_{\mathrm{f}} + \mathrm{grad}^T \boldsymbol{v}_{\mathrm{f}}) \,. \tag{13}$$

Thus, taking the divergence of Eq. 12 as required by Eq. 8_3 and insertion of Eq. 7 into Eq. 5, introduces a porosity gradient as well as a Laplacian of the pore fluid

velocity (shown in red):

$$\begin{aligned}\frac{\partial \sigma^{\mathrm{f}}_{ij(E)}}{\partial X_J} F^{-1}_{Jj(s)} = &\left(\kappa_{\mathrm{f}} \frac{\partial v_{k(\mathrm{f})}}{\partial X_K} F^{-1}_{Kk(s)} F^{-1}_{Ji(s)} + \eta_{\mathrm{f}} \left[\frac{\partial v_{i(\mathrm{f})}}{\partial X_K} F^{-1}_{Kj(s)} + \frac{\partial v_{j(\mathrm{f})}}{\partial X_K} F^{-1}_{Ki(s)}\right] F^{-1}_{Jj(s)}\right) \frac{\partial n^{\mathrm{f}}}{\partial X_J} \\ &+ n^{\mathrm{f}} \kappa_{\mathrm{f}} \frac{\partial^2 v_{k(\mathrm{f})}}{\partial X_J \partial X_K} F^{-1}_{Kk(s)} F^{-1}_{Ji(s)} \\ &+ n^{\mathrm{f}} \eta_{\mathrm{f}} \left(\frac{\partial^2 v_{i(\mathrm{f})}}{\partial X_J \partial X_K} F^{-1}_{Kj(s)} F^{-1}_{Jj(s)} + \frac{\partial^2 v_{j(\mathrm{f})}}{\partial X_J \partial X_K} F^{-1}_{Ki(s)} F^{-1}_{Jj(s)}\right),\end{aligned} \tag{14}$$

where the porosity gradient, under the assumption of a mechanically incompressible solid (s) constituent, can be expressed as

$$\begin{aligned}\frac{\partial n^{\mathrm{f}}}{\partial x_j} &= \frac{\partial n^{\mathrm{f}}}{\partial X_J} F^{-1}_{Jj(s)} = -\frac{\partial n^{\mathrm{s}}}{\partial X_J} F^{-1}_{Jj(s)} = \frac{\partial}{\partial X_J}\left(\frac{n^{\mathrm{s}}_0}{J_{\mathrm{s}}}\right) F^{-1}_{Jj(s)} = \frac{n^{\mathrm{s}}_0}{J^2_{\mathrm{s}}} \frac{\partial J_{\mathrm{s}}}{\partial X_J} F^{-1}_{Jj(s)} \\ &= \frac{n^{\mathrm{s}}_0}{J^2_{\mathrm{s}}} \frac{\partial \det(1 + \partial u_{i(s)}/\partial X_I)}{\partial X_J} F^{-1}_{Jj(s)} = \frac{n^{\mathrm{s}}_0}{J_{\mathrm{s}}} \frac{\partial^2 u_{i(s)}}{\partial X_I \partial X_J} F^{-1}_{Ii(s)} F^{-1}_{Jj(s)}\,.\end{aligned} \tag{15}$$

The terms highlighted in red in Eqs. 14 and 15 possess second derivatives and thus convergence is not guaranteed for standard FE implementations if not weakened appropriately. In other words, they would require finite elements (for the respective fields) that possess C^1 continuity rather than the standard C^0 continuity (e.g., a typical Lagrange element). We will proceed to show that such a weakening of these terms will be very difficult.

Dropping now the $(\cdot)^{\mathrm{s}}$ and $(\cdot)_{\mathrm{s}}$ superscripts and subscripts for notational convenience, the strong form of the balance of mass for the biphasic mixture under the assumption of locally homogeneous temperatures and barotropic constituents is written as

$$\begin{aligned}&\frac{J n^{\mathrm{f}}}{K^{\eta}_{\mathrm{f}}} D_t p_{\mathrm{f}} + D_t J + \frac{J}{K^{\eta}_{\mathrm{f}}} \operatorname{GRAD}(p_{\mathrm{f}}) \cdot \boldsymbol{F}^{-1} \cdot (n^{\mathrm{f}} \tilde{\boldsymbol{v}}_{\mathrm{f}}) + J \operatorname{GRAD}(n^{\mathrm{f}} \tilde{\boldsymbol{v}}_{\mathrm{f}}) : \boldsymbol{F}^{-T} = 0\,, \\ &p_{\mathrm{f}}(\boldsymbol{X}, t) = g^p(\boldsymbol{X}, t)\ \forall \boldsymbol{X} \in \Gamma^p_0\,, \\ &-\left[J \boldsymbol{F}^{-1} \cdot (n^{\mathrm{f}} \tilde{\boldsymbol{v}}_{\mathrm{f}})\right] \cdot \boldsymbol{N} = Q_{\mathrm{f}}(\boldsymbol{X}, t)\ \forall \boldsymbol{X} \in \Gamma^{Q_{\mathrm{f}}}_0\,,\end{aligned} \tag{16}$$

where g^p is the prescribed pore fluid pressure on Γ^p_0 (typically set for the "drained" boundary condition), and Q_{f} is the prescribed fluid flux (positive inward) on $\Gamma^{Q_{\mathrm{f}}}_0$, where we have assumed that the mass supply of the pore fluid (f) constituent is

negligible.

Let $\mathcal{H}(\boldsymbol{u}, \boldsymbol{u}_{\mathrm{f}}, p_{\mathrm{f}}, w^{p_{\mathrm{f}}})$ be the variational form of Eq. 16, and let $w^{p_{\mathrm{f}}}$ be a set of scalar valued weighting (test) functions associated with pore fluid pressure p_{f}. We may then rewrite Eq. 16 in indicial notation as

$$\begin{aligned}\mathcal{H}(u_i, u_{i(\mathrm{f})}, p_{\mathrm{f}}, w^{p_{\mathrm{f}}}) = &\int_{\mathcal{B}_0} w^{p_{\mathrm{f}}} \left(\frac{J n^{\mathrm{f}}}{K_{\mathrm{f}}^{\eta}} \dot{p}_{\mathrm{f}} + \dot{J} \right) dV \\ &+ \int_{\mathcal{B}_0} w^{p_{\mathrm{f}}} \frac{J}{K_{\mathrm{f}}^{\eta}} \frac{\partial p_{\mathrm{f}}}{\partial X_I} F_{Ii}^{-1} \left(n^{\mathrm{f}} \tilde{v}_{i(\mathrm{f})} \right) dV \\ &+ \int_{\mathcal{B}_0} w^{p_{\mathrm{f}}} J \frac{\partial \left(n^{\mathrm{f}} \tilde{v}_{i(\mathrm{f})} \right)}{\partial X_I} F_{Ii}^{-1} \, dV = 0 \,. \end{aligned} \tag{17}$$

Using chain rule, the last term in Eq. 17 can be rewritten as follows:

$$\begin{aligned}\int_{\mathcal{B}_0} w^{p_{\mathrm{f}}} J \frac{\partial \left(n^{\mathrm{f}} \tilde{v}_{i(\mathrm{f})} \right)}{\partial X_I} F_{Ii}^{-1} \, dV = &\int_{\mathcal{B}_0} \frac{\partial \left(w^{p_{\mathrm{f}}} J \left(n^{\mathrm{f}} \tilde{v}_{i(\mathrm{f})} \right) F_{Ii}^{-1} \right)}{\partial X_I} \, dV \\ &- \int_{\mathcal{B}_0} \frac{\partial w^{p_{\mathrm{f}}}}{\partial X_I} J \left(n^{\mathrm{f}} \tilde{v}_{i(\mathrm{f})} \right) F_{Ii}^{-1} \, dV \\ &- \int_{\mathcal{B}_0} w^{p_{\mathrm{f}}} \left(n^{\mathrm{f}} \tilde{v}_{i(\mathrm{f})} \right) \frac{\partial (J F_{Ii}^{-1})}{\partial X_I} \, dV \,, \end{aligned} \tag{18}$$

wherein the last term goes to zero because of the Piola identity (as shown in Holzapfel[31] p. 146). Substitution of Eq. 18 into Eq. 17 gives

$$\begin{aligned}\mathcal{H}(u_i, u_{i(\mathrm{f})}, p_{\mathrm{f}}, w^{p_{\mathrm{f}}}) = &\int_{\mathcal{B}_0} w^{p_{\mathrm{f}}} \left(\frac{J n^{\mathrm{f}}}{K_{\mathrm{f}}^{\eta}} \dot{p}_{\mathrm{f}} + \dot{J} \right) dV \\ &+ \int_{\mathcal{B}_0} w^{p_{\mathrm{f}}} \frac{J}{K_{\mathrm{f}}^{\eta}} \frac{\partial p_{\mathrm{f}}}{\partial X_I} F_{Ii}^{-1} \left(n^{\mathrm{f}} \tilde{v}_{i(\mathrm{f})} \right) dV \\ &+ \int_{\mathcal{B}_0} \frac{\partial \left(w^{p_{\mathrm{f}}} J \left(n^{\mathrm{f}} \tilde{v}_{i(\mathrm{f})} \right) F_{Ii}^{-1} \right)}{\partial X_I} \, dV \\ &- \int_{\mathcal{B}_0} \frac{\partial w^{p_{\mathrm{f}}}}{\partial X_I} J \left(n^{\mathrm{f}} \tilde{v}_{i(\mathrm{f})} \right) F_{Ii}^{-1} \, dV = 0 \,. \end{aligned} \tag{19}$$

Applying the divergence theorem to the third term in Eq. 19, using the boundary

conditions in Eq. 16_2 (where $w^{p_\mathrm{f}} \to 0$ on Γ_0^p) and Eq. 16_3, the variational form for the balance of mass of the biphasic mixture becomes

$$\begin{aligned}\mathcal{H}(u_i, u_{i(\mathrm{f})}, p_\mathrm{f}, w^{p_\mathrm{f}}) = &\int_{\mathcal{B}_0} w^{p_\mathrm{f}} \left(\frac{J n^\mathrm{f}}{K_\mathrm{f}^\eta} \dot{p}_\mathrm{f} + \dot{J} \right) dV \\ &+ \int_{\mathcal{B}_0} w^{p_\mathrm{f}} \frac{J}{K_\mathrm{f}^\eta} \frac{\partial p_\mathrm{f}}{\partial X_I} F_{Ii}^{-1} \left(n^\mathrm{f} \tilde{v}_{i(\mathrm{f})} \right) dV \\ &- \int_{\mathcal{B}_0} \frac{\partial w^{p_\mathrm{f}}}{\partial X_I} J \left(n^\mathrm{f} \tilde{v}_{i(\mathrm{f})} \right) F_{Ii}^{-1} \, dV - \int_{\Gamma_0^{Q_\mathrm{f}}} w^{p_\mathrm{f}} Q_\mathrm{f} \, dA = 0 \,. \end{aligned} \tag{20}$$

Given the Darcy-Brinkman equation (Eq. 7), for notational simplicity, we will denote the separate terms as

$$\mathcal{H} = \mathcal{H}_1^{\mathrm{INT}} + \mathcal{H}_2^{\mathrm{INT}} + \mathcal{H}_3^{\mathrm{INT}} + \mathcal{H}_4^{\mathrm{INT}} + \mathcal{H}_5^{\mathrm{INT}} - \mathcal{H}^{\mathrm{EXT}} = 0 \,, \tag{21}$$

where

$$\begin{aligned}\mathcal{H}_1^{\mathrm{INT}} &= \int_{\mathcal{B}_0} w^{p_\mathrm{f}} \left(\frac{J n^\mathrm{f}}{K_\mathrm{f}^\eta} \dot{p}_\mathrm{f} + \dot{J} \right) dV \,, \\ \mathcal{H}_2^{\mathrm{INT}} &= \int_{\mathcal{B}_0} w^{p_\mathrm{f}} \frac{J}{K_\mathrm{f}^\eta} \frac{\partial p_\mathrm{f}}{\partial X_I} F_{Ii}^{-1} \left(n^\mathrm{f} \tilde{v}_{i(\mathrm{f})} \right) dV \,, \\ \mathcal{H}_3^{\mathrm{INT}} &= \int_{\mathcal{B}_0} \frac{\partial w^{p_\mathrm{f}}}{\partial X_I} J F_{Ii}^{-1} \hat{k} \frac{\partial p_\mathrm{f}}{\partial X_K} F_{Ki}^{-1} \, dV \,, \\ \mathcal{H}_4^{\mathrm{INT}} &= \int_{\mathcal{B}_0} \frac{\partial w^{p_\mathrm{f}}}{\partial X_I} J F_{Ii}^{-1} \hat{k} \rho^{\mathrm{fR}} \left(a_{i(\mathrm{f})} - g_i \right) dV \,, \\ \mathcal{H}_5^{\mathrm{INT}} &= -\int_{\mathcal{B}_0} \frac{\partial w^{p_\mathrm{f}}}{\partial X_I} \frac{\hat{k}}{n^\mathrm{f}} J F_{Ii}^{-1} \frac{\partial \sigma_{ij(E)}^\mathrm{f}}{\partial X_J} F_{Jj}^{-1} \, dV \,, \\ \mathcal{H}^{\mathrm{EXT}} &= \int_{\Gamma_0^{Q_\mathrm{f}}} w^{p_\mathrm{f}} Q_\mathrm{f} \, dA \,. \end{aligned} \tag{22}$$

Considering $\mathcal{H}_2^{\text{INT}}$, we have, upon expanding the Darcy-Brinkman term:

$$\mathcal{H}_2^{\text{INT}} = -\int_{\mathcal{B}_0} w^{p_\text{f}} \frac{J\hat{k}}{K_\text{f}^\eta} \frac{\partial p_\text{f}}{\partial X_I} F_{Ii}^{-1} \frac{\partial p_\text{f}}{\partial X_K} F_{Kk}^{-1} \, dV - \int_{\mathcal{B}_0} w^{p_\text{f}} \frac{J\hat{k}}{K_\text{f}^\eta} \frac{\partial p_\text{f}}{\partial X_I} F_{Ii}^{-1} \rho^{\text{fR}} (a_{i(\text{f})} - g_i) \, dV$$
$$+ \int_{\mathcal{B}_0} w^{p_\text{f}} \frac{J\hat{k}}{K_\text{f}^\eta} \frac{\partial p_\text{f}}{\partial X_I} F_{Ii}^{-1} \Bigg(\frac{1}{n^\text{f}} \Big(\kappa_\text{f} \frac{\partial v_{k(\text{f})}}{\partial X_K} F_{Kk}^{-1} F_{Ji}^{-1} + \eta_\text{f} \Big[\frac{\partial v_{i(\text{f})}}{\partial X_K} F_{Kj}^{-1} + \frac{\partial v_{j(\text{f})}}{\partial X_K} F_{Ki}^{-1} \Big] F_{Jj}^{-1} \Big) \frac{\partial n^\text{f}}{\partial X_J}$$
$$+ \kappa_\text{f} \frac{\partial^2 v_{k(\text{f})}}{\partial X_J \partial X_K} F_{Kk}^{-1} F_{Ji}^{-1} + \eta_\text{f} \Big(\frac{\partial^2 v_{i(\text{f})}}{\partial X_J \partial X_K} F_{Kj}^{-1} F_{Jj}^{-1} + \frac{\partial^2 v_{j(\text{f})}}{\partial X_J \partial X_K} F_{Ki}^{-1} F_{Jj}^{-1} \Big) \Bigg) \, dV \ . \tag{23}$$

The first two terms can be integrated normally; however, the last cannot be integrated by parts to reduce continuity requirements of the solid skeleton (s) displacement and pore fluid (f) displacement given that a gradient is also applied to pore fluid pressure p_f (i.e., weakening continuity requirements on the displacements in turn strengthens the continuity requirement on pore fluid pressure). This problem also arises in $\mathcal{H}_5^{\text{INT}}$, although there the gradient is applied to the weighting function w^{p_f}:

$$\mathcal{H}_5^{\text{INT}} = -\int_{\mathcal{B}_0} \frac{\partial w^{p_\text{f}}}{\partial X_I} J F_{Ii}^{-1} \Bigg(\frac{1}{n^\text{f}} \Big(\kappa_\text{f} \frac{\partial v_{k(\text{f})}}{\partial X_K} F_{Kk}^{-1} F_{Ji}^{-1} + \eta_\text{f} \Big[\frac{\partial v_{i(\text{f})}}{\partial X_K} F_{Kj}^{-1} + \frac{\partial v_{j(\text{f})}}{\partial X_K} F_{Ki}^{-1} \Big] F_{Jj}^{-1} \Big) \frac{\partial n^\text{f}}{\partial X_J}$$
$$+ \kappa_\text{f} \frac{\partial^2 v_{k(\text{f})}}{\partial X_J \partial X_K} F_{Kk}^{-1} F_{Ji}^{-1} + \eta_\text{f} \Big(\frac{\partial^2 v_{i(\text{f})}}{\partial X_J \partial X_K} F_{Kj}^{-1} F_{Jj}^{-1} + \frac{\partial^2 v_{j(\text{f})}}{\partial X_J \partial X_K} F_{Ki}^{-1} F_{Jj}^{-1} \Big) \Bigg) \, dV \ . \tag{24}$$

Furthermore, the "mixed approach" taken by Vuong et al.[32,33] to treat porosity n^f as an independent field variable in the FE implementation (with the assumption of incompressible pore fluid (f) constituent, i.e., $\nabla \cdot \boldsymbol{v}_\text{f} = 0$), thereby eliminating strict dependence on solid skeleton (s) displacement, does not in and of itself relieve the issue of higher-order continuity requirements since second derivatives appear for pore fluid velocity when the pore fluid is assumed to be compressible ($\nabla \cdot \boldsymbol{v}_\text{f} \neq 0$), in both the balance of mass of the mixture and the balance of linear momentum of the pore fluid (assuming the divergence on the pore fluid extra stress is not weakened in the latter; details to follow in Section 3).

One potential remedy is to ignore the pore fluid extra stress tensor $\boldsymbol{\sigma}_E^\text{f}$ altogether.

It was shown by Markert[34] and Ehlers[35] (originally in Ehlers et al.[36]) that the fluid friction (viscous) forces are negligible when compared to the drag forces on the macroscale. The derivation from Ehlers[35] proceeds as follows.

Begin by assuming an incompressible pore fluid constituent and a rigid, non-deforming solid constituent:

$$D_t^{\mathrm{f}} \rho^{\mathrm{fR}} \to 0\,, \quad \boldsymbol{u} \to \boldsymbol{0}\,. \tag{25}$$

Then, the balance of mass of phase α reduces to (still under the assumption of negligible mass supply to phase α)

$$D_t^{\alpha} n^{\alpha} + n^{\alpha} \operatorname{div} \boldsymbol{v}_{\alpha} = 0\,. \tag{26}$$

Given that

$$\sum_{\alpha} D_t^{\alpha} n^{\alpha} = \operatorname{grad}(n^{\mathrm{f}}) \cdot \tilde{\boldsymbol{v}}_{\mathrm{f}} = \operatorname{div}(n^{\mathrm{f}} \tilde{\boldsymbol{v}}_{\mathrm{f}}) - n^{\mathrm{f}} \operatorname{div} \boldsymbol{v}_{\mathrm{f}} + (1 - n^{\mathrm{s}}) \operatorname{div} \boldsymbol{v}_{\mathrm{s}}\,, \tag{27}$$

the balance of mass of the mixture for incompressible constituents reduces to

$$\operatorname{div}(n^{\mathrm{f}} \tilde{\boldsymbol{v}}_{\mathrm{f}}) = 0\,. \tag{28}$$

For non-deforming solid, n^{s} is constant ($\operatorname{grad}(n^{\mathrm{f}}) \to \boldsymbol{0}$), and thus

$$\operatorname{div} \boldsymbol{v}_{\mathrm{f}} = 0\,. \tag{29}$$

Pore fluid momentum balance is written as

$$\rho^{\mathrm{f}} \boldsymbol{a}_{\mathrm{f}} + \operatorname{div}(n^{\mathrm{f}} p_{\mathrm{f}}) - \operatorname{div} \boldsymbol{\sigma}_E^{\mathrm{f}} - \boldsymbol{h}^{\mathrm{f}} - \rho^{\mathrm{f}} \boldsymbol{g} = \boldsymbol{0}\,. \tag{30}$$

In a prior report,[27] it was shown that the drag force

$$\boldsymbol{h}^{\mathrm{f}} = \boldsymbol{h}_E^{\mathrm{f}} + p_{\mathrm{f}} \operatorname{grad} n^{\mathrm{f}}\,, \tag{31}$$

with

$$\boldsymbol{h}_E^{\mathrm{f}} = -\boldsymbol{S}_w \tilde{\boldsymbol{v}}_{\mathrm{f}} = -\frac{(n^{\mathrm{f}})^2}{\hat{k}} \tilde{\boldsymbol{v}}_{\mathrm{f}}\,, \quad \boldsymbol{S}_w \coloneqq \frac{(n^{\mathrm{f}})^2}{\hat{k}} \boldsymbol{1}\,. \tag{32}$$

With this, and by inserting the Newtonian fluid law given by Eq. 12 (using the identity $\mathrm{tr}(\boldsymbol{d}_\mathrm{f}) = \mathrm{div}\,\boldsymbol{v}_\mathrm{f}$, which is zero by Eq. 29) into Eq. 30 gives the pore fluid momentum balance for incompressible constituents and non-deforming solid skeleton:

$$\rho^\mathrm{f}\boldsymbol{a}_\mathrm{f} + n^\mathrm{f}\mathrm{grad}p_\mathrm{f} - n^\mathrm{f}\eta_\mathrm{f}\,\mathrm{div}\,\mathrm{grad}\boldsymbol{v}_\mathrm{f} + \frac{(n^\mathrm{f})^2}{\hat{k}}\boldsymbol{v}_\mathrm{f} - \rho^\mathrm{f}\boldsymbol{g} = \boldsymbol{0}\,. \tag{33}$$

Introducing the dimensionless quantities

$$\overset{*}{\boldsymbol{x}} \coloneqq \frac{\boldsymbol{x}}{L}\,, \quad \overset{*}{\boldsymbol{v}}_\mathrm{f} \coloneqq \frac{\boldsymbol{v}_\mathrm{f}}{V}\,, \tag{34}$$

with L as a characteristic length scale and V as a characteristic velocity allows us to write the dimensionless gradient and divergence operators as

$$\overset{*}{\mathrm{grad}}(\cdot) = L\mathrm{grad}(\cdot)\,, \quad \overset{*}{\mathrm{div}}(\cdot) = L\,\mathrm{div}(\cdot)\,. \tag{35}$$

Then we may recast the viscous and drag forces in Eq. 33 as, respectively,

$$\begin{aligned} \mathrm{div}\,\boldsymbol{\sigma}^\mathrm{f}_E &= n^\mathrm{f}\eta_\mathrm{f}\frac{V}{L^2}\overset{*}{\mathrm{div}}(\overset{*}{\mathrm{grad}}\overset{*}{\boldsymbol{v}}_\mathrm{f})\,, \\ \boldsymbol{h}^\mathrm{f}_E &= -\frac{(n^\mathrm{f})^2}{\hat{k}}V\overset{*}{\boldsymbol{v}}_\mathrm{f}\,. \end{aligned} \tag{36}$$

Taking the ratio of the viscous force to the drag force yields

$$\frac{\text{Viscous force}}{\text{Drag force}} \propto \frac{\eta_\mathrm{f}\hat{k}}{n^\mathrm{f}L^2} = \frac{\varkappa}{n^\mathrm{f}L^2}\,. \tag{37}$$

For porous media applications, $\varkappa$ is typically several orders of magnitude smaller than the length scale of interest L (e.g., in the current work $\varkappa \sim \mathcal{O}(10^{-10}\ \mathrm{m}^2)$ for lung parenchyma[37] and $L \sim \mathcal{O}(10^{-2}\ \mathrm{m})$). Thus, it may be appropriate to ignore the pore fluid extra stress (the viscous force) when solving the balance equations for the macroscale regime, but not necessarily for the microscale regime where the pore size $\sqrt{\varkappa}$ is on the order of L.

However, as Vuong points out (see Section 3.3.6 of Vuong[33] and the figures therein), a nearly inviscid fluid creates infinitesimally large velocity gradients at the porous channel walls to counteract an infinitesimally small boundary layer, which could lead to numerical instability for 3-D simulations, particularly for highly permeable

materials, that is, those with larger pore sizes (larger fluid domains). Whether or not it is necessary to account for the boundary layer in a numerical simulation where flow is modeled on the macroscale regime is an area of debate.[38] This boundary layer has thickness of order $(\tilde{\eta}_{\mathrm{f}}\varkappa/\eta_{\mathrm{f}})^{1/2}$, where $\tilde{\eta}_{\mathrm{f}}$ is an effective viscosity of the pore fluid. For lung parenchyma,[37] $\varkappa \sim 10^{-10}$ m^2, thus these viscous effects are probably negligible at the mesoscale level of interest for lung parenchyma, which is $\mathcal{O}(10^{-2})$ m.

Generally speaking, it is believed that both the Darcy and Darcy-Brinkman equations only hold in the range of Reynolds numbers[33,38–40] $1 < \mathrm{Re} < 10$—for reference, in prior work,[28,29] the maximum Reynolds number resulting from numerical simulations was roughly $\mathrm{Re} = 10.7$. Nevertheless, the Reynolds number-based limits are based upon experimental data wherein it is difficult to measure the inertia forces,[41] and, with the exception of Vuong et al.,[32,33] many authors do not include the inertia term in Darcy's law, and use instead the classical form that relates seepage velocity to pore fluid pressure gradient and (if applicable) body forces.

2.2 Satisfying C^1 Continuity

If the pore fluid extra stress is to be included, elements with continuous first derivatives along their boundaries must be used to guarantee convergence. The approach taken by Vuong et al.[32,33] to guarantee C^1 continuity was to use Non-Uniform Rational Basis Splines (NURBS) (refer to work by Hughes et al.[42] for a FE application). However, for the simple 1-D geometry considered herein, NURBS would introduce an additional layer of complexity given that the basis functions are not interpolatory.

A simpler solution would be to invoke the Hermite cubic polynomial element (which is C^1 continous), typically employed in FE analysis of beams. Herein, the analogy to a rotational degree of freedom (DOF) in beam analysis is the gradient DOF. However, unlike beam analysis, the gradient DOFs of the field variables of interest (u and u_{f}) are allowed to "float," that is, no Dirichlet nor Neumann boundary conditions are prescribed on these DOFs; in essence, they go unused outside of their interpolatory functionality.

The element (refer to Fig. 2) will not be isoparametric, that is,

$$x^{h^e}(\xi) = \boldsymbol{N}^e(\xi) \cdot \boldsymbol{x}^e\,, \quad u^{h^e}(\xi) = \boldsymbol{N}_H^{e,u}(\boldsymbol{\xi}) \cdot \boldsymbol{d}^e\,, \tag{38}$$

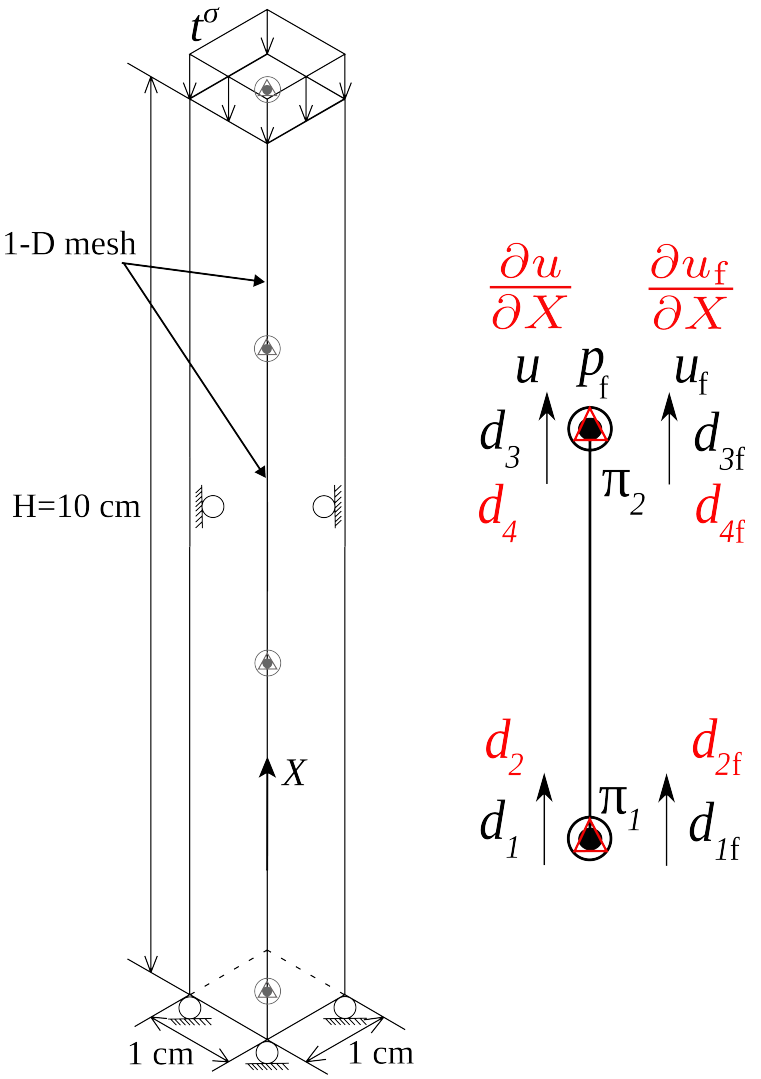

Fig. 2 The Q3H-Q3H-P1 line element used for C^1 continuity of the field variables u and u_f. Shown in red are the gradient DOFs that are allowed to "float," that is, no boundary conditions are prescribed for these DOFs.

with

$$
\begin{aligned}
N_1^e &:= \frac{1}{2}(1-\xi)\,, \\
N_2^e &:= \frac{1}{2}(1+\xi)\,,
\end{aligned}
\tag{39}
$$

and

$$\boldsymbol{d}^e = \begin{Bmatrix} d_1^e \\ d_2^e \\ d_3^e \\ d_4^e \end{Bmatrix} = \begin{Bmatrix} u^{h^e}(\xi = -1) \\ u_{,x}^{h^e}(-1) \\ u^{h^e}(1) \\ u_{,x}^{h^e}(1) \end{Bmatrix}, \tag{40}$$

such that

$$u^{h^e}(\xi) = \begin{bmatrix} N_{1(H)}^{e,u} & j^e N_{2(H)}^{e,u} & N_{3(H)}^{e,u} & j^e N_{4(H)}^{e,u} \end{bmatrix} \begin{bmatrix} d_1^e \\ d_2^e \\ d_3^e \\ d_4^e \end{bmatrix} = \boldsymbol{N}_H^{e,u}(\xi) \cdot \boldsymbol{d}^e \,, \tag{41}$$

where $\boldsymbol{N}_H^{e,u}(\xi)$ are the element Hermite cubic polynomials:

$$\begin{aligned} N_{1(H)}^{e,u} &\coloneqq \frac{1}{4}(1-\xi)^2(2+\xi)\,, \\ N_{2(H)}^{e,u} &\coloneqq \frac{1}{4}(1-\xi)^2(1+\xi)\,, \\ N_{3(H)}^{e,u} &\coloneqq \frac{1}{4}(1+\xi)^2(2-\xi)\,, \\ N_{4(H)}^{e,u} &\coloneqq \frac{1}{4}(1+\xi)^2(-1+\xi)\,, \end{aligned} \tag{42}$$

and

$$\begin{aligned} j^e &\coloneqq \frac{\partial x^{h^e}}{\partial \xi} = \frac{h^e}{2}\,, \\ \frac{\partial u^{h^e}}{\partial \xi} &= j^e \frac{\partial u^{h^e}}{\partial X}, \\ w^{u^{h^e}}(\xi) &= \boldsymbol{N}_H^{e,u} \cdot \boldsymbol{c}^{u,e} = (\boldsymbol{c}^{u,e})^T \cdot (\boldsymbol{N}_H^{e,u})^T\,. \end{aligned} \tag{43}$$

Herein, the "strain-displacement" matrix $\boldsymbol{H}^{e,u}$ is defined as

$$\frac{\partial^2 u^{h^e}(\xi)}{\partial X^2} = \frac{d^2 \boldsymbol{N}_H^{e,u}(\xi)}{\partial X^2} \cdot \boldsymbol{d}^e = \frac{1}{(j^e)^2} \frac{d^2 \boldsymbol{N}_H^{e,u}(\xi)}{\partial \xi^2} \cdot \boldsymbol{d}^e = \boldsymbol{H}^{e,u}(\xi) \cdot \boldsymbol{d}^e\,, \tag{44}$$

and

$$\frac{\partial u^{h^e}(\xi)}{\partial X} = \frac{d \boldsymbol{B}_H^{e,u}(\xi)}{\partial X} \cdot \boldsymbol{d}^e = \frac{1}{j^e} \frac{d \boldsymbol{B}_H^{e,u}(\xi)}{\partial \xi^2} \cdot \boldsymbol{d}^e = \boldsymbol{B}_H^{e,u}(\xi) \cdot \boldsymbol{d}^e\,. \tag{45}$$

For notational purposes, the $(\cdot)_H$ subscript will be dropped from $\boldsymbol{N}_H^{e,u}$ and $\boldsymbol{B}_H^{e,u}$. In the finite element equations where $\boldsymbol{H}^{e,u}$ is used, the reader should assume that the shape functions for the respective field, and its first derivative, are the Hermite shape functions shown here (i.e., only one element type will be used to represent a field variable, not a mix of element types). Of course the same interpolation applies to the shape functions $\boldsymbol{N}_H^{e,u_\mathrm{f}}$, $\boldsymbol{B}_H^{e,u_\mathrm{f}}$, and $\boldsymbol{H}^{e,u_\mathrm{f}}$ when the pore fluid displacement u_f requires a C^1 continuous element.

3. Numerical Implementation

3.1 1-D Kinematics

One-dimensional uniaxial solid skeleton strain and unidirectional pore fluid flow simplifications are implemented for (s) and (f) phases, respectively. If we assume that the soft porous material only undergoes compression or expansion in one dimension, specifically the vertical direction X, then both the solid skeleton displacements in the transverse directions as well as all shear terms in the deformation gradient go to zero. The solid skeleton deformation gradient becomes

$$\boldsymbol{F}_\mathrm{s} = \begin{bmatrix} 1+\dfrac{\partial u}{\partial X} & 0 & 0 \\ 0 & 1 & 0 \\ 0 & 0 & 1 \end{bmatrix}, \qquad J_\mathrm{s} = \det \boldsymbol{F}_\mathrm{s} = F_{11(\mathrm{s})} = 1+\frac{\partial u}{\partial X} \tag{46}$$

where $u(X,t)$ is the axial displacement in the X direction. Similarly, if we assume that pore fluid flow is confined in direction X (i.e., surrounded by an impermeable sleeve, drained or undrained at its ends), then

$$\boldsymbol{v}_\mathrm{f} = \begin{bmatrix} v_\mathrm{f} \\ 0 \\ 0 \end{bmatrix}, \qquad \boldsymbol{a}_\mathrm{f} = \begin{bmatrix} a_\mathrm{f} \\ 0 \\ 0 \end{bmatrix}, \qquad \boldsymbol{u}_\mathrm{f} = \begin{bmatrix} u_\mathrm{f} \\ 0 \\ 0 \end{bmatrix} \tag{47}$$

where in the X direction, v_f is the pore fluid velocity, a_f is the pore fluid acceleration, and u_f is the pore fluid displacement. Variational forms that follow are first presented in a general 3-D regime before simplifications to the 1-D regime; the $(\cdot)^\mathrm{s}$ and $(\cdot)_\mathrm{s}$ superscripts and subscripts are dropped for notational convenience.

3.2 Variational Formulation

The strong and variational form of the balance of mass of the mixture was given in Section 2, but is briefly restated here as

$$\begin{aligned}
&\frac{Jn^{\mathrm{f}}}{K_{\mathrm{f}}^{\eta}} D_t p_{\mathrm{f}} + D_t J + \frac{J}{K_{\mathrm{f}}^{\eta}} \operatorname{GRAD}(p_{\mathrm{f}}) \cdot \boldsymbol{F}^{-1} \cdot (n^{\mathrm{f}} \tilde{\boldsymbol{v}}_{\mathrm{f}}) + J \operatorname{GRAD}(n^{\mathrm{f}} \tilde{\boldsymbol{v}}_{\mathrm{f}}) : \boldsymbol{F}^{-T} = 0 \,, \\
&p_{\mathrm{f}}(\boldsymbol{X}, t) = g^p(\boldsymbol{X}, t) \; \forall \boldsymbol{X} \in \Gamma_0^p \,, \\
&- [J \boldsymbol{F}^{-1} \cdot (n^{\mathrm{f}} \tilde{\boldsymbol{v}}_{\mathrm{f}})] \cdot \boldsymbol{N} = Q_{\mathrm{f}}(\boldsymbol{X}, t) \; \forall \boldsymbol{X} \in \Gamma_0^{Q_{\mathrm{f}}} \,,
\end{aligned} \tag{48}$$

where g^p is the prescribed pore fluid pressure on Γ_0^p (typically set for the "drained" boundary condition), and Q_{f} is the prescribed fluid flux (positive inward) on $\Gamma_0^{Q_{\mathrm{f}}}$, where we have assumed that the mass supply of the pore fluid (f) constituent is negligible.

Let $\mathcal{H}(\boldsymbol{u}, \boldsymbol{u}_{\mathrm{f}}, p_{\mathrm{f}}, w^{p_{\mathrm{f}}})$ be the variational form of Eq. 48, and let $w^{p_{\mathrm{f}}}$ be a set of scalar valued weighting (test) functions associated with pore fluid pressure p_{f}. We may then rewrite Eq. 48 in indicial notation as

$$\begin{aligned}
\mathcal{H}(u_i, u_{i(\mathrm{f})}, p_{\mathrm{f}}, w^{p_{\mathrm{f}}}) = &\int_{\mathcal{B}_0} w^{p_{\mathrm{f}}} \left(\frac{Jn^{\mathrm{f}}}{K_{\mathrm{f}}^{\eta}} \dot{p}_{\mathrm{f}} + \dot{J} \right) dV \\
&+ \int_{\mathcal{B}_0} w^{p_{\mathrm{f}}} \frac{J}{K_{\mathrm{f}}^{\eta}} \frac{\partial p_{\mathrm{f}}}{\partial X_I} F_{Ii}^{-1} \left(n^{\mathrm{f}} \tilde{v}_{i(\mathrm{f})} \right) dV \\
&- \int_{\mathcal{B}_0} \frac{\partial w^{p_{\mathrm{f}}}}{\partial X_I} J \left(n^{\mathrm{f}} \tilde{v}_{i(\mathrm{f})} \right) F_{Ii}^{-1} \, dV - \int_{\Gamma_0^{Q_{\mathrm{f}}}} w^{p_{\mathrm{f}}} Q_{\mathrm{f}} \, dA = 0 \,.
\end{aligned} \tag{49}$$

For notational simplicity, we will denote the separate terms as

$$\mathcal{H} = \mathcal{H}_1^{\mathrm{INT}} + \mathcal{H}_2^{\mathrm{INT}} + \mathcal{H}_3^{\mathrm{INT}} + \mathcal{H}_4^{\mathrm{INT}} + \mathcal{H}_5^{\mathrm{INT}} - \mathcal{H}^{\mathrm{EXT}} = 0 \,, \tag{50}$$

where

$$
\begin{aligned}
\mathcal{H}_1^{\text{INT}} &= \int_{\mathcal{B}_0} w^{p_{\text{f}}} \left(\frac{J n^{\text{f}}}{K_{\text{f}}^{\eta}} \dot{p}_{\text{f}} + \dot{J} \right) dV \,, \\
\mathcal{H}_2^{\text{INT}} &= \int_{\mathcal{B}_0} w^{p_{\text{f}}} \frac{J}{K_{\text{f}}^{\eta}} \frac{\partial p_{\text{f}}}{\partial X_I} F_{Ii}^{-1} \left(n^{\text{f}} \tilde{v}_{i(\text{f})} \right) dV \,, \\
\mathcal{H}_3^{\text{INT}} &= \int_{\mathcal{B}_0} \frac{\partial w^{p_{\text{f}}}}{\partial X_I} J F_{Ii}^{-1} \hat{k} \frac{\partial p_{\text{f}}}{\partial X_K} F_{Ki}^{-1} \, dV \,, \\
\mathcal{H}_4^{\text{INT}} &= \int_{\mathcal{B}_0} \frac{\partial w^{p_{\text{f}}}}{\partial X_I} J F_{Ii}^{-1} \hat{k} \rho^{\text{fR}} \left(a_{i(\text{f})} - g_i \right) dV \,, \\
\mathcal{H}_5^{\text{INT}} &= - \int_{\mathcal{B}_0} \frac{\partial w^{p_{\text{f}}}}{\partial X_I} \frac{\hat{k}}{n^{\text{f}}} J F_{Ii}^{-1} \frac{\partial \sigma_{ij(E)}^{\text{f}}}{\partial X_J} F_{Jj}^{-1} \, dV \,, \\
\mathcal{H}^{\text{EXT}} &= \int_{\Gamma_0^{Q_{\text{f}}}} w^{p_{\text{f}}} Q_{\text{f}} \, dA \,.
\end{aligned}
\tag{51}
$$

The 1-D reduction of Eq. 51 is

$$
\begin{aligned}
\mathcal{H}_1^{\text{INT}} &= \int_0^{X=H} w^{p_{\text{f}}} \left(\frac{J n^{\text{f}}}{K_{\text{f}}^{\eta}} \dot{p}_{\text{f}} + \dot{J} \right) A \, dX \,, \\
\mathcal{H}_2^{\text{INT}} &= \int_0^{X=H} w^{p_{\text{f}}} \frac{1}{K_{\text{f}}^{\eta}} \frac{\partial p_{\text{f}}}{\partial X} n^{\text{f}} \tilde{v}_{\text{f}} A \, dX \,, \\
\mathcal{H}_3^{\text{INT}} &= \int_0^{X=H} \frac{\partial w^{p_{\text{f}}}}{\partial X} \hat{k} \frac{\partial p_{\text{f}}}{\partial X} F_{11}^{-1} A \, dX \,, \\
\mathcal{H}_4^{\text{INT}} &= \int_0^{X=H} \frac{\partial w^{p_{\text{f}}}}{\partial X} \hat{k} \rho^{\text{fR}} \left(a_{\text{f}} + g \right) A \, dX \,, \\
\mathcal{H}_5^{\text{INT}} &= - \int_0^{X=H} \frac{\partial w^{p_{\text{f}}}}{\partial X} \frac{\hat{k}}{n^{\text{f}}} \frac{\partial \sigma_{11(E)}^{\text{f}}}{\partial X} F_{11}^{-1} A \, dX \,, \\
\mathcal{H}^{\text{EXT}} &= \int_{\Gamma_0^{Q_{\text{f}}}} w^{p_{\text{f}}} Q_{\text{f}} \, dA = Q_{\text{f}}|_{X=H} A \,.
\end{aligned}
\tag{52}
$$

The strong form of the balance of linear momentum of the biphasic mixture is given

as

$$\begin{aligned}
&\mathrm{DIV}\,\boldsymbol{P} + \rho_0 \boldsymbol{g} - \left(\rho_0^{\mathrm{s}} \boldsymbol{a} + \rho_0^{\mathrm{f}} \boldsymbol{a}_{\mathrm{f}}\right) = \boldsymbol{0}\,, \\
&\boldsymbol{u}(\boldsymbol{X}, t) = \boldsymbol{g}^u(\boldsymbol{X}, t)\ \forall \boldsymbol{X} \in \Gamma_0^u\,, \\
&\boldsymbol{P}(\boldsymbol{X}, t) \cdot \boldsymbol{N}(\boldsymbol{X}) = \boldsymbol{t}^\sigma(\boldsymbol{X}, t)\ \forall \boldsymbol{X} \in \Gamma_0^t\,.
\end{aligned} \tag{53}$$

Let $\mathcal{G}(u_i, u_{i(\mathrm{f})}, p_{\mathrm{f}}, w_i^u)$ be the variational form of Eq. 53 and let w_i^u be a set of vector-valued weighting (test) functions associated with solid skeleton displacement u_i. We may then rewrite Eq. 53 as

$$\begin{aligned}
\mathcal{G}(u_i, u_{i(\mathrm{f})}, p_{\mathrm{f}}, w_i^u) = &\int_{\mathcal{B}_0} w_i^u \left(\rho_0^{\mathrm{s}} a_i + \rho_0^{\mathrm{f}} a_{i(\mathrm{f})}\right) dV + \int_{\mathcal{B}_0} \frac{\partial w_i^u}{\partial X_I} P^{\mathrm{s}}_{iI(E)}\, dV \\
&- \int_{\mathcal{B}_0} \frac{\partial w_i^u}{\partial X_I} J F^{-1}_{Ii} p_{\mathrm{f}}\, dV + \int_{\mathcal{B}_0} \frac{\partial w_i^u}{\partial X_I} P^{\mathrm{f}}_{iI(E)}\, dV - \int_{\mathcal{B}_0} w_i^u \rho_0 g_i\, dV \\
&- \left(\int_{\Gamma_0^t} w_i^u t_i^{\sigma^{\mathrm{s}}_E}\, dA - \int_{\Gamma_0^t} w_i^u p_{\mathrm{f}} J F^{-1}_{Ii} N_I\, dA + \int_{\Gamma_0^t} w_i^u t_i^{\sigma^{\mathrm{f}}_E}\, dA \right) = 0\,,
\end{aligned} \tag{54}$$

where the divergence on total first Piola-Kirchhoff stress of the mixture was weakened using divergence theorem, producing the second, third, fourth, and last terms in Eq. 54. The last term represents the *total* traction applied to solid and fluid phases (the mixture). Thus, there is no need to compute any of its components, for example, the integrand of the "viscous traction" $t_i^{\sigma^{\mathrm{f}}_E}$ term. For notational simplicity, we denote the separate terms as

$$\mathcal{G} = \mathcal{G}_1^{\mathrm{INT}} + \mathcal{G}_2^{\mathrm{INT}} + \mathcal{G}_3^{\mathrm{INT}} + \mathcal{G}_4^{\mathrm{INT}} - (\mathcal{G}_1^{\mathrm{EXT}} + \mathcal{G}_2^{\mathrm{EXT}} + \mathcal{G}_3^{\mathrm{EXT}}) = 0\,, \tag{55}$$

where

$$
\begin{aligned}
\mathcal{G}_1^{\text{INT}} &= \int_{\mathcal{B}_0} w_i^u \left(\rho_0^{\text{s}} a_i + \rho_0^{\text{f}} a_{i(\text{f})}\right) dV \,, \\
\mathcal{G}_2^{\text{INT}} &= \int_{\mathcal{B}_0} \frac{\partial w_i^u}{\partial X_I} P_{iI(E)}^{\text{s}} \, dV \,, \\
\mathcal{G}_3^{\text{INT}} &= -\int_{\mathcal{B}_0} \frac{\partial w_i^u}{\partial X_I} J F_{Ii}^{-1} p_{\text{f}} \, dV \,, \\
\mathcal{G}_4^{\text{INT}} &= -\int_{\mathcal{B}_0} w_i^u \rho_0 g_i \, dV \,, \\
\mathcal{G}_5^{\text{INT}} &= \int_{\mathcal{B}_0} \frac{\partial w_i^u}{\partial X_I} P_{iI(E)}^{\text{f}} \, dV \,, \\
\mathcal{G}_1^{\text{EXT}} &= \int_{\Gamma_0^t} w_i^u t_i^{\sigma_E^{\text{s}}} \, dA \,, \\
\mathcal{G}_2^{\text{EXT}} &= -\int_{\Gamma_0^t} w_i^u p_{\text{f}} J F_{Ii}^{-1} N_I \, dA \,, \\
\mathcal{G}_3^{\text{EXT}} &= \int_{\Gamma_0^t} w_i^u t_i^{\sigma_E^{\text{f}}} \, dA \,.
\end{aligned}
\tag{56}
$$

The 1-D reduction of Eq. 56 is

$$
\begin{aligned}
\mathcal{G}_1^{\text{INT}} &= \int_0^{X=H} w^u \left(\rho_0^{\text{s}} a_{\text{s}} + \rho_0^{\text{f}} a_{\text{f}}\right) A \, dX \,, \\
\mathcal{G}_2^{\text{INT}} &= \int_0^{X=H} \frac{\partial w^u}{\partial X} P_{11(E)}^{\text{s}} A \, dX \,, \\
\mathcal{G}_3^{\text{INT}} &= -\int_0^{X=H} \frac{\partial w^u}{\partial X} p_{\text{f}} A \, dX \,, \\
\mathcal{G}_4^{\text{INT}} &= \int_0^{X=H} w^u \rho_0 g A \, dX \,, \\
\mathcal{G}_5^{\text{INT}} &= \int_0^{X=H} \frac{\partial w^u}{\partial X} P_{11(E)}^{\text{f}} A \, dX \,, \\
\mathcal{G}_1^{\text{EXT}} &= \int_{\Gamma_0^t} w^u t^{\sigma_E^{\text{s}}} \, dA = t^{\sigma_E^{\text{s}}} A \,, \\
\mathcal{G}_2^{\text{EXT}} &= -\int_{\Gamma_0^t} w^u p_{\text{f}} \, dA = -p_{\text{f}} A \,, \\
\mathcal{G}_3^{\text{EXT}} &= \int_{\Gamma_0^t} w^u t^{\sigma_E^{\text{f}}} \, dA = t^{\sigma_E^{\text{f}}} A \,.
\end{aligned}
\tag{57}
$$

If we combine Eq. $57_{6,7,8}$ we see that

$$
\mathcal{G}_1^{\text{EXT}} + \mathcal{G}_2^{\text{EXT}} + \mathcal{G}_3^{\text{EXT}} = A \left(t^{\sigma_E^{\text{s}}} - p_{\text{f}} + t^{\sigma_E^{\text{f}}}\right) = A t^{\sigma} \,. \tag{58}
$$

The strong formulation of the balance of linear momentum for a viscous pore fluid is given as

$$
\begin{aligned}
&\rho_0^{\text{f}} \boldsymbol{a}_{\text{f}} + J n^{\text{f}} \, \text{GRAD}(p_{\text{f}}) \cdot \boldsymbol{F}^{-1} - \text{DIV} \, \boldsymbol{P}_E^{\text{f}} + J \frac{\left(n^{\text{f}}\right)^2}{\hat{k}} (\boldsymbol{v}_{\text{f}} - \boldsymbol{v}) - \rho_0^{\text{f}} \boldsymbol{g} = \boldsymbol{0} \,, \\
&\boldsymbol{u}_{\text{f}}(\boldsymbol{X}, t) = \boldsymbol{g}_{u_{\text{f}}}(\boldsymbol{X}, t) \; \forall \boldsymbol{X} \in \Gamma_0^{u_{\text{f}}} \,.
\end{aligned}
\tag{59}
$$

Let $\mathcal{I}(u_i, u_{i(\text{f})}, p_{\text{f}}, w_i^{u_{\text{f}}})$ be the variational form of Eq. 59 and let $w_i^{u_{\text{f}}}$ be a set of vector-valued weighting functions associated with pore fluid displacement $u_{i(\text{f})}$. We

may then rewrite Eq. 59 as follows:

$$\begin{aligned}\mathcal{I}(u_i, u_{i(\mathrm{f})}, p_\mathrm{f}, w_i^{u_\mathrm{f}}) = &\int_{\mathcal{B}_0} w_i^{u_\mathrm{f}} \rho_0^\mathrm{f} a_{i(\mathrm{f})}\, dV + \int_{\mathcal{B}_0} w_i^{u_\mathrm{f}} J n^\mathrm{f} \frac{\partial p_\mathrm{f}}{\partial X_I} F_{Ii}^{-1}\, dV \\ &+ \int_{\mathcal{B}_0} w_i^{u_\mathrm{f}} J \frac{\left(n^\mathrm{f}\right)^2}{\hat{k}} (v_{i(\mathrm{f})} - v_i)\, dV \\ &- \int_{\mathcal{B}_0} w_i^{u_\mathrm{f}} \frac{\partial P_{iI(E)}^\mathrm{f}}{\partial X_I}\, dV - \int_{\mathcal{B}_0} w_i^{u_\mathrm{f}} \rho_0^\mathrm{f} g_i\, dV = 0\,, \end{aligned} \tag{60}$$

wherein the second to last term in Eq. 60 can be split into two terms, similar to the procedure in the balance of momentum of the mixture, as follows:

$$\begin{aligned}\mathcal{I}(u_i, u_{i(\mathrm{f})}, p_\mathrm{f}, w_i^{u_\mathrm{f}}) = &\int_{\mathcal{B}_0} w_i^{u_\mathrm{f}} \rho_0^\mathrm{f} a_{i(\mathrm{f})}\, dV + \int_{\mathcal{B}_0} w_i^{u_\mathrm{f}} J n^\mathrm{f} \frac{\partial p_\mathrm{f}}{\partial X_I} F_{Ii}^{-1}\, dV \\ &+ \int_{\mathcal{B}_0} w_i^{u_\mathrm{f}} J \frac{\left(n^\mathrm{f}\right)^2}{\hat{k}} (v_{i(\mathrm{f})} - v_i)\, dV \\ &+ \int_{\mathcal{B}_0} \frac{\partial w_i^{u_\mathrm{f}}}{\partial X_I} P_{iI(E)}^\mathrm{f}\, dV - \int_{\Gamma_0} w_i^{u_\mathrm{f}} t_i^{\sigma_E^\mathrm{f}}\, dA \\ &- \int_{\mathcal{B}_0} w_i^{u_\mathrm{f}} \rho_0^\mathrm{f} g_i\, dV = 0\,. \end{aligned} \tag{61}$$

However, doing so creates an additional complexity, namely that now $t_i^{\sigma_E^\mathrm{f}}$ must be determined. In Vuong et al.,[32,33] such a traction is merely a stress balance between solid and fluid phases, and does not take into account an external load as implied here. There are at least two ways in which one might approximate the viscous traction.

The first follows from analysis by Heider[43] for a nearly inviscid pore fluid. It involves applying traction to the solid and fluid phases *separately*, which thus necessitates an equation that solves balance of linear momentum of the solid phase, rather than an equation that solves the balance of linear momentum of the mixture. Supposing then that the total traction

$$\boldsymbol{t}^\sigma = \underbrace{\boldsymbol{t}^{\sigma^\mathrm{s}}}_{\text{applied to solid mom. bal.}} + \underbrace{\boldsymbol{t}^{\sigma^\mathrm{f}}}_{\text{applied to fluid mom. bal.}} \tag{62}$$

is specified (e.g., from known data), one may deduce the viscous traction component $\boldsymbol{t}^{\sigma^{\mathrm{f}}_E}$ via an implicit solve using the solutions $\boldsymbol{u}$ and p_{f}, that is,

$$\boldsymbol{t}^{\sigma^{\mathrm{f}}} = \boldsymbol{t}^{\sigma} - \boldsymbol{t}^{\sigma^{\mathrm{s}}} \Rightarrow \boldsymbol{t}^{\sigma^{\mathrm{f}}_E}(\boldsymbol{u}, p_{\mathrm{f}}) = \boldsymbol{t}^{\sigma} - (\boldsymbol{\sigma}^{\mathrm{s}}_E - n^{\mathrm{s}} p_{\mathrm{f}} \mathbf{1}) \cdot \boldsymbol{n} + n^{\mathrm{f}} p_{\mathrm{f}} \boldsymbol{n}\,, \tag{63}$$

where $\boldsymbol{\sigma}^{\mathrm{s}}_E, n^{\mathrm{s}}, n^{\mathrm{f}}$ are functions of solid displacement $\boldsymbol{u}$. Heider[43] observed inaccurate pore fluid pressure solutions with such a scheme for low permeabilities, small strain theory and low-strain-rate loadings, unless additional stabilization parameters were provided. Given difficulties obtaining stable solutions at finite strain for high-strain-rate loadings,[28,29] it is outside the current scope to pursue such a method.

The other approach would be to use the mixture linear momentum balance equation, and approximate the value of $\boldsymbol{t}^{\sigma^{\mathrm{f}}_E}$ using the interpolated values of porosity and pore fluid velocity gradient at the Gauss point closest to the boundary where $\boldsymbol{t}^{\sigma^{\mathrm{f}}_E}$ is applied. However, this would be inconsistent with how the total traction is applied to the mixture in the balance of linear momentum of the mixture; there, no such approximations are used for $\boldsymbol{t}^{\sigma^{\mathrm{f}}_E}$, nor $\boldsymbol{t}^{\sigma^{\mathrm{s}}_E}$ nor the pore fluid pressure component.

The most consistent assumption, in contrast to the previous two cumbersome alternatives, is to not weaken the divergence of the pore fluid extra stress term, in other words, to use Eq. 60. We have already established in Section 2 that the pore fluid velocity cannot be weakened in the balance of mass of the mixture equations; therefore, requiring C^1 continuity in the balance of linear momentum of the pore fluid raises no issues, and alleviates the problem of specifying the "viscous traction" term.

For notational simplicity, we will denote the separate terms in Eq. 60 as

$$\mathcal{I} = \mathcal{I}^{\mathrm{INT}}_1 + \mathcal{I}^{\mathrm{INT}}_2 + \mathcal{I}^{\mathrm{INT}}_3 + \mathcal{I}^{\mathrm{INT}}_4 + \mathcal{I}^{\mathrm{INT}}_5 = 0\,, \tag{64}$$

where

$$
\begin{aligned}
\mathcal{I}_1^{\text{INT}} &= \int_{\mathcal{B}_0} w_i^{u_{\text{f}}} \rho_0^{\text{f}} a_{i(\text{f})} \, dV \,, \\
\mathcal{I}_2^{\text{INT}} &= \int_{\mathcal{B}_0} w_i^{u_{\text{f}}} J n^{\text{f}} \frac{\partial p_{\text{f}}}{\partial X_I} F_{Ii}^{-1} \, dV \,, \\
\mathcal{I}_3^{\text{INT}} &= \int_{\mathcal{B}_0} w_i^{u_{\text{f}}} J \frac{(n^{\text{f}})^2}{\hat{k}} (v_{i(\text{f})} - v_i) \, dV \,, \\
\mathcal{I}_4^{\text{INT}} &= -\int_{\mathcal{B}_0} w_i^{u_{\text{f}}} \rho_0^{\text{f}} g_i \, dV \,, \\
\mathcal{I}_5^{\text{INT}} &= -\int_{\mathcal{B}_0} w_i^{u_{\text{f}}} \frac{\partial P_{iI(E)}^{\text{f}}}{\partial X_I} dV \,.
\end{aligned}
\tag{65}
$$

The 1-D reduction of Eq. 65 is

$$
\begin{aligned}
\mathcal{I}_1^{\text{INT}} &= \int_0^{X=H} w^{u_{\text{f}}} \rho_0^{\text{f}} a_{\text{f}} A \, dX \,, \\
\mathcal{I}_2^{\text{INT}} &= \int_0^{X=H} w^{u_{\text{f}}} n^{\text{f}} \frac{\partial p_{\text{f}}}{\partial X} A \, dX \,, \\
\mathcal{I}_3^{\text{INT}} &= \int_0^{X=H} w^{u_{\text{f}}} J \frac{(n^{\text{f}})^2}{\hat{k}} (v_{\text{f}} - v) A \, dX \,, \\
\mathcal{I}_4^{\text{INT}} &= \int_0^{X=H} w^{u_{\text{f}}} \rho_0^{\text{f}} g A \, dX \,, \\
\mathcal{I}_5^{\text{INT}} &= -\int_0^{X=H} w^{u_{\text{f}}} \frac{\partial P_{11(E)}^{\text{f}}}{\partial X} A \, dX \,.
\end{aligned}
\tag{66}
$$

3.3 FE Implementation

The FE implementation follows from Irwin et al.,[29,30] though in the present work we invoke the Q3H-Q3H-P1 element as discussed in Section 2 to be able to handle second-order spatial derivatives of solid and fluid displacements. In other words, the Hermite cubic polynomials are used to interpolate solid skeleton and pore fluid displacement and their associated gradients, and linear shape functions are used to interpolate pore fluid pressure and associated gradients.

For our solution variables of interest (i.e., u, u_{f}, and p_{f}) we introduce the corresponding discretizations $\boldsymbol{d}$, $\boldsymbol{d}_{\mathrm{f}}$, and $\boldsymbol{\pi}$, respectively. For solid skeleton displacement $\boldsymbol{d}$, we have

$$u^{h^e}(\xi,t) = \sum_{a=1}^{n_{\mathrm{dof}}^{s,e}} N_a^u(\xi) d_a^e(t) = \underbrace{\left\{\boldsymbol{N}^{e,u}\right\}}_{1\times n_{\mathrm{dof}}^{s,e}} \cdot \underbrace{\left\{\boldsymbol{d}^e\right\}}_{n_{\mathrm{dof}}^{s,e}\times 1}, \tag{67}$$

where for the Q3H-Q3H-P1 element $n_{\mathrm{dof}}^{s,e} := 4$. The solid skeleton velocity and acceleration are defined similarly:

$$\begin{aligned} v^{h^e}(\xi,t) &= \sum_{a=1}^{n_{\mathrm{dof}}^{s,e}} N_a^u(\xi) \dot{d}_a^e(t) = \underbrace{\left\{\boldsymbol{N}^{e,u}\right\}}_{1\times n_{\mathrm{dof}}^{s,e}} \cdot \underbrace{\left\{\dot{\boldsymbol{d}}^e\right\}}_{n_{\mathrm{dof}}^{s,e}\times 1}, \\ a^{h^e}(\xi,t) &= \sum_{a=1}^{n_{\mathrm{dof}}^{s,e}} N_a^u(\xi) \ddot{d}_a^e(t) = \underbrace{\left\{\boldsymbol{N}^{e,u}\right\}}_{1\times n_{\mathrm{dof}}^{s,e}} \cdot \underbrace{\left\{\ddot{\boldsymbol{d}}^e\right\}}_{n_{\mathrm{dof}}^{s,e}\times 1}. \end{aligned} \tag{68}$$

Solid skeleton displacement gradient, velocity gradient, and acceleration gradient

are defined as follows, respectively:

$$\begin{aligned}
\frac{\partial u^{h^e}(\xi,t)}{\partial X} &= \sum_{a=1}^{n_{\text{dof}}^{s,e}} B_a^u(\xi) d_a^e(t) = \underbrace{\left\{\boldsymbol{B}^{e,u}\right\}}_{1\times n_{\text{dof}}^{s,e}} \cdot \underbrace{\left\{\boldsymbol{d}^e\right\}}_{n_{\text{dof}}^{s,e}\times 1}, \\
\frac{\partial v^{h^e}(\xi,t)}{\partial X} &= \sum_{a=1}^{n_{\text{dof}}^{s,e}} B_a^u(\xi) \dot{d}_a^e(t) = \underbrace{\left\{\boldsymbol{B}^{e,u}\right\}}_{1\times n_{\text{dof}}^{s,e}} \cdot \underbrace{\left\{\dot{\boldsymbol{d}}^e\right\}}_{n_{\text{dof}}^{s,e}\times 1}, \\
\frac{\partial a^{h^e}(\xi,t)}{\partial X} &= \sum_{a=1}^{n_{\text{dof}}^{s,e}} B_a^u(\xi) \ddot{d}_a^e(t) = \underbrace{\left\{\boldsymbol{B}^{e,u}\right\}}_{1\times n_{\text{dof}}^{s,e}} \cdot \underbrace{\left\{\ddot{\boldsymbol{d}}^e\right\}}_{n_{\text{dof}}^{s,e}\times 1}.
\end{aligned} \tag{69}$$

Second-order gradients are defined as follows:

$$\begin{aligned}
\frac{\partial^2 u^{h^e}(\xi,t)}{\partial X^2} &= \sum_{a=1}^{n_{\text{dof}}^{s,e}} H_a^u(\xi) d_a^e(t) = \underbrace{\left\{\boldsymbol{H}^{e,u}\right\}}_{1\times n_{\text{dof}}^{s,e}} \cdot \underbrace{\left\{\boldsymbol{d}^e\right\}}_{n_{\text{dof}}^{s,e}\times 1}, \\
\frac{\partial^2 v^{h^e}(\xi,t)}{\partial X^2} &= \sum_{a=1}^{n_{\text{dof}}^{s,e}} H_a^u(\xi) \dot{d}_a^e(t) = \underbrace{\left\{\boldsymbol{H}^{e,u}\right\}}_{1\times n_{\text{dof}}^{s,e}} \cdot \underbrace{\left\{\dot{\boldsymbol{d}}^e\right\}}_{n_{\text{dof}}^{s,e}\times 1}, \\
\frac{\partial^2 a^{h^e}(\xi,t)}{\partial X^2} &= \sum_{a=1}^{n_{\text{dof}}^{s,e}} H_a^u(\xi) \ddot{d}_a^e(t) = \underbrace{\left\{\boldsymbol{H}^{e,u}\right\}}_{1\times n_{\text{dof}}^{s,e}} \cdot \underbrace{\left\{\ddot{\boldsymbol{d}}^e\right\}}_{n_{\text{dof}}^{s,e}\times 1}.
\end{aligned} \tag{70}$$

Discretizations of the pore fluid displacement $\boldsymbol{d}_{\text{f}}$ are given as follows, where for the

Q3H-Q3H-P1 element $n_{\text{dof}}^{f,e} := 4$:

$$
\begin{aligned}
u_{\text{f}}^{h^e}(\xi,t) &= \sum_{a=1}^{n_{\text{dof}}^{f,e}} N_a^{u_{\text{f}}}(\xi) d_{a,\text{f}}^e(t) = \underbrace{\left\{\boldsymbol{N}^{e,u_{\text{f}}}\right\}}_{1\times n_{\text{dof}}^{f,e}} \cdot \underbrace{\left\{\boldsymbol{d}_{\text{f}}^e\right\}}_{n_{\text{dof}}^{f,e}\times 1}, \\
v_{\text{f}}^{h^e}(\xi,t) &= \sum_{a=1}^{n_{\text{dof}}^{f,e}} N_a^{u_{\text{f}}}(\xi) \dot{d}_{a,\text{f}}^e(t) = \underbrace{\left\{\boldsymbol{N}^{e,u_{\text{f}}}\right\}}_{1\times n_{\text{dof}}^{f,e}} \cdot \underbrace{\left\{\dot{\boldsymbol{d}}_{\text{f}}^e\right\}}_{n_{\text{dof}}^{s,e}\times 1}, \\
a_{\text{f}}^{h^e}(\xi,t) &= \sum_{a=1}^{n_{\text{dof}}^{f,e}} N_a^{u_{\text{f}}}(\xi) \ddot{d}_{a,\text{f}}^e(t) = \underbrace{\left\{\boldsymbol{N}^{e,u_{\text{f}}}\right\}}_{1\times n_{\text{dof}}^{f,e}} \cdot \underbrace{\left\{\ddot{\boldsymbol{d}}_{\text{f}}^e\right\}}_{n_{\text{dof}}^{f,e}\times 1}, \\
\frac{\partial u_{\text{f}}^{h^e}(\xi,t)}{\partial X} &= \sum_{a=1}^{n_{\text{dof}}^{f,e}} B_a^{u_{\text{f}}}(\xi) d_{a,\text{f}}^e(t) = \underbrace{\left\{\boldsymbol{B}^{e,u_{\text{f}}}\right\}}_{1\times n_{\text{dof}}^{f,e}} \cdot \underbrace{\left\{\boldsymbol{d}_{\text{f}}^e\right\}}_{n_{\text{dof}}^{f,e}\times 1}, \\
\frac{\partial v_{\text{f}}^{h^e}(\xi,t)}{\partial X} &= \sum_{a=1}^{n_{\text{dof}}^{f,e}} B_a^{u_{\text{f}}}(\xi) \dot{d}_{a,\text{f}}^e(t) = \underbrace{\left\{\boldsymbol{B}^{e,u_{\text{f}}}\right\}}_{1\times n_{\text{dof}}^{f,e}} \cdot \underbrace{\left\{\dot{\boldsymbol{d}}_{\text{f}}^e\right\}}_{n_{\text{dof}}^{f,e}\times 1}, \\
\frac{\partial a_{\text{f}}^{h^e}(\xi,t)}{\partial X} &= \sum_{a=1}^{n_{\text{dof}}^{f,e}} B_a^{u_{\text{f}}}(\xi) \ddot{d}_{a,\text{f}}^e(t) = \underbrace{\left\{\boldsymbol{B}^{e,u_{\text{f}}}\right\}}_{1\times n_{\text{dof}}^{f,e}} \cdot \underbrace{\left\{\ddot{\boldsymbol{d}}_{\text{f}}^e\right\}}_{n_{\text{dof}}^{f,e}\times 1}, \\
\frac{\partial^2 u_{\text{f}}^{h^e}(\xi,t)}{\partial X^2} &= \sum_{a=1}^{n_{\text{dof}}^{f,e}} H_a^{u_{\text{f}}}(\xi) d_{a,\text{f}}^e(t) = \underbrace{\left\{\boldsymbol{H}^{e,u_{\text{f}}}\right\}}_{1\times n_{\text{dof}}^{f,e}} \cdot \underbrace{\left\{\boldsymbol{d}_{\text{f}}^e\right\}}_{n_{\text{dof}}^{f,e}\times 1}, \\
\frac{\partial^2 v_{\text{f}}^{h^e}(\xi,t)}{\partial X^2} &= \sum_{a=1}^{n_{\text{dof}}^{f,e}} H_a^{u_{\text{f}}}(\xi) \dot{d}_{a,\text{f}}^e(t) = \underbrace{\left\{\boldsymbol{H}^{e,u_{\text{f}}}\right\}}_{1\times n_{\text{dof}}^{f,e}} \cdot \underbrace{\left\{\dot{\boldsymbol{d}}_{\text{f}}^e\right\}}_{n_{\text{dof}}^{f,e}\times 1}, \\
\frac{\partial^2 a_{\text{f}}^{h^e}(\xi,t)}{\partial X^2} &= \sum_{a=1}^{n_{\text{dof}}^{f,e}} H_a^{u_{\text{f}}}(\xi) \ddot{d}_{a,\text{f}}^e(t) = \underbrace{\left\{\boldsymbol{H}^{e,u_{\text{f}}}\right\}}_{1\times n_{\text{dof}}^{f,e}} \cdot \underbrace{\left\{\ddot{\boldsymbol{d}}_{\text{f}}^e\right\}}_{n_{\text{dof}}^{f,e}\times 1}.
\end{aligned}
\tag{71}
$$

Pore fluid pressure discretizations $\boldsymbol{\pi}$ are given as follows:

$$
\begin{aligned}
p_{\mathrm{f}}^{h^e}(\xi,t) &= \sum_{a=1}^{n_{\mathrm{dof}}^{p_{\mathrm{f}},e}} N_a^{p_{\mathrm{f}}}(\xi)\pi_a^e(t) = \underbrace{\left\{\boldsymbol{N}^{e,p_{\mathrm{f}}}\right\}}_{1\times n_{\mathrm{dof}}^{p_{\mathrm{f}},e}} \cdot \underbrace{\left\{\boldsymbol{\pi}^e\right\}}_{n_{\mathrm{dof}}^{p_{\mathrm{f}},e}\times 1}, \\
\dot{p}_{\mathrm{f}}^{h^e}(\xi,t) &= \sum_{a=1}^{n_{\mathrm{dof}}^{p_{\mathrm{f}},e}} N_a^{p_{\mathrm{f}}}(\xi)\dot{\pi}_{\mathrm{f}}^e(t) = \underbrace{\left\{\boldsymbol{N}^{e,p_{\mathrm{f}}}\right\}}_{1\times n_{\mathrm{dof}}^{p_{\mathrm{f}},e}} \cdot \underbrace{\left\{\dot{\boldsymbol{\pi}}^e\right\}}_{n_{\mathrm{dof}}^{p_{\mathrm{f}},e}\times 1}, \\
\ddot{p}_{\mathrm{f}}^{h^e}(\xi,t) &= \sum_{a=1}^{n_{\mathrm{dof}}^{p_{\mathrm{f}},e}} N_a^{p_{\mathrm{f}}}(\xi)\ddot{\pi}_{\mathrm{f}}^e(t) = \underbrace{\left\{\boldsymbol{N}^{e,p_{\mathrm{f}}}\right\}}_{1\times n_{\mathrm{dof}}^{p_{\mathrm{f}},e}} \cdot \underbrace{\left\{\ddot{\boldsymbol{\pi}}^e\right\}}_{n_{\mathrm{dof}}^{p_{\mathrm{f}},e}\times 1}, \\
\frac{\partial p_{\mathrm{f}}^{h^e}(\xi,t)}{\partial X} &= \sum_{a=1}^{n_{\mathrm{dof}}^{p_{\mathrm{f}},e}} B_a^{p_{\mathrm{f}}}(\xi)\pi_a^e(t) = \underbrace{\left\{\boldsymbol{B}^{e,p_{\mathrm{f}}}\right\}}_{1\times n_{\mathrm{dof}}^{p_{\mathrm{f}},e}} \cdot \underbrace{\left\{\boldsymbol{\pi}^e\right\}}_{n_{\mathrm{dof}}^{p_{\mathrm{f}},e}\times 1}, \\
\frac{\partial \dot{p}_{\mathrm{f}}^{h^e}(\xi,t)}{\partial X} &= \sum_{a=1}^{n_{\mathrm{dof}}^{p_{\mathrm{f}},e}} B_a^{p_{\mathrm{f}}}(\xi)\dot{\pi}_{\mathrm{f}}^e(t) = \underbrace{\left\{\boldsymbol{B}^{e,p_{\mathrm{f}}}\right\}}_{1\times n_{\mathrm{dof}}^{p_{\mathrm{f}},e}} \cdot \underbrace{\left\{\dot{\boldsymbol{\pi}}^e\right\}}_{n_{\mathrm{dof}}^{p_{\mathrm{f}},e}\times 1}, \\
\frac{\partial \ddot{p}_{\mathrm{f}}^{h^e}(\xi,t)}{\partial X} &= \sum_{a=1}^{n_{\mathrm{dof}}^{p_{\mathrm{f}},e}} B_a^{p_{\mathrm{f}}}(\xi)\ddot{\pi}_{\mathrm{f}}^e(t) = \underbrace{\left\{\boldsymbol{B}^{e,p_{\mathrm{f}}}\right\}}_{1\times n_{\mathrm{dof}}^{p_{\mathrm{f}},e}} \cdot \underbrace{\left\{\ddot{\boldsymbol{\pi}}^e\right\}}_{n_{\mathrm{dof}}^{p_{\mathrm{f}},e}\times 1}.
\end{aligned}
\tag{72}
$$

The weighting functions for solid skeleton displacement $\boldsymbol{d}$ and their interpolations (including gradients) are given as follows:

$$
\begin{aligned}
w^{u^{h^e}}(\xi) &= \underbrace{\left\{\boldsymbol{N}^{e,u}\right\}}_{1\times n_{\mathrm{dof}}^{s,e}} \cdot \underbrace{\left\{\boldsymbol{c}^{u,e}\right\}}_{n_{\mathrm{dof}}^{s,e}\times 1} = \underbrace{\left\{\boldsymbol{c}^{u,e}\right\}^T}_{1\times n_{\mathrm{dof}}^{s,e}} \cdot \underbrace{\left\{\boldsymbol{N}^{e,u}\right\}^T}_{n_{\mathrm{dof}}^{s,e}\times 1}, \\
\frac{\partial w^{u^{h^e}}(\xi,t)}{\partial X} &= \underbrace{\left\{\boldsymbol{B}^{e,u}\right\}}_{1\times n_{\mathrm{dof}}^{s,e}} \cdot \underbrace{\left\{\boldsymbol{c}^{u,e}\right\}}_{n_{\mathrm{dof}}^{s,e}\times 1} = \underbrace{\left\{\boldsymbol{c}^{u,e}\right\}^T}_{1\times n_{\mathrm{dof}}^{s,e}} \cdot \underbrace{\left\{\boldsymbol{B}^{e,u}\right\}^T}_{n_{\mathrm{dof}}^{s,e}\times 1}, \\
\frac{\partial^2 w^{u^{h^e}}(\xi,t)}{\partial X^2} &= \underbrace{\left\{\boldsymbol{H}^{e,u}\right\}}_{1\times n_{\mathrm{dof}}^{s,e}} \cdot \underbrace{\left\{\boldsymbol{c}^{u,e}\right\}}_{n_{\mathrm{dof}}^{s,e}\times 1} = \underbrace{\left\{\boldsymbol{c}^{u,e}\right\}^T}_{1\times n_{\mathrm{dof}}^{s,e}} \cdot \underbrace{\left\{\boldsymbol{H}^{e,u}\right\}^T}_{n_{\mathrm{dof}}^{s,e}\times 1}.
\end{aligned}
\tag{73}
$$

The weighting functions for pore fluid displacement $\boldsymbol{d}_{\mathrm{f}}$ and their interpolations (in-

cluding gradients) are given as follows:

$$
\begin{aligned}
w^{u_{\mathrm{f}}^{h^e}}(\xi) &= \underbrace{\left\{\boldsymbol{N}^{e,u_{\mathrm{f}}}\right\}}_{1\times n_{\mathrm{dof}}^{f,e}} \cdot \underbrace{\left\{\boldsymbol{c}^{u_{\mathrm{f}},e}\right\}}_{n_{\mathrm{dof}}^{f,e}\times 1} = \underbrace{\left\{\boldsymbol{c}^{u_{\mathrm{f}},e}\right\}^T}_{1\times n_{\mathrm{dof}}^{f,e}} \cdot \underbrace{\left\{\boldsymbol{N}^{e,u_{\mathrm{f}}}\right\}^T}_{n_{\mathrm{dof}}^{f,e}\times 1}, \\
\frac{\partial w^{u_{\mathrm{f}}^{h^e}}(\xi,t)}{\partial X} &= \underbrace{\left\{\boldsymbol{B}^{e,u_{\mathrm{f}}}\right\}}_{1\times n_{\mathrm{dof}}^{f,e}} \cdot \underbrace{\left\{\boldsymbol{c}^{u_{\mathrm{f}},e}\right\}}_{n_{\mathrm{dof}}^{f,e}\times 1} = \underbrace{\left\{\boldsymbol{c}^{u_{\mathrm{f}},e}\right\}^T}_{1\times n_{\mathrm{dof}}^{f,e}} \cdot \underbrace{\left\{\boldsymbol{B}^{e,u_{\mathrm{f}}}\right\}^T}_{n_{\mathrm{dof}}^{f,e}\times 1}, \\
\frac{\partial^2 w^{u_{\mathrm{f}}^{h^e}}(\xi,t)}{\partial X^2} &= \underbrace{\left\{\boldsymbol{H}^{e,u_{\mathrm{f}}}\right\}}_{1\times n_{\mathrm{dof}}^{f,e}} \cdot \underbrace{\left\{\boldsymbol{c}^{u_{\mathrm{f}},e}\right\}}_{n_{\mathrm{dof}}^{f,e}\times 1} = \underbrace{\left\{\boldsymbol{c}^{u_{\mathrm{f}},e}\right\}^T}_{1\times n_{\mathrm{dof}}^{f,e}} \cdot \underbrace{\left\{\boldsymbol{H}^{e,u_{\mathrm{f}}}\right\}^T}_{n_{\mathrm{dof}}^{f,e}\times 1}.
\end{aligned}
\tag{74}
$$

The weighting functions for pore fluid pressure $\boldsymbol{\pi}$ and their interpolations (including gradients) are given as follows:

$$
\begin{aligned}
w^{p_{\mathrm{f}}^{h^e}}(\xi) &= \underbrace{\left\{\boldsymbol{N}^{e,p_{\mathrm{f}}}\right\}}_{1\times n_{\mathrm{dof}}^{p_{\mathrm{f}},e}} \cdot \underbrace{\left\{\boldsymbol{c}^{p_{\mathrm{f}},e}\right\}}_{n_{\mathrm{dof}}^{p_{\mathrm{f}},e}\times 1} = \underbrace{\left\{\boldsymbol{c}^{p_{\mathrm{f}},e}\right\}^T}_{1\times n_{\mathrm{dof}}^{p_{\mathrm{f}},e}} \cdot \underbrace{\left\{\boldsymbol{N}^{e,p_{\mathrm{f}}}\right\}^T}_{n_{\mathrm{dof}}^{p_{\mathrm{f}},e}\times 1}, \\
\frac{\partial w^{p_{\mathrm{f}}^{h^e}}(\xi,t)}{\partial X} &= \underbrace{\left\{\boldsymbol{B}^{e,p_{\mathrm{f}}}\right\}}_{1\times n_{\mathrm{dof}}^{p_{\mathrm{f}},e}} \cdot \underbrace{\left\{\boldsymbol{c}^{p_{\mathrm{f}},e}\right\}}_{n_{\mathrm{dof}}^{p_{\mathrm{f}},e}\times 1} = \underbrace{\left\{\boldsymbol{c}^{p_{\mathrm{f}},e}\right\}^T}_{1\times n_{\mathrm{dof}}^{p_{\mathrm{f}},e}} \cdot \underbrace{\left\{\boldsymbol{B}^{e,p_{\mathrm{f}}}\right\}^T}_{n_{\mathrm{dof}}^{p_{\mathrm{f}},e}\times 1}.
\end{aligned}
\tag{75}
$$

3.4 Numerical Integration

After applying the Galerkin approximation[44] to the coupled variational equations in Section 3 substituting interpolations and their derivatives in Section 3 applying boundary conditions at the nodes, and assembling the FE equations, the general coupled system of matrix-vector equations resembles the following nonlinear form:

$$
\boldsymbol{M}\ddot{\boldsymbol{x}} + \boldsymbol{C}\dot{\boldsymbol{x}} + \boldsymbol{F}^{INT}(\ddot{\boldsymbol{x}}, \boldsymbol{x}) = \boldsymbol{F}^{EXT}\,, \tag{76}
$$

where $\boldsymbol{M}$ is the mass matrix, $\boldsymbol{C}$ is the viscous matrix, $\boldsymbol{F}^{INT}$ is the nonlinear internal "force" vector, and $\boldsymbol{F}^{EXT}$ is the vector of applied external forces and fluxes for the full coupled variational form. Similarly, the accelerations, velocities, and

displacements are given by the global DOF vectors $\ddot{\boldsymbol{x}}$, $\dot{\boldsymbol{x}}$, and $\boldsymbol{x}$, respectively, as

$$\boldsymbol{x} = \begin{Bmatrix} \boldsymbol{d} \\ \boldsymbol{d}_{\mathrm{f}} \\ \boldsymbol{\pi} \end{Bmatrix}, \quad \dot{\boldsymbol{x}} = \begin{Bmatrix} \dot{\boldsymbol{d}} \\ \dot{\boldsymbol{d}}_{\mathrm{f}} \\ \dot{\boldsymbol{\pi}} \end{Bmatrix}, \quad \ddot{\boldsymbol{x}} = \begin{Bmatrix} \ddot{\boldsymbol{d}} \\ \ddot{\boldsymbol{d}}_{\mathrm{f}} \\ \ddot{\boldsymbol{\pi}} \end{Bmatrix} \tag{77}$$

where $\boldsymbol{d}$, $\boldsymbol{d}_{\mathrm{f}}$, and $\boldsymbol{\pi}$ are the global nodal DOFs of solid skeleton displacement, pore fluid displacement (part of the time integration procedure, not used in any of the balance equations), and pore fluid pressure, respectively.

3.4.1 Newmark-beta Integrators

For the dynamic equations that retain inertia terms, we apply the Newmark-beta (NB) method[44,45] and a nonlinear solver (Newton-Raphson method; for details, refer to Irwin et al.[30]) for solving Eq. 76 wherein

$$\begin{aligned} &\boldsymbol{M}\ddot{\boldsymbol{x}}_{n+1} + \boldsymbol{C}\dot{\boldsymbol{x}}_{n+1} + \boldsymbol{F}^{\mathrm{INT}}(\ddot{\boldsymbol{x}}_{n+1}, \boldsymbol{x}_{n+1}) = \boldsymbol{F}^{\mathrm{EXT}}_{n+1}\,, \\ &\boldsymbol{x}_{n+1} = \boldsymbol{x}_n + \Delta t\dot{\boldsymbol{x}}_n + \frac{(\Delta t)^2}{2}\left[(1-2\beta)\,\ddot{\boldsymbol{x}}_n + 2\beta\ddot{\boldsymbol{x}}_{n+1}\right]\,, \\ &\dot{\boldsymbol{x}}_{n+1} = \dot{\boldsymbol{x}}_n + \Delta t\left[(1-\gamma)\,\ddot{\boldsymbol{x}}_n + \gamma\ddot{\boldsymbol{x}}_{n+1}\right]\,. \end{aligned} \tag{78}$$

Here $(\bullet)_{n+1}$ implies a quantity to be solved or updated at current time t_{n+1}, $(\bullet)_n$ implies a quantity known at previous time t_n, β and γ are integration parameters, and the time increment $\Delta t = t_{n+1} - t_n$ may be variable or held constant during the time marching solution.

The predictors are written as

$$\begin{aligned} \tilde{\boldsymbol{x}}_{n+1} &= \boldsymbol{x}_n + \Delta t\dot{\boldsymbol{x}}_n + \frac{(\Delta t)^2}{2}\,(1-2\beta)\,\ddot{\boldsymbol{x}}_n\,, \\ \dot{\tilde{\boldsymbol{x}}}_{n+1} &= \dot{\boldsymbol{x}}_n + \Delta t\,(1-\gamma)\,\ddot{\boldsymbol{x}}_n\,, \end{aligned} \tag{79}$$

such that the correctors are

$$\begin{aligned} \boldsymbol{x}_{n+1} &= \tilde{\boldsymbol{x}}_{n+1} + \beta(\Delta t)^2\ddot{\boldsymbol{x}}_{n+1}\,, \\ \dot{\boldsymbol{x}}_{n+1} &= \dot{\tilde{\boldsymbol{x}}}_{n+1} + \gamma\Delta t\ddot{\boldsymbol{x}}_{n+1}\,. \end{aligned} \tag{80}$$

Writing in residual form for solution via the Newton-Raphson method, this allows

us to solve for the accelerations $\ddot{\boldsymbol{x}}_{n+1}$ at the next time step t_{n+1} as follows:

$$\boldsymbol{R}(\ddot{\boldsymbol{x}}_{n+1}) = \boldsymbol{M}\ddot{\boldsymbol{x}}_{n+1} + \boldsymbol{C}\dot{\boldsymbol{x}}_{n+1} + \boldsymbol{F}^{\text{INT}}(\ddot{\boldsymbol{x}}_{n+1}, \boldsymbol{x}_{n+1}) - \boldsymbol{F}^{\text{EXT}}_{n+1} = \boldsymbol{0} \tag{81}$$

In Eq. 81, the internal forces are nonlinear, therefore requiring us to employ a nonlinear solver (e.g., the Newton-Raphson method).

With the linearized equations, we can construct the coupled linear equations to solve at each current iteration $k+1$ as

$$\underbrace{\begin{bmatrix} \boldsymbol{K}_{u,u} & \boldsymbol{K}_{u,u_{\text{f}}} & \boldsymbol{K}_{u,p_{\text{f}}} \\ \boldsymbol{K}_{u_{\text{f}},u} & \boldsymbol{K}_{u_{\text{f}},u_{\text{f}}} & \boldsymbol{K}_{u_{\text{f}},p_{\text{f}}} \\ \boldsymbol{K}_{p_{\text{f}},u} & \boldsymbol{K}_{p_{\text{f}},u_{\text{f}}} & \boldsymbol{K}_{p_{\text{f}},p_{\text{f}}} \end{bmatrix}^{k}}_{(n^s_{\text{dof}}+n^f_{\text{dof}}+n^{p_{\text{f}}}_{\text{dof}})\times(n^s_{\text{dof}}+n^f_{\text{dof}}+n^{p_{\text{f}}}_{\text{dof}})} \cdot \underbrace{\begin{Bmatrix} \delta\ddot{\boldsymbol{d}} \\ \delta\ddot{\boldsymbol{d}}_{\text{f}} \\ \delta\ddot{\boldsymbol{\pi}} \end{Bmatrix}}_{(n^s_{\text{dof}}+n^f_{\text{dof}}+n^{p_{\text{f}}}_{\text{dof}})\times 1} = \underbrace{\begin{Bmatrix} -\boldsymbol{R}_u \\ -\boldsymbol{R}_{u_{\text{f}}} \\ -\boldsymbol{R}_{p_{\text{f}}} \end{Bmatrix}^{k}}_{(n^s_{\text{dof}}+n^f_{\text{dof}}+n^{p_{\text{f}}}_{\text{dof}})\times 1} \tag{82}$$

The "stiffness" matrices in Eq. 82 remain mostly unchanged from those given in Irwin et al.[29,30] Minor differences arise with the inclusion of the pore fluid extra stress. Specifically, variations of the pore fluid extra stress tensor and the divergence of the pore fluid extra stress tensor contribute to block matrices $\boldsymbol{K}_{u,u}, \boldsymbol{K}_{u,u_{\text{f}}}, \boldsymbol{K}_{u_{\text{f}},u}$, $\boldsymbol{K}_{u_{\text{f}},u_{\text{f}}}, \boldsymbol{K}_{p_{\text{f}},u}, \boldsymbol{K}_{p_{\text{f}},u_{\text{f}}}$. The derivation of the Gateaux derivative of the pore fluid extra stress tensor, which contributes to block matrices $\boldsymbol{K}_{u,u}, \boldsymbol{K}_{u,u_{\text{f}}}$, proceeds as follows:

$$\delta(\sigma^{\text{f}}_{11(E)}) = \delta\left(n^{\text{f}}\frac{\partial v_{\text{f}}}{\partial X}\right)(\kappa_{\text{f}} + 2\eta_{\text{f}}) = \left(\frac{n^{\text{s}}}{J}\big(\beta\Delta t^2\big)\frac{\partial(\delta a)}{\partial X} + n^{\text{f}}(\gamma\Delta t)\frac{\partial(\delta a_{\text{f}})}{\partial X}\right)(\kappa_{\text{f}} + 2\eta_{\text{f}})\,, \tag{83}$$

where we assume pore fluid bulk viscosity κ_{f} and pore fluid shear viscosity η_{f} are not functions of the independent variables $u, u_{\text{f}}, p_{\text{f}}$. Thus, $\delta\mathcal{G}^{\text{INT}}_5$ is

$$\delta\mathcal{G}^{\text{INT}}_5 = \int_0^{X=H} \frac{\partial w^u}{\partial X}\left(\frac{n^{\text{s}}}{J}\big(\beta\Delta t^2\big)\frac{\partial(\delta a)}{\partial X} + n^{\text{f}}(\gamma\Delta t)\frac{\partial(\delta a_{\text{f}})}{\partial X}\right)(\kappa_{\text{f}} + 2\eta_{\text{f}})A\,dX\ . \tag{84}$$

Divergence of the pore fluid extra stress tensor simplifies to the following with the 1-D uniaxial strain assumption:

$$\left[\frac{\partial n^{\text{f}}}{\partial X}\frac{\partial v_{\text{f}}}{\partial X} + n^{\text{f}}\frac{\partial^2 v_{\text{f}}}{\partial X^2}\right](\kappa_{\text{f}} + 2\eta_{\text{f}})F_{11}^{-2}\,. \tag{85}$$

The Gateaux derivatives of new variables are given as follows:

$$
\begin{aligned}
\delta\Big(\frac{\partial n^{\mathrm{f}}}{\partial X}\Big) &= \delta\Big(n^{\mathrm{s}}\frac{\partial^2 u}{\partial X^2}F_{11}^{-2}\Big) \\
&= \big(\beta\Delta t^2\big)\left(-\frac{n^{\mathrm{s}}}{J}\frac{\partial^2 u}{\partial X^2}F_{11}^{-2}\frac{\partial(\delta a)}{\partial X} + n^{\mathrm{s}}F_{11}^{-2}\frac{\partial^2(\delta a)}{\partial X^2} - 2\frac{n^{\mathrm{s}}}{J}F_{11}^{-2}\frac{\partial^2 u}{\partial X^2}\frac{\partial(\delta a)}{\partial X}\right) \\
&= \big(\beta\Delta t^2\big)\left(n^{\mathrm{s}}F_{11}^{-2}\frac{\partial^2(\delta a)}{\partial X} - \frac{3}{J}\frac{\partial n^{\mathrm{f}}}{\partial X}\frac{\partial(\delta a)}{\partial X}\right), \\
\delta\Big(\frac{\partial v_{\mathrm{f}}}{\partial X}\Big) &= (\gamma\Delta t)\frac{\partial(\delta a_{\mathrm{f}})}{\partial X}\,, \\
\delta\Big(\frac{\partial^2 v_{\mathrm{f}}}{\partial X^2}\Big) &= (\gamma\Delta t)\frac{\partial^2(\delta a_{\mathrm{f}})}{\partial X^2}\,.
\end{aligned}
\tag{86}
$$

Thus, the variation of the divergence of the pore fluid extra stress term, which contributes to block matrices $\boldsymbol{K}_{u_{\mathrm{f}},u}$, $\boldsymbol{K}_{u_{\mathrm{f}},u_{\mathrm{f}}}$, is

$$
\begin{aligned}
\delta\left(\frac{\partial\sigma^{\mathrm{f}}_{11(E)}}{\partial X}\right) = (\kappa_{\mathrm{f}}+2\eta_{\mathrm{f}})\Bigg(&\left[(n^{\mathrm{s}}-n^{\mathrm{f}})\frac{\partial^2 v_{\mathrm{f}}}{\partial X^2} - 4\frac{\partial n^{\mathrm{f}}}{\partial X}\frac{\partial v_{\mathrm{f}}}{\partial X}\right]F_{11}^{-2}\big(\beta\Delta t^2\big)\frac{\partial(\delta a)}{\partial X} \\
&+ (\gamma\Delta t)F_{11}^{-1}\left[\frac{\partial n^{\mathrm{f}}}{\partial X}\frac{\partial(\delta a_{\mathrm{f}})}{\partial X} + n^{\mathrm{f}}\frac{\partial^2(\delta a_{\mathrm{f}})}{\partial X^2}\right]\Bigg)\,.
\end{aligned}
\tag{87}
$$

With that, $\delta\mathcal{I}_5^{\mathrm{INT}}$ is

$$
\begin{aligned}
\delta\mathcal{I}_5^{\mathrm{INT}} = \int_0^{X=H} w^{u_{\mathrm{f}}}(\kappa_{\mathrm{f}}+2\eta_{\mathrm{f}})\Bigg(&\left[(n^{\mathrm{s}}-n^{\mathrm{f}})\frac{\partial^2 v_{\mathrm{f}}}{\partial X^2} - 4\frac{\partial n^{\mathrm{f}}}{\partial X}\frac{\partial v_{\mathrm{f}}}{\partial X}\right]F_{11}^{-2}\big(\beta\Delta t^2\big)\frac{\partial(\delta a)}{\partial X} \\
&+ (\gamma\Delta t)F_{11}^{-1}\left[\frac{\partial n^{\mathrm{f}}}{\partial X}\frac{\partial(\delta a_{\mathrm{f}})}{\partial X} + n^{\mathrm{f}}\frac{\partial^2(\delta a_{\mathrm{f}})}{\partial X^2}\right]\Bigg)A\,dX\,.
\end{aligned}
\tag{88}
$$

The Gateaux derivative of the divergence of the pore fluid extra stress term that is scaled by porosity, hydraulic conductivity, and inverse deformation gradient, is used

in variation of $\mathcal{H}_2^{\text{INT}}$, $\mathcal{H}_5^{\text{INT}}$, and is given by

$$\delta\left(\frac{\hat{k}}{n^{\text{f}}}\frac{\partial\sigma^{\text{f}}_{11(E)}}{\partial X}F_{11}^{-1}\right) = \left(\frac{\hat{k}}{n^{\text{f}}}F_{11}^{-2}\left[\frac{\partial\sigma^{\text{f}}_{11(E)}}{\partial X}\left(n^{\text{s}}\left[\left(\frac{3}{n^{\text{f}}}-\frac{2n^{\text{f}}}{1-(n^{\text{f}})^2}\right)-\frac{1}{n^{\text{f}}}\right]-2\right)\right.\right.$$
$$\left.\left.+(\kappa_{\text{f}}+2\eta_{\text{f}})\left[\frac{n^{\text{s}}}{J}\frac{\partial^2 v_{\text{f}}}{\partial X^2}-\frac{3}{J}\frac{\partial n^{\text{f}}}{\partial X}\frac{\partial v_{\text{f}}}{\partial X}\right]\right)\big(\beta\Delta t^2\big)\frac{\partial(\delta a)}{\partial X}$$
$$+\frac{\hat{k}}{n^{\text{f}}}\frac{n^{\text{s}}}{J}\frac{\partial v_{\text{f}}}{\partial X}F_{11}^{-3}(\kappa_{\text{f}}+2\eta_{\text{f}})\big(\beta\Delta t^2\big)\frac{\partial^2(\delta a)}{\partial X^2}$$
$$+\frac{\hat{k}}{n^{\text{f}}}F_{11}^{-2}(\gamma\Delta t)\left(\frac{\partial n^{\text{f}}}{\partial X}\frac{\partial(\delta a_{\text{f}})}{\partial X}+n^{\text{f}}\frac{\partial^2(\delta a_{\text{f}})}{\partial X^2}\right) \tag{89}$$

Thus, δH_2^{INT} becomes

$$\delta\mathcal{H}_2^{\text{INT}} = \int_0^{X=H} w^{p_{\text{f}}}\left(\left[\big(n^{\text{f}}\tilde{v}_{\text{f}}\big)-\hat{k}\frac{\partial p_{\text{f}}}{\partial X}\right]\big(\beta\Delta t^2\big)\frac{\partial(\delta\ddot{p}_{\text{f}})}{\partial X}-\hat{k}\frac{\partial p_{\text{f}}}{\partial X}(a_{\text{f}}+g)\frac{\rho^{\text{fR}}}{K_{\text{f}}^{\eta}}\right.$$
$$\times\big(\beta\Delta t^2\big)\delta\ddot{p}_{\text{f}}+\frac{\partial p_{\text{f}}}{\partial X}\left[\frac{n^{\text{s}}}{J}\left(\frac{3}{n^{\text{f}}}-\frac{2n^{\text{f}}}{1-(n^{\text{f}})^2}\right)\big(n^{\text{f}}\tilde{v}_{\text{f}}\big)+\hat{k}\frac{\partial p_{\text{f}}}{\partial X}F_{11}^{-2}\right.$$
$$+\frac{\hat{k}}{n^{\text{f}}}F_{11}^{-2}\left(\frac{\partial\sigma^{\text{f}}_{11(E)}}{\partial X}\left[n^{\text{s}}\left(\left[\frac{3}{n^{\text{f}}}-\frac{2n^{\text{f}}}{1-(n^{\text{f}})^2}\right]-\frac{1}{n^{\text{f}}}\right)-2\right]\right.$$
$$\left.\left.+(\kappa_{\text{f}}+2\eta_{\text{f}})\left(\frac{n^{\text{s}}}{J}\frac{\partial^2 v_{\text{f}}}{\partial X^2}-\frac{3}{J}\frac{\partial n^{\text{f}}}{\partial X}\frac{\partial v_{\text{f}}}{\partial X}\right)\right]\big(\beta\Delta t^2\big)\frac{\partial(\delta a)}{\partial X}\right.$$
$$-\frac{\partial p_{\text{f}}}{\partial X}\frac{\hat{k}}{n^{\text{f}}}\frac{n^{\text{s}}}{J}\frac{\partial v_{\text{f}}}{\partial X}F_{11}^{-3}(\kappa_{\text{f}}+2\eta_{\text{f}})\big(\beta\Delta t^2\big)\frac{\partial^2(\delta a)}{\partial X^2}-\frac{\partial p_{\text{f}}}{\partial X}\hat{k}\rho^{\text{fR}}\delta a_{\text{f}}$$
$$\left.\left.-\frac{\partial p_{\text{f}}}{\partial X}\frac{\hat{k}}{n^{\text{f}}}F_{11}^{-2}(\gamma\Delta t)\left[\frac{\partial n^{\text{f}}}{\partial X}\frac{\partial(\delta a_{\text{f}})}{\partial X}+n^{\text{f}}\frac{\partial^2(\delta a_{\text{f}})}{\partial X^2}\right]\right)\frac{A}{K_{\text{f}}^{\eta}}\,dX\ . \tag{90}$$

Next, $\delta\mathcal{H}_5^{\text{INT}}$ is given as

$$\delta\mathcal{H}_5^{\text{INT}} = -\int_0^{X=H} \frac{\partial w^{p_{\text{f}}}}{\partial X}\left(\frac{\hat{k}}{n^{\text{f}}}F_{11}^{-2}\left[\frac{\partial \sigma_{11(E)}^{\text{f}}}{\partial X}\left(n^{\text{s}}\left[\left(\frac{3}{n^{\text{f}}}-\frac{2n^{\text{f}}}{1-(n^{\text{f}})^2}\right)-\frac{1}{n^{\text{f}}}\right]-2\right)\right.\right.$$
$$\left.\left.+(\kappa_{\text{f}}+2\eta_{\text{f}})\left(\frac{n^{\text{s}}}{J}\frac{\partial^2 v_{\text{f}}}{\partial X^2}-\frac{3}{J}\frac{\partial n^{\text{f}}}{\partial X}\frac{\partial v_{\text{f}}}{\partial X}\right)\right](\beta\Delta t^2)\frac{\partial(\delta a)}{\partial X}\right.$$
$$+\frac{\hat{k}}{n^{\text{f}}}\frac{n^{\text{s}}}{J}\frac{\partial v_{\text{f}}}{\partial X}F_{11}^{-3}(\kappa_{\text{f}}+2\eta_{\text{f}})\big(\beta\Delta t^2\big)\frac{\partial^2(\delta a)}{\partial X^2}$$
$$\left.+\frac{\hat{k}}{n^{\text{f}}}F_{11}^{-2}(\gamma\Delta t)\left[\frac{\partial n^{\text{f}}}{\partial X}\frac{\partial(\delta a_{\text{f}})}{\partial X}+n^{\text{f}}\frac{\partial^2(\delta a_{\text{f}})}{\partial X^2}\right]\right)A\,dX\ . \tag{91}$$

Following the procedure described in Irwin et al.,[30] the global residual for the solid skeleton displacement is given by

$$\boldsymbol{c}^{u,T}\cdot\boldsymbol{R}_u = \mathcal{G}^h = \mathcal{G}_1^{\text{INT},h}+\mathcal{G}_2^{\text{INT},h}+\mathcal{G}_3^{\text{INT},h}+\mathcal{G}_4^{\text{INT},h}+\mathcal{G}_5^{\text{INT},h}-\mathcal{G}^{\text{EXT},h}=0\,, \tag{92}$$

which remains unchanged from Irwin et al.,[29,30] with the exception of

$$\mathcal{G}_5^{\text{INT},h} = \mathop{\mathsf{A}}_{e}^{n_e}\underbrace{\left\{\boldsymbol{c}^{u,e}\right\}^T}_{1\times n_{\text{dof}}^{s,e}}\cdot\left(\int_{-1}^{1}\underbrace{\left\{\boldsymbol{B}^{e,u}\right\}^T}_{n_{\text{dof}}^{s,e}\times 1}P_{11(E)}^{\text{f},h^e}Aj^e\,d\xi\right). \tag{93}$$

The global residual for the pore fluid displacement is given by

$$\boldsymbol{c}^{u_{\text{f}},T}\cdot\boldsymbol{R}_{u_{\text{f}}} = \mathcal{I}^h = \mathcal{I}_1^{\text{INT},h}+\mathcal{I}_2^{\text{INT},h}+\mathcal{I}_3^{\text{INT},h}+\mathcal{I}_4^{\text{INT},h}+\mathcal{I}_5^{\text{INT},h}=0\,, \tag{94}$$

which remains unchanged from Irwin et al.,[29,30] with the exception of

$$\mathcal{I}_5^{\text{INT},h} = \mathop{\mathsf{A}}_{e}^{n_e}\underbrace{\left\{\boldsymbol{c}^{u_{\text{f}},e}\right\}^T}_{1\times n_{\text{dof}}^{f,e}}\cdot\left(-\int_{-1}^{1}\underbrace{\left\{\boldsymbol{N}^{e,u_{\text{f}}}\right\}^T}_{n_{\text{dof}}^{f,e}\times 1}\frac{\partial P_{11(E)}^{\text{f},h^e}}{\partial X}Aj^e\,d\xi\right). \tag{95}$$

The global residual for the pore fluid pressure is given by

$$\boldsymbol{c}^{p_\mathrm{f},T}\cdot\boldsymbol{R}_{p_\mathrm{f}}=\mathcal{H}^h=\mathcal{H}_1^{\mathrm{INT},h}+\mathcal{H}_2^{\mathrm{INT},h}+\mathcal{H}_3^{\mathrm{INT},h}+\mathcal{H}_4^{\mathrm{INT},h}+\mathcal{H}_5^{\mathrm{INT},h}-\mathcal{H}_1^{\mathrm{EXT},h}=0\,, \tag{96}$$

which remains unchanged from Irwin et al.,[29,30] with the exception of

$$\begin{aligned}
\mathcal{H}_2^{\mathrm{INT},h}&=\mathop{\mathsf{A}}_{e}^{n_e}\underbrace{\left\{\boldsymbol{c}^{p_\mathrm{f},e}\right\}^T}_{1\times n_{\mathrm{dof}}^{p_\mathrm{f},e}}\cdot\left(\int_{-1}^{1}\underbrace{\left\{\boldsymbol{N}^{e,p_\mathrm{f}}\right\}^T}_{n_{\mathrm{dof}}^{p_\mathrm{f},e}\times 1}\frac{1}{K_\mathrm{f}^\eta}\frac{\partial p_\mathrm{f}^{h^e}}{\partial X}\left(n^\mathrm{f}\tilde{v}_\mathrm{f}\right)^{h^e}Aj^e\,d\xi\right),\\
\mathcal{H}_5^{\mathrm{INT},h}&=\mathop{\mathsf{A}}_{e}^{n_e}\underbrace{\left\{\boldsymbol{c}^{p_\mathrm{f},e}\right\}^T}_{1\times n_{\mathrm{dof}}^{p_\mathrm{f},e}}\cdot\left(-\int_{-1}^{1}\underbrace{\left\{\boldsymbol{B}^{e,p_\mathrm{f}}\right\}^T}_{n_{\mathrm{dof}}^{p_\mathrm{f},e}\times 1}\frac{\hat{k}^{h^e}}{n^{\mathrm{f},h^e}}\frac{\partial\sigma_{11(E)}^{\mathrm{f},h^e}}{\partial X}(F_{11}^{h^e})^{-1}Aj^e\,d\xi\right),
\end{aligned} \tag{97}$$

where the pore fluid extra stress is embedded within the discretized Darcy velocity in $\mathcal{H}_2^{\mathrm{INT},h}$. When pressure stabilization is enabled, an additional term $\mathcal{H}^{\mathrm{stab}}$ is added to the left-hand side of Eq. 96 and is defined as

$$\mathcal{H}^{\mathrm{stab}}=\mathop{\mathsf{A}}_{e}^{n_e}\underbrace{\left\{\boldsymbol{c}^{p_\mathrm{f},e}\right\}^T}_{1\times n_{\mathrm{dof}}^{p_\mathrm{f},e}}\cdot\left(\int_{-1}^{1}\underbrace{\left\{\boldsymbol{B}^{e,p_\mathrm{f}}\right\}^T}_{n_{\mathrm{dof}}^{p_\mathrm{f},e}\times 1}\alpha^{\mathrm{stab}}\frac{\partial p_\mathrm{f}^{h^e}}{\partial X}\left(F_{11}^{h^e}\right)^{-1}Aj^e\,d\xi\right) \tag{98}$$

Recall that the tangent matrix for each iteration must be of the form

$$\mathbf{0}=\boldsymbol{R}^k=\underbrace{\begin{bmatrix}\boldsymbol{K}_{u,u} & \boldsymbol{K}_{u,u_\mathrm{f}} & \boldsymbol{K}_{u,p_\mathrm{f}}\\ \boldsymbol{K}_{u_\mathrm{f},u} & \boldsymbol{K}_{pu_\mathrm{f},u_\mathrm{f}} & \boldsymbol{K}_{u_\mathrm{f},p_\mathrm{f}}\\ \boldsymbol{K}_{p_\mathrm{f},u} & \boldsymbol{K}_{p_\mathrm{f},u_\mathrm{f}} & \boldsymbol{K}_{p_\mathrm{f},p_\mathrm{f}}\end{bmatrix}}_{(n_{\mathrm{dof}}^s+n_{\mathrm{dof}}^f+n_{\mathrm{dof}}^{p_\mathrm{f}})\times(n_{\mathrm{dof}}^s+n_{\mathrm{dof}}^f+n_{\mathrm{dof}}^{p_\mathrm{f}})}\cdot\underbrace{\begin{Bmatrix}\delta\ddot{\boldsymbol{d}}\\ \delta\ddot{\boldsymbol{d}}_\mathrm{f}\\ \delta\ddot{\boldsymbol{\pi}}\end{Bmatrix}}_{(n_{\mathrm{dof}}^s+n_{\mathrm{dof}}^f+n_{\mathrm{dof}}^{p_\mathrm{f}})\times 1} \tag{99}$$

Block stiffness matrices remain unchanged from Irwin et al.,[29,30] with the following

exceptions:

$$
\begin{aligned}
\underbrace{\Big[\boldsymbol{K}_{u,u}\Big]}_{n^s_{\text{dof}}\times n^s_{\text{dof}}} &= \mathop{\mathsf{A}}_{e}^{n_e} \underbrace{\Big\{\boldsymbol{c}^{u,e}\Big\}^T}_{1\times n^{s,e}_{\text{dof}}} \cdot \sum_{i=1,2,5} \underbrace{\Big[\boldsymbol{k}^{\mathcal{G}^{\text{INT}}_i,e}_{u,u}\Big]}_{n^{s,e}_{\text{dof}}\times n^{s,e}_{\text{dof}}}, \\
\underbrace{\Big[\boldsymbol{K}_{u,u_{\text{f}}}\Big]}_{n^s_{\text{dof}}\times n^f_{\text{dof}}} &= \mathop{\mathsf{A}}_{e}^{n_e} \underbrace{\Big\{\boldsymbol{c}^{u,e}\Big\}^T}_{1\times n^{s,e}_{\text{dof}}} \cdot \sum_{i=1,5} \underbrace{\Big[\boldsymbol{k}^{\mathcal{G}^{\text{INT}}_i,e}_{u,u_{\text{f}}}\Big]}_{n^{s,e}_{\text{dof}}\times n^{f,e}_{\text{dof}}}, \\
\underbrace{\Big[\boldsymbol{K}_{u_{\text{f}},u}\Big]}_{n^f_{\text{dof}}\times n^s_{\text{dof}}} &= \mathop{\mathsf{A}}_{e}^{n_e} \underbrace{\Big\{\boldsymbol{c}^{u_{\text{f}},e}\Big\}^T}_{1\times n^{f,e}_{\text{dof}}} \cdot \sum_{i=1}^{5} \underbrace{\Big[\boldsymbol{k}^{\mathcal{I}^{\text{INT}}_i,e}_{u_{\text{f}},u}\Big]}_{n^{f,e}_{\text{dof}}\times n^{s,e}_{\text{dof}}}, \\
\underbrace{\Big[\boldsymbol{K}_{u_{\text{f}},u_{\text{f}}}\Big]}_{n^f_{\text{dof}}\times n^f_{\text{dof}}} &= \mathop{\mathsf{A}}_{e}^{n_e} \underbrace{\Big\{\boldsymbol{c}^{u_{\text{f}},e}\Big\}^T}_{1\times n^{f,e}_{\text{dof}}} \cdot \sum_{i=1,3,5} \underbrace{\Big[\boldsymbol{k}^{\mathcal{I}^{\text{INT}}_i,e}_{u_{\text{f}},u_{\text{f}}}\Big]}_{n^{f,e}_{\text{dof}}\times n^{f,e}_{\text{dof}}}, \\
\underbrace{\Big[\boldsymbol{K}_{p_{\text{f}},u}\Big]}_{n^{p_{\text{f}}}_{\text{dof}}\times n^s_{\text{dof}}} &= \mathop{\mathsf{A}}_{e}^{n_e} \underbrace{\Big\{\boldsymbol{c}^{p_{\text{f}},e}\Big\}^T}_{1\times n^{p_{\text{f}},e}_{\text{dof}}} \cdot \sum_{i=1}^{5} \underbrace{\Big[\boldsymbol{k}^{\mathcal{H}^{\text{INT}}_i,e}_{p_{\text{f}},u}\Big]}_{n^{p_{\text{f}},e}_{\text{dof}}\times n^{s,e}_{\text{dof}}}, \\
\underbrace{\Big[\boldsymbol{K}_{p_{\text{f}},u_{\text{f}}}\Big]}_{n^{p_{\text{f}}}_{\text{dof}}\times n^f_{\text{dof}}} &= \mathop{\mathsf{A}}_{e}^{n_e} \underbrace{\Big\{\boldsymbol{c}^{p_{\text{f}},e}\Big\}^T}_{1\times n^{p_{\text{f}},e}_{\text{dof}}} \cdot \sum_{i=1}^{5} \underbrace{\Big[\boldsymbol{k}^{\mathcal{H}^{\text{INT}}_i,e}_{p_{\text{f}},u_{\text{f}}}\Big]}_{n^{p_{\text{f}},e}_{\text{dof}}\times n^{f,e}_{\text{dof}}}.
\end{aligned}
\tag{100}
$$

Specifically, the following new additions (denoted by $i = 5$ in all of Eq. 100, as well as $i = 2$ in Eq. $100_{5,6}$) are made to account for the pore fluid extra stress:

$$
\begin{aligned}
\underbrace{\Big[\boldsymbol{k}^{\mathcal{G}^{\text{INT}}_5,e}_{u,u}\Big]}_{n^{s,e}_{\text{dof}}\times n^{s,e}_{\text{dof}}} &= \int_{-1}^{1} \frac{\partial v^{h^e}_{\text{f}}}{\partial X}(n^{\text{s},h^e} - n^{\text{f},h^e})(\kappa_{\text{f}} + 2\eta_{\text{f}})\big(F^{h^e}_{11}\big)^{-2}\big(\beta\Delta t^2\big) \underbrace{\Big\{\boldsymbol{B}^{e,u}\Big\}^T}_{n^{s,e}_{\text{dof}}\times 1} \underbrace{\Big\{\boldsymbol{B}^{e,u}\Big\}}_{1\times n^{s,e}_{\text{dof}}} Aj^e\, d\xi\,, \\
\underbrace{\Big[\boldsymbol{k}^{\mathcal{G}^{\text{INT}}_5,e}_{u,u_{\text{f}}}\Big]}_{n^{s,e}_{\text{dof}}\times n^{f,e}_{\text{dof}}} &= \int_{-1}^{1} \frac{n^{\text{f},h^e}}{F^{h^e}_{11}}(\kappa_{\text{f}} + 2\eta_{\text{f}})(\gamma\Delta t) \underbrace{\Big\{\boldsymbol{B}^{e,u}\Big\}^T}_{n^{s,e}_{\text{dof}}\times 1} \underbrace{\Big\{\boldsymbol{B}^{e,u_{\text{f}}}\Big\}}_{1\times n^{f,e}_{\text{dof}}} Aj^e\, d\xi\,, \\
\underbrace{\Big[\boldsymbol{k}^{\mathcal{I}^{\text{INT}}_5,e}_{u_{\text{f}},u}\Big]}_{n^{f,e}_{\text{dof}}\times n^{s,e}_{\text{dof}}} &= -\int_{-1}^{1} \underbrace{\Big\{\boldsymbol{N}^{e,u_{\text{f}}}\Big\}^T}_{n^{f,e}_{\text{dof}}\times 1} \Bigg(\Bigg[(n^{\text{s},h^e} - n^{\text{f},h^e}) \frac{\partial^2 v^{h^e}_{\text{f}}}{\partial X^2} - 4\frac{\partial n^{\text{f},h^e}}{\partial X}\frac{\partial n^{\text{f},h^e}}{\partial X} \Bigg] \underbrace{\Big\{\boldsymbol{B}^{e,u}\Big\}}_{1\times n^{s,e}_{\text{dof}}} \\
&\qquad + \frac{n^{\text{s},h^e}}{J^{h^e}} \frac{\partial v^{h^e}_{\text{f}}}{\partial X} \underbrace{\Big\{\boldsymbol{H}^{e,u}\Big\}}_{1\times n^{s,e}_{\text{dof}}} \Bigg) \big(F^{h^e}_{11}\big)^{-2}(\kappa_{\text{f}} + 2\eta_{\text{f}})\big(\beta\Delta t^2\big) Aj^e\, d\xi\,,
\end{aligned}
$$

$$\underbrace{\left[\boldsymbol{k}^{\mathcal{I}_5^{\mathrm{INT}},e}_{u_{\mathrm{f}},u_{\mathrm{f}}}\right]}_{n^{f,e}_{\mathrm{dof}}\times n^{f,e}_{\mathrm{dof}}} = -\int_{-1}^{1} \underbrace{\left\{\boldsymbol{N}^{e,u_{\mathrm{f}}}\right\}^T}_{n^{f,e}_{\mathrm{dof}}\times 1} \left(\frac{\partial n^{\mathrm{f},h^e}}{\partial X} \underbrace{\left\{\boldsymbol{B}^{e,u_{\mathrm{f}}}\right\}}_{1\times n^{f,e}_{\mathrm{dof}}} + n^{\mathrm{f},h^e} \underbrace{\left\{\boldsymbol{H}^{e,u_{\mathrm{f}}}\right\}}_{1\times n^{f,e}_{\mathrm{dof}}} \right) (\kappa_{\mathrm{f}}+2\eta_{\mathrm{f}}) \left(F_{11}^{h^e}\right)^{-2} (\gamma\Delta t) A j^e \, d\xi \,,$$

$$\begin{aligned}
\underbrace{\left[\boldsymbol{k}^{\mathcal{H}_2^{\mathrm{INT}},e}_{p_{\mathrm{f}},u}\right]}_{n^{p_{\mathrm{f}},e}_{\mathrm{dof}}\times n^{s,e}_{\mathrm{dof}}} = \int_{-1}^{1} \underbrace{\left\{\boldsymbol{N}^{e,p_{\mathrm{f}}}\right\}^T}_{n^{p_{\mathrm{f}},e}_{\mathrm{dof}}\times 1} \Bigg(\Bigg(\Bigg[\frac{3}{n^{\mathrm{f},h^e}} - \frac{2n^{\mathrm{f},h^e}}{1-\left(n^{\mathrm{f},h^e}\right)^2} \Bigg] \left(n^{\mathrm{f}}\tilde{v}_{\mathrm{f}}\right)^{h^e} \frac{n^{\mathrm{s},h^e}}{J^{h^e}} \\
+ \frac{\hat{k}^{h^e}}{n^{\mathrm{f},h^e}} \left(F_{11}^{h^e}\right)^{-2} \Bigg[\frac{\partial \sigma^{\mathrm{f},h^e}_{11(E)}}{\partial X} \Bigg(n^{\mathrm{s},h^e} \Bigg[\Bigg(\frac{3}{n^{\mathrm{f},h^e}} - \frac{2n^{\mathrm{f},h^e}}{1-\left(n^{\mathrm{f},h^e}\right)^2} \Bigg) - \frac{1}{n^{\mathrm{f},h^e}} \Bigg] - 2 \Bigg) \\
+ (\kappa_{\mathrm{f}}+2\eta_{\mathrm{f}}) \Bigg(\frac{n^{\mathrm{s},h^e}}{J^{h^e}} \frac{\partial^2 v_{\mathrm{f}}^{h^e}}{\partial X^2} - \frac{3}{J^{h^e}} \frac{\partial n^{\mathrm{f},h^e}}{\partial X} \frac{\partial v_{\mathrm{f}}^{h^e}}{\partial X} \Bigg) \Bigg] + \hat{k}^{h^e} \frac{\partial p_{\mathrm{f}}^{h^e}}{\partial X} \left[F_{11}^{h^e}\right]^{-2} \Bigg) \underbrace{\left\{\boldsymbol{B}^{e,u}\right\}}_{1\times n^{s,e}_{\mathrm{dof}}} \\
(\kappa_{\mathrm{f}}+2\eta_{\mathrm{f}}) \frac{\hat{k}^{h^e}}{n^{\mathrm{f},h^e}} n^{\mathrm{s},h^e} \frac{\partial v_{\mathrm{f}}^{h^e}}{\partial X} \left(F_{11}^{h^e}\right)^{-4} \underbrace{\left\{\boldsymbol{H}^{e,u}\right\}}_{1\times n^{s,e}_{\mathrm{dof}}} \Bigg] \frac{1}{K_{\mathrm{f}}^{\eta}} \frac{\partial p_{\mathrm{f}}^{h^e}}{\partial X} \left(\beta\Delta t^2\right) A j^e \, d\xi \,,
\end{aligned}$$

$$\begin{aligned}
\underbrace{\left[\boldsymbol{k}^{\mathcal{H}_5^{\mathrm{INT}},e}_{p_{\mathrm{f}},u}\right]}_{n^{p_{\mathrm{f}},e}_{\mathrm{dof}}\times n^{s,e}_{\mathrm{dof}}} = -\int_{-1}^{1} \underbrace{\left\{\boldsymbol{N}^{e,u_{\mathrm{f}}}\right\}^T}_{n^{f,e}_{\mathrm{dof}}\times 1} \Bigg(\Bigg[\frac{\partial \sigma^{\mathrm{f},h^e}_{11(E)}}{\partial X} \Bigg(n^{\mathrm{s},h^e} \Bigg[\Bigg(\frac{3}{n^{\mathrm{f},h^e}} - \frac{2n^{\mathrm{f},h^e}}{1-\left(n^{\mathrm{f},h^e}\right)^2} \Bigg) - \frac{1}{n^{\mathrm{f},h^e}} \Bigg] - 2 \Bigg) \\
+ (\kappa_{\mathrm{f}}+2\eta_{\mathrm{f}}) \Bigg(\frac{n^{\mathrm{s},h^e}}{J^{h^e}} \frac{\partial^2 v_{\mathrm{f}}^{h^e}}{\partial X^2} - \frac{3}{J^{h^e}} \frac{\partial n^{\mathrm{f},h^e}}{\partial X} \frac{\partial v_{\mathrm{f}}^{h^e}}{\partial X} \Bigg) \Bigg] \underbrace{\left\{\boldsymbol{B}^{e,u}\right\}}_{1\times n^{s,e}_{\mathrm{dof}}} \\
+ (\kappa_{\mathrm{f}}+2\eta_{\mathrm{f}}) \frac{n^{\mathrm{s},h^e}}{\left(F_{11}^{h^e}\right)^2} \frac{\partial v_{\mathrm{f}}^{h^e}}{\partial X} \underbrace{\left\{\boldsymbol{H}^{e,u}\right\}}_{1\times n^{s,e}_{\mathrm{dof}}} \Bigg) \frac{\hat{k}^{h^e}}{\left(F_{11}^{h^e}\right)^2} \left(\beta\Delta t^2\right) A j^e \, d\xi \,,
\end{aligned}$$

$$\begin{aligned}
\underbrace{\left[\boldsymbol{k}^{\mathcal{H}_2^{\mathrm{INT}},e}_{p_{\mathrm{f}},u_{\mathrm{f}}}\right]}_{n^{p_{\mathrm{f}},e}_{\mathrm{dof}}\times n^{f,e}_{\mathrm{dof}}} = -\int_{-1}^{1} \underbrace{\left\{\boldsymbol{N}^{e,p_{\mathrm{f}}}\right\}^T}_{n^{p_{\mathrm{f}},e}_{\mathrm{dof}}\times 1} \Bigg(\rho^{\mathrm{fR},h^e} \underbrace{\left\{\boldsymbol{N}^{e,u_{\mathrm{f}}}\right\}}_{1\times n^{f,e}_{\mathrm{dof}}} \\
- (\kappa_{\mathrm{f}}+2\eta_{\mathrm{f}}) (\gamma\Delta t) \left(F_{11}^{h^e}\right)^{-2} \Bigg[\frac{1}{n^{\mathrm{f},h^e}} \frac{\partial n^{\mathrm{f},h^e}}{\partial X} \underbrace{\left\{\boldsymbol{B}^{e,u_{\mathrm{f}}}\right\}}_{1\times n^{f,e}_{\mathrm{dof}}} + \underbrace{\left\{\boldsymbol{H}^{e,u_{\mathrm{f}}}\right\}}_{1\times n^{f,e}_{\mathrm{dof}}} \Bigg] \Bigg) \frac{\partial p_{\mathrm{f}}^{h^e}}{\partial X} \frac{\hat{k}^{h^e}}{K_{\mathrm{f}}^{\eta}} A j^e \,,
\end{aligned}$$

$$\underbrace{\left[\boldsymbol{k}_{p_\mathrm{f},u_\mathrm{f}}^{\mathcal{H}_5^{\mathrm{INT}},e}\right]}_{n_{\mathrm{dof}}^{p_\mathrm{f},e}\times n_{\mathrm{dof}}^{f,e}} = -\int_{-1}^{1} \underbrace{\left\{\boldsymbol{B}^{e,p_\mathrm{f}}\right\}^T}_{n_{\mathrm{dof}}^{p_\mathrm{f},e}\times 1} \left(\frac{1}{n^{\mathrm{f},h^e}} \frac{\partial n^{\mathrm{f},h^e}}{\partial X} \underbrace{\left\{\boldsymbol{B}^{e,u_\mathrm{f}}\right\}}_{1\times n_{\mathrm{dof}}^{f,e}} + \underbrace{\left\{\boldsymbol{H}^{e,u_\mathrm{f}}\right\}}_{1\times n_{\mathrm{dof}}^{f,e}} \right) (\kappa_\mathrm{f} + 2\eta_\mathrm{f}) \frac{\hat{k}^{h^e}}{\left(F_{11}^{h^e}\right)^2} (\gamma\Delta t) A j^e \,. \tag{101}$$

3.4.2 Runge-Kutta Integrators

For explicit time integration of the matrix-vector equations, we apply a generalized adaptive time-stepping Runge-Kutta method (specifically, the Runge-Kutta Cash-Karp scheme,[46] henceforth referred to as "RKFNC") for solving Eq. 76, which involves transforming the second-order ordinary differential equations (ODEs) into first-order ODEs by variable substitution:

$$\boldsymbol{z} \coloneqq \begin{Bmatrix} \boldsymbol{z}_x \\ \boldsymbol{z}_{\dot{x}} \end{Bmatrix} = \begin{Bmatrix} \boldsymbol{x} \\ \dot{\boldsymbol{x}} \end{Bmatrix} , \tag{102}$$

such that

$$\dot{\boldsymbol{z}} = \begin{Bmatrix} \dot{\boldsymbol{z}}_x \\ \dot{\boldsymbol{z}}_{\dot{x}} \end{Bmatrix} = \begin{Bmatrix} \dot{\boldsymbol{x}} \\ \ddot{\boldsymbol{x}} \end{Bmatrix} . \tag{103}$$

For a general nonlinear multi-degree-of-freedom ODE

$$\dot{\boldsymbol{z}} = \boldsymbol{f}(t, \boldsymbol{z}) \,, \tag{104}$$

where $\boldsymbol{f}(t, \boldsymbol{z})$ is in general a nonlinear equation in terms of time t and unknown variable $\boldsymbol{z}$. For a general Runge-Kutta method of m^{th} order, the intermediate stages $\boldsymbol{k}_i$ are defined as follows using standard notation for a Butcher table:

$$\boldsymbol{k}_i = \boldsymbol{f}\left(t_n + c_i \Delta t, \boldsymbol{z}(t_n) + \Delta t \sum_{j=1}^{i-1} a_{ij} \boldsymbol{k}_j \right) . \tag{105}$$

The higher-order solution is given by

$$\boldsymbol{z}^m(t_{n+1}) = \boldsymbol{z}(t_n) + \Delta t \sum_{i=1}^{m+1} b_i^m \boldsymbol{k}_i \,, \tag{106}$$

and the lower-order solution is given by

$$\boldsymbol{z}^{m-1}(t_{n+1}) = \boldsymbol{z}(t_n) + \Delta t \sum_{i=1}^{m} b_i^{m-1} \boldsymbol{k}_i \,, \tag{107}$$

where the b_i^m coefficients are different from the b_i^{m-1} coefficients; refer to the literature[46,47] for specific values. The difference between the higher and lower order solutions allows us to define a truncation error

$$\epsilon_{TE} \coloneqq \left|\left| \boldsymbol{z}^m(t_{n+1}) - \boldsymbol{z}^{m-1}(t_{n+1}) \right|\right|_2 . \tag{108}$$

Note that in comparison to prior work,[28–30] here we define the truncation error with the L_2 norm rather than the L_∞ norm because the former has better performance with the new Q3H-Q3H-P1 element than the latter. The adapted time step Δt^* is typically adjusted as follows:

$$\Delta t^* = \text{SF} \times \left(\frac{\epsilon_a}{\epsilon_{TE}} \right)^{1/(m-1)} \Delta t \,, \tag{109}$$

where SF is a safety factor, typically set to 0.9, and ϵ_a is a user-defined absolute tolerance, typically set to $\epsilon_a \in [10^{-8}, 10^{-2}]$. If the absolute error

$$\left(\frac{\epsilon_{TE}}{\epsilon_a} \right)^{1/(m-1)} < 1 \,, \tag{110}$$

then the solution $\boldsymbol{z}^m$ is accepted with $\Delta t_{n+1} \leftarrow \Delta t^*$. Otherwise, the stages $\boldsymbol{k}_i$ are recomputed at time t_n with $\Delta t_n \leftarrow \Delta t^*$, new solutions are computed, and a new absolute error is computed until the condition defined by Eq. 110 is met.

The Runge-Kutta integrators transform the general solution variables given by Eq. 104 to

$$\left\{ \dot{\boldsymbol{z}} \right\} \coloneqq \begin{Bmatrix} \dot{\boldsymbol{z}}_u \\ \dot{\boldsymbol{z}}_v \\ \dot{\boldsymbol{z}}_{u_\mathrm{f}} \\ \dot{\boldsymbol{z}}_{v_\mathrm{f}} \\ \dot{\boldsymbol{z}}_{p_\mathrm{f}} \end{Bmatrix} = \left\{ \boldsymbol{f}(t, \boldsymbol{z}) \right\} = \begin{Bmatrix} \boldsymbol{f}_v(t, \boldsymbol{z}) \\ \boldsymbol{f}_a(t, \boldsymbol{z}) \\ \boldsymbol{f}_{v_\mathrm{f}}(t, \boldsymbol{z}) \\ \boldsymbol{f}_{a_\mathrm{f}}(t, \boldsymbol{z}) \\ \boldsymbol{f}_{\dot{p}_\mathrm{f}}(t, \boldsymbol{z}) \end{Bmatrix} , \tag{111}$$

such that

$$\left\{\boldsymbol{z}\right\} = \begin{Bmatrix} \boldsymbol{d} \\ \dot{\boldsymbol{d}} \\ \boldsymbol{d}_{\mathrm{f}} \\ \dot{\boldsymbol{d}}_{\mathrm{f}} \\ \boldsymbol{\pi} \end{Bmatrix}, \; \dot{\boldsymbol{z}} = \begin{Bmatrix} \dot{\boldsymbol{d}} \\ \ddot{\boldsymbol{d}} \\ \dot{\boldsymbol{d}}_{\mathrm{f}} \\ \ddot{\boldsymbol{d}}_{\mathrm{f}} \\ \dot{\boldsymbol{\pi}} \end{Bmatrix} . \tag{112}$$

The FE formulation for the balance of momentum of the mixture, variational Eq. 54, is written in block-matrix form as

$$\underbrace{\left\{\boldsymbol{R}_u\right\}}_{n^s_{\mathrm{dof}}\times 1} = \boldsymbol{0} \,, \tag{113}$$

where the global residual for the solid skeleton displacement is given as

$$\boldsymbol{c}^{u,T} \cdot \boldsymbol{R}_u = \mathcal{G}^h = \mathcal{G}_1^{\mathrm{INT},h} + \mathcal{G}_2^{\mathrm{INT},h} + \mathcal{G}_3^{\mathrm{INT},h} + \mathcal{G}_4^{\mathrm{INT},h} + \mathcal{G}_5^{\mathrm{INT},h} - \mathcal{G}^{\mathrm{EXT},h} = 0 \,. \tag{114}$$

The weighted residual remains unchanged from Irwin et al.,[29,30] with the exception of

$$\begin{aligned} \mathcal{G}_5^{\mathrm{INT},h} \qquad &= \mathop{\mathbf{A}}_{e}^{n_e} \underbrace{\left\{\boldsymbol{c}^{u,e}\right\}^T}_{1\times n^{s,e}_{\mathrm{dof}}} \cdot \underbrace{\left\{\boldsymbol{f}^{\mathcal{G}_5^{\mathrm{INT}},e}\right\}}_{n^{s,e}_{\mathrm{dof}}\times 1} , \\ \underbrace{\left\{\boldsymbol{f}^{\mathcal{G}_5^{\mathrm{INT}},e}\right\}}_{n^{s,e}_{\mathrm{dof}}\times 1} \quad &= \int_{-1}^{1} \underbrace{\left\{\boldsymbol{B}^{e,u}\right\}^T}_{n^{s,e}_{\mathrm{dof}}\times 1} P^{\mathrm{f},h^e}_{11(E)} A j^e \, d\xi \; . \end{aligned} \tag{115}$$

The FE formulation for the balance of mass, variational Eq. 49, is written in block-matrix form as

$$\underbrace{\left\{\boldsymbol{R}_{p_{\mathrm{f}}}\right\}}_{n^{p_{\mathrm{f}}}_{\mathrm{dof}}\times 1} = \boldsymbol{0} \,, \tag{116}$$

where the global residual for the pore fluid pressure is given as

$$\boldsymbol{c}^{p_{\mathrm{f}},T} \cdot \boldsymbol{R}_{p_{\mathrm{f}}} = \mathcal{H}^h = \mathcal{H}_1^{\mathrm{INT},h} + \mathcal{H}_2^{\mathrm{INT},h} + \mathcal{H}_3^{\mathrm{INT},h} + \mathcal{H}_4^{\mathrm{INT},h} + \mathcal{H}_5^{\mathrm{INT},h} - \mathcal{H}_1^{\mathrm{EXT},h} = 0 \,. \tag{117}$$

The weighted residual remains unchanged from Irwin et al.,[29,30] with the exception of

$$
\begin{aligned}
\mathcal{H}_2^{\text{INT},h} &= \mathop{\mathsf{A}}_{e}^{n_e} \underbrace{\left\{ \boldsymbol{c}^{p_\text{f},e} \right\}^T}_{1\times n_\text{dof}^{p_\text{f},e}} \cdot \underbrace{\left\{ \boldsymbol{f}^{\mathcal{H}_2^{\text{INT}},e} \right\}}_{n_\text{dof}^{p_\text{f},e}\times 1}, \\
\mathcal{H}_5^{\text{INT},h} &= \mathop{\mathsf{A}}_{e}^{n_e} \underbrace{\left\{ \boldsymbol{c}^{p_\text{f},e} \right\}^T}_{1\times n_\text{dof}^{p_\text{f},e}} \cdot \underbrace{\left\{ \boldsymbol{f}\mathcal{H}_5^{\text{INT}},e \right\}}_{n_\text{dof}^{p_\text{f},e}\times 1}, \\
\underbrace{\left\{ \boldsymbol{f}^{\mathcal{H}_2^{\text{INT}},e} \right\}}_{n_\text{dof}^{p_\text{f},e}\times 1} &= \int_{-1}^{1} \underbrace{\left\{ \boldsymbol{N}^{e,p_\text{f}} \right\}^T}_{n_\text{dof}^{p_\text{f},e}\times 1} \frac{\partial p_\text{f}^{h^e}}{\partial X} \left(n^\text{f} \tilde{v}_\text{f} \right)^{h^e} \frac{1}{K_\text{f}^\eta} A j^e \, d\xi \,, \\
\underbrace{\left\{ \boldsymbol{f}^{\mathcal{H}_5^{\text{INT}},e} \right\}}_{n_\text{dof}^{p_\text{f},e}\times 1} &= -\int_{-1}^{1} \underbrace{\left\{ \boldsymbol{B}^{e,p_\text{f}} \right\}^T}_{n_\text{dof}^{p_\text{f},e}\times 1} \frac{\hat{k}}{n^\text{f}} \frac{\partial \sigma_{11(E)}^{\text{f},h^e}}{\partial X} \left(F_{11}^{h^e} \right)^{-1} \frac{1}{K_\text{f}^\eta} A j^e \, d\xi \,,
\end{aligned}
\tag{118}
$$

where the pore fluid extra stress is embedded within the discretized Darcy velocity in $\boldsymbol{f}^{\mathcal{H}_2^{\text{INT}},e}$.

The FE formulation for the balance of momentum of the fluid, variational Eq. 60, is written in block-matrix form

$$
\underbrace{\left\{ \boldsymbol{R}_{u_\text{f}} \right\}}_{n_\text{dof}^{f}\times 1} = \boldsymbol{0} \,, \tag{119}
$$

where the global residual for the pore fluid displacement is given as

$$
\boldsymbol{c}^{u_\text{f},T} \cdot \boldsymbol{R}_{u_\text{f}} = \mathcal{I}^h = \mathcal{I}_1^{\text{INT},h} + \mathcal{I}_2^{\text{INT},h} + \mathcal{I}_3^{\text{INT},h} + \mathcal{I}_4^{\text{INT},h} + \mathcal{I}_5^{\text{INT},h} = 0 \,. \tag{120}
$$

The weighted residual remains unchanged from Irwin et al.,[29,30] with the exception of

$$
\begin{aligned}
\mathcal{I}_5^{\text{INT},h} &= \mathop{\mathsf{A}}_{e}^{n_e} \underbrace{\left\{ \boldsymbol{c}^{u_\text{f},e} \right\}^T}_{1\times n_\text{dof}^{f,e}} \cdot \underbrace{\left\{ \boldsymbol{f}^{\mathcal{I}_5^{\text{INT}},e} \right\}}_{n_\text{dof}^{f,e}\times 1}, \\
\underbrace{\left\{ \boldsymbol{f}^{\mathcal{I}_5^{\text{INT}},e} \right\}}_{n_\text{dof}^{f,e}\times 1} &= -\int_{-1}^{1} \underbrace{\left\{ \boldsymbol{N}^{e,u_\text{f}} \right\}^T}_{n_\text{dof}^{f,e}\times 1} \frac{\partial P_{11(E)}^{\text{f},h^e}}{\partial X} A j^e \, d\xi \,.
\end{aligned}
\tag{121}
$$

The block system of equations to solve is

$$\underbrace{\left\{\dot{\boldsymbol{z}}\right\}}_{(2\times n_{\text{dof}}^{s}+2\times n_{\text{dof}}^{f}+n_{\text{dof}}^{p_{\text{f}}})\times 1} = \left\{ \begin{array}{c} \underbrace{\left\{\dot{\boldsymbol{d}}\right\}}_{n_{\text{dof}}^{s}\times 1} \\ \underbrace{\left[\boldsymbol{M}_{u,u}^{\mathcal{G}_1^{\text{INT}}}\right]^{-1}}_{n_{\text{dof}}^{s}\times n_{\text{dof}}^{s}} \cdot \\ \left(-\underbrace{\left\{\boldsymbol{F}^{\mathcal{G}_1^{\text{INT}}}\right\}}_{n_{\text{dof}}^{s}\times 1} - \underbrace{\left\{\boldsymbol{F}^{\mathcal{G}_2^{\text{INT}}}\right\}}_{n_{\text{dof}}^{s}\times 1} - \underbrace{\left\{\boldsymbol{F}^{\mathcal{G}_3^{\text{INT}}}\right\}}_{n_{\text{dof}}^{s}\times 1} - \right. \\ \left. \underbrace{\left\{\boldsymbol{F}^{\mathcal{G}_4^{\text{INT}}}\right\}}_{n_{\text{dof}}^{s}\times 1} - \underbrace{\left\{\boldsymbol{F}^{\mathcal{G}_5^{\text{INT}}}\right\}}_{n_{\text{dof}}^{s}\times 1} + \underbrace{\left\{\boldsymbol{F}^{\mathcal{G}^{\text{EXT}}}\right\}}_{n_{\text{dof}}^{s}\times 1} \right) \\ \underbrace{\left\{\dot{\boldsymbol{d}}_{\text{f}}\right\}}_{n_{\text{dof}}^{f}\times 1} \\ \underbrace{\left[\boldsymbol{M}_{u_{\text{f}},u_{\text{f}}}^{\mathcal{I}_1^{\text{INT}}}\right]^{-1}}_{n_{\text{dof}}^{f}\times n_{\text{dof}}^{f}} \cdot \\ \left(-\underbrace{\left\{\boldsymbol{F}^{\mathcal{I}_2^{\text{INT}}}\right\}}_{n_{\text{dof}}^{f}\times 1} - \underbrace{\left\{\boldsymbol{F}^{\mathcal{I}_3^{\text{INT}}}\right\}}_{n_{\text{dof}}^{f}\times 1} - \underbrace{\left\{\boldsymbol{F}^{\mathcal{I}_4^{\text{INT}}}\right\}}_{n_{\text{dof}}^{f}\times 1} - \underbrace{\left\{\boldsymbol{F}^{\mathcal{I}_5^{\text{INT}}}\right\}}_{n_{\text{dof}}^{f}\times 1} \right) \\ \underbrace{\left[\boldsymbol{M}_{p_{\text{f}},p_{\text{f}}}^{\mathcal{H}_1^{\text{INT}}}\right]^{-1}}_{n_{\text{dof}}^{p_{\text{f}}}\times n_{\text{dof}}^{p_{\text{f}}}} \cdot \left(-\underbrace{\left\{\boldsymbol{F}^{\mathcal{H}_1^{\text{INT}}}\right\}}_{n_{\text{dof}}^{p_{\text{f}}}\times 1} - \underbrace{\left\{\boldsymbol{F}^{\mathcal{H}_2^{\text{INT}}}\right\}}_{n_{\text{dof}}^{p_{\text{f}}}\times 1} - \underbrace{\left\{\boldsymbol{F}^{\mathcal{H}_3^{\text{INT}}}\right\}}_{n_{\text{dof}}^{p_{\text{f}}}\times 1} - \right. \\ \left. \underbrace{\left\{\boldsymbol{F}^{\mathcal{H}_4^{\text{INT}}}\right\}}_{n_{\text{dof}}^{p_{\text{f}}}\times 1} - \underbrace{\left\{\boldsymbol{F}^{\mathcal{H}_5^{\text{INT}}}\right\}}_{n_{\text{dof}}^{p_{\text{f}}}\times 1} + \underbrace{\left\{\boldsymbol{F}^{\mathcal{H}^{\text{EXT}}}\right\}}_{n_{\text{dof}}^{p_{\text{f}}}\times 1} \right) \end{array} \right\}, \tag{122}$$

where assembled mass matrices and vectors remain unchanged from those given in

Irwin et al.,[29,30] with the exception of

$$\begin{aligned}
\underbrace{\left\{\boldsymbol{F}^{\mathcal{G}_5^{\mathrm{INT}}}\right\}}_{n_{\mathrm{dof}}^{s}\times 1} &= \mathop{\mathsf{A}}_{e}^{n_e} \underbrace{\left\{\boldsymbol{f}^{\mathcal{G}_5^{\mathrm{INT}},e}\right\}}_{n_{\mathrm{dof}}^{s,e}\times 1}, \\
\underbrace{\left\{\boldsymbol{F}^{\mathcal{I}_5^{\mathrm{INT}}}\right\}}_{n_{\mathrm{dof}}^{f}\times 1} &= \mathop{\mathsf{A}}_{e}^{n_e} \underbrace{\left\{\boldsymbol{f}^{\mathcal{I}_5^{\mathrm{INT}},e}\right\}}_{n_{\mathrm{dof}}^{f,e}\times 1}, \\
\underbrace{\left\{\boldsymbol{F}^{\mathcal{H}_5^{\mathrm{INT}}}\right\}}_{n_{\mathrm{dof}}^{p_{\mathrm{f}}}\times 1} &= \mathop{\mathsf{A}}_{e}^{n_e} \underbrace{\left\{\boldsymbol{f}^{\mathcal{H}_5^{\mathrm{INT}},e}\right\}}_{n_{\mathrm{dof}}^{p_{\mathrm{f}},e}\times 1}.
\end{aligned} \tag{123}$$

4. Results

4.1 Verification

Here, we present results comparing the numerical solutions to an analytical solution developed by de Boer et al.[48]

A porous column is subjected to an external traction load while its base and sides remain fixed. Values of material and geometric parameters used in this example are given in Tables 1 and 2, respectively, where different load amplitudes and frequencies are included in the latter. The top of the porous column is perfectly drained with reference pressure $p_{\mathrm{f}}(X = H, t) = 0$ atm and subjected to a harmonic loading, as shown in Fig. 3. The analytical solution for this problem was given in Irwin et al.[28] (originally by de Boer et al.[48]), and is not repeated here for brevity.

Table 1 Material parameters for the poroelastodynamics verification example. Viscosity values are obtained from Holmes et al.,[49] assuming a temperature $= 20^{\circ}$ C.

λ (MPa)	μ (MPa)	ρ_0^{sR} (kg/m^3)	ρ_0^{fR} (kg/m^3)	$\mathrm{n}_0^{\mathrm{f}}$	k_0 (m/s)	η_{f} (mPa-s)	κ_{f} (mPa-s)
5.6	8.4	2700	1000	0.42	10^{-2}	1	2.86

Table 2 Geometrical and loading parameters for the poroelastodynamics verification example

H (m)	A (m^2)	$\mathrm{h}_0^{\mathrm{e}}$ (m)	$\mathrm{t}_0^{\boldsymbol{\sigma}}$ (kPa)	ω (rad/s)
10	1	0.1	40	50

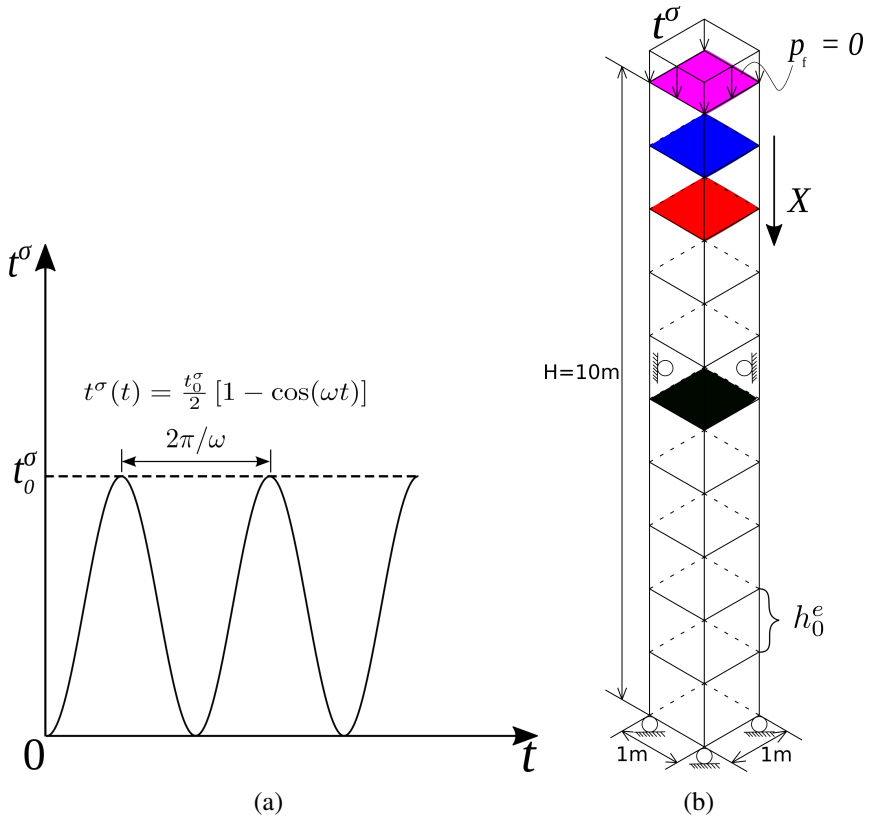

Fig. 3 (a) Traction application and (b) schematic of column mesh for the poroelastodynamics verification example

Here we compare the results between the analytical solution, the new Q3H-Q3H-P1 element type—with and without the pore fluid extra stress—and the old Q2-Q2-P1 element type, which is restricted to the nearly inviscid assumption. Solid skeleton displacement results (refer to Fig. 4(a)) are improved for the Hermite cubic element, but pore fluid displacement results (refer to Fig. 4(b)) suffer slightly, though remain reasonably accurate. Excellent agreement is observed between pore fluid pressure and solid skeleton extra (effective) stress for all element types. Appearance of improvement of the Hermite cubic element over the standard Lagrange quadratic element arises only since the Hermite cubic element is integrated with 4-point quadrature rather than 3-point quadrature; thus, the quadrature points that are sampled for the Hermite cubic element are closer to the nodes where the analytical solution is defined.

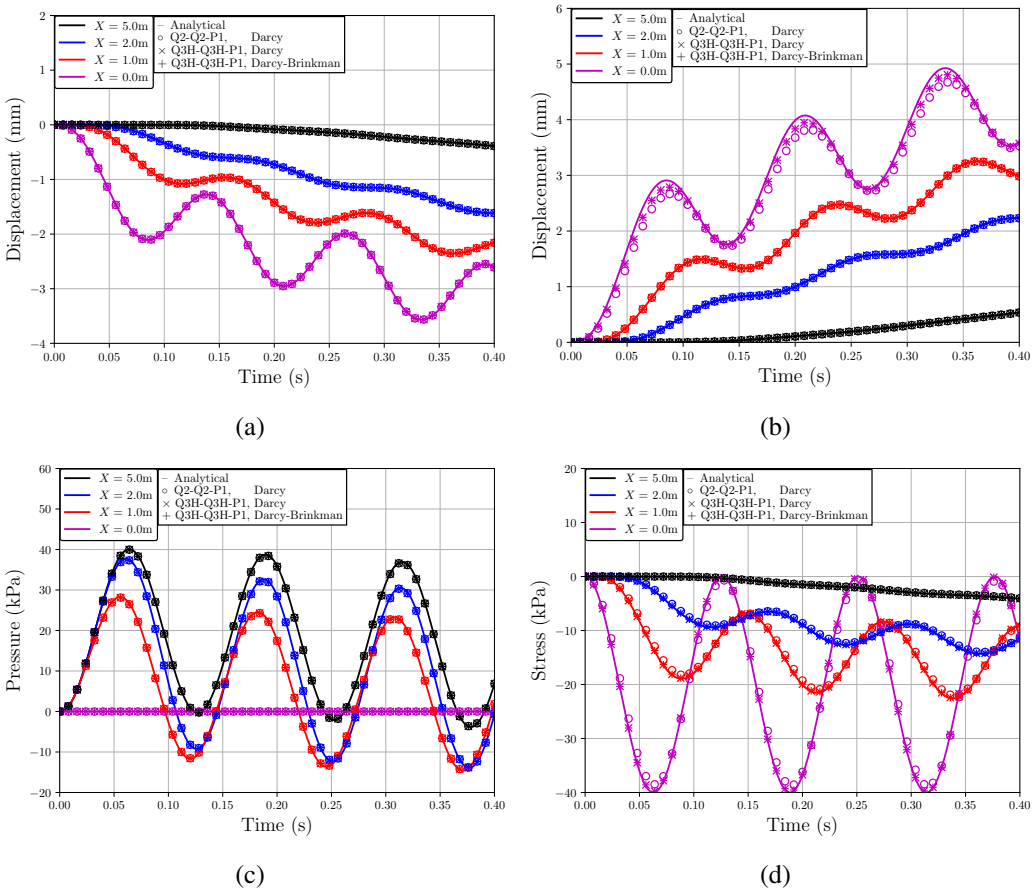

Fig. 4 Verification results for the numerical approximation to the de Boer analytical solution showing (a) solid skeleton displacement, (b) pore fluid displacement, (c) pore fluid pressure, and (d) solid extra stress

Pore fluid extra stress is shown in Fig. 5(a); it is six orders of magnitude smaller than the pore fluid pressure contribution (refer to Fig. 5(b)). This is in agreement with the argument laid out in Section 2 (originally in Ehlers et al.[36]), where the soil column in this example is essentially a low permeability, rigid, non-deforming solid skeleton (approximate for small strain) and the pore fluid is nearly incompressible (via large pore fluid bulk modulus given in Table1). Furthermore, porosity gradients for this example are inherently small for small strains, rendering that contribution to the divergence of the pore fluid extra stress negligible as well.

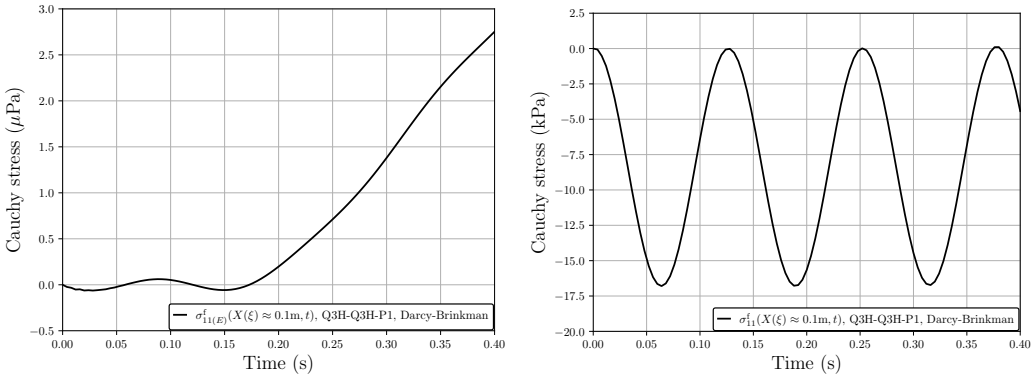

(a) (b)

Fig. 5 Pore fluid stress results for the numerical approximation to the de Boer analytical solution for (a) pore fluid extra stress at the Gauss point closest to $X = H$, and (b) total pore fluid stress $\sigma^{\mathrm{f}}_{11} \coloneqq \sigma^{\mathrm{f}}_{11(E)} - n^{\mathrm{f}} p_{\mathrm{f}}$ at the Gauss point closest to $X = H$

4.2 Shockwave Loading of Lung

Of key importance for dynamic injury predictions is how lung tissue deforms under shock loading. In Section 4 we present our findings for a column of lung parenchyma subjected to external traction loadings on the order of milliseconds or less. In all of the simulations, the lung parenchyma column is fixed on its sides and base. In contrast to prior work,[28,29] the pore fluid pressure boundary condition at the top of the column is allowed to vary, such that the top of the membrane can be represented as both impermeable (i.e., "undrained") or permeable (i.e., "drained"). The latter might be more experimentally feasible and is an advantage of our model to the one implemented by Clayton et al.[10] For example, one might excise a small section of lung parenchyma, place it in a sleeve such that the sleeve need not enclose the end of excised tissue, and then load it uniaxially wherein the impacting device would need only to maintain contact with a part of the tissue during loading. Material, geometrical, and loading parameters are given in Tables 3 and 4.

We begin our discussion of the effects of the pore fluid extra stress with a simulation that mimics a shock tube test in a laboratory setting. The traction is a linear triangular impulse, hereafter referred to as the Yen impulse,[50] shown in Fig. 6(a), which rises to a maximum overpressure $t_0^\sigma = 50$ kPa (relative to atmospheric pressure at sea level) at a time $t_0 = 170$ μs. It then decays to $t^\sigma = 0$ kPa at time $2t_0 = t_1 = 340$ μs. The time scales and pressure profile were chosen based on an experimental study of rabbit lung exposed to shock tubes by Yen et al.[50] Overpressure amplitude

was chosen arbitrarily, though we note that Yen et al.[50] observed that overpressures greater than 2 psi (≈ 14 kPa) resulted in edema of the exposed rabbit lung.

Table 3 Material parameters for multiphase lung parenchyma simulations. Values taken from Clayton et al., Lande and Mitzner, Holmes et al., Rand et al. and Shang et al.[10,37,49,51,52] Viscosity values for air are interpolated for resting body temperature 37° C; bulk modulus, density and bulk viscosity for blood are estimated using values for water at resting body temperature 37° C, while shear viscosity is estimated from Rand et al.[51]

$\mathbf{K^{skel}}$ **(kPa)**	$\mathbf{G}$ **(kPa)**	$\mathbf{K_s}$ **(kPa)**	$\mathbf{K_f^\eta}$ **(kPa)**	$\boldsymbol{\rho_0^{sR}}$ **(kg/m^3)**
7.5	3	2.2×10^6	140; 2.2×10^6	1000
$\boldsymbol{\rho_0^{fR}}$ **(kg/m^3)**	$\mathbf{n_0^f}$	$\hat{\mathbf{k}}_0$ **(m^2/Pa-s)**	$\boldsymbol{\eta_f}$ **(mPa-s)**	$\boldsymbol{\kappa_f}$ **(mPa-s)**
1.2; 1000	0.664; 0.99	10^{-5}; 6.3×10^{-8}	1.89×10^{-2}; 3	2.03×10^{-2}; 1.93

Table 4 Geometrical and loading parameters for multiphase lung parenchyma simulations

Overpressure load type	**H (cm)**	**A (cm^2)**	$\mathbf{h_0^e}$ **(cm)**	$\mathbf{t_0^\sigma}$ **(kPa)**	$\mathbf{t_0}$ **(ms)**	$\mathbf{t_1}$ **(ms)**
Yen impulse	10	1	0.1	25; 50	0.17	0.34
Friedlander impulse	10	1	0.1	25; 50	10	N/A

To start, we assume an impermeable membrane of lung parenchyma, in other words, the pore air is allowed to move freely within the column of lung parenchyma, but cannot escape at either end. Displacement profiles between the nearly inviscid (Darcy) and viscous (Darcy-Brinkman, inclusion of pore fluid extra stress) simulations are shown in Fig. 7. It is evident that inclusion of the pore fluid extra stress for this example has a negligible effect on the motion of the lung parenchyma and pore fluid within. This is likely due to how small of a contribution the pore fluid extra stress, shown in Fig. 8(a), has on the total fluid stress, shown in Fig. 8(b). Pore fluid extra stress is three orders of magnitude smaller than the pore fluid pressure for this application.

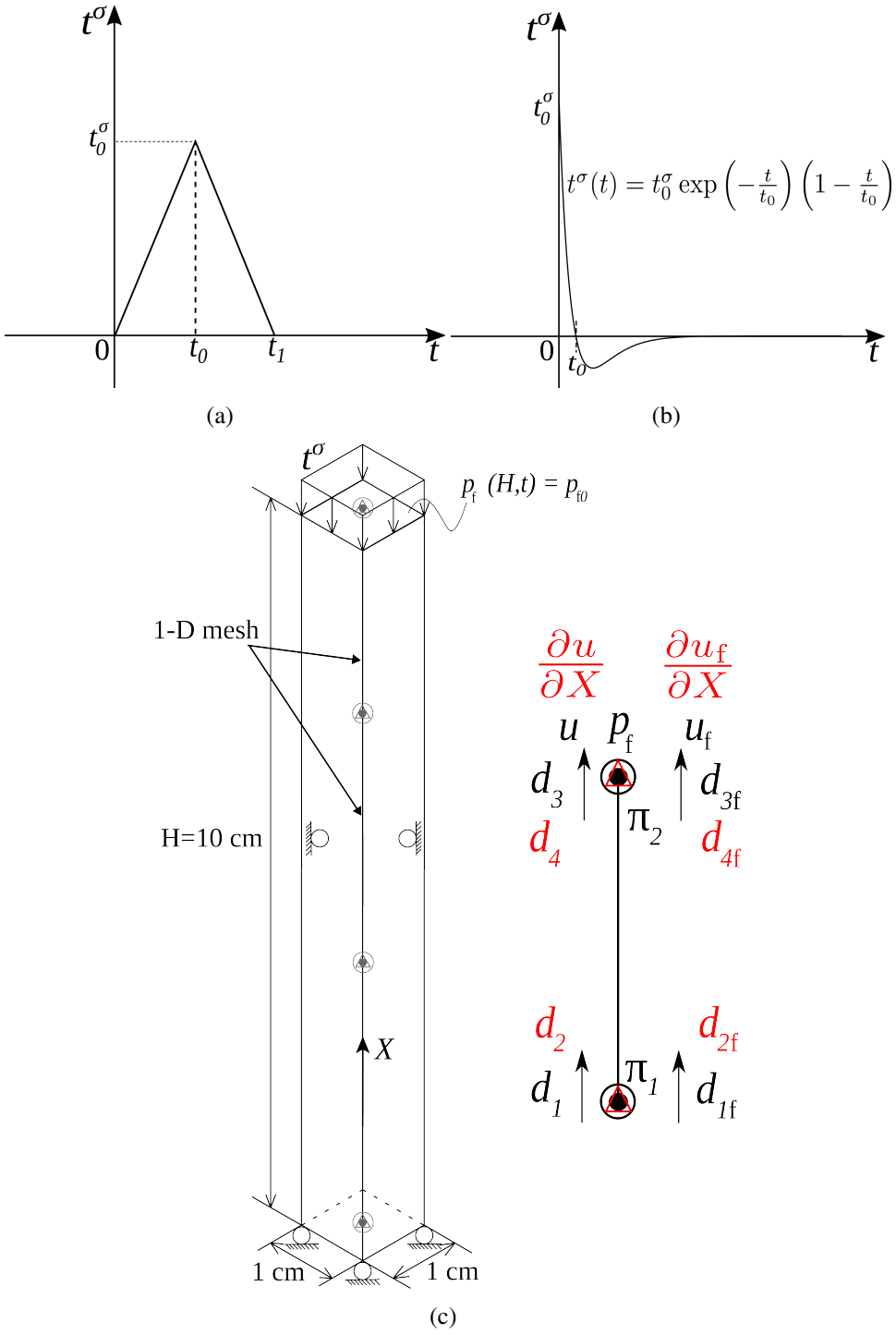

Fig. 6 (a) Yen impulse traction application (b) Friedlander traction application (c) schematic of multiphase column mesh for examples of lung parenchyma deformations. Note that in (c), for the impermeable membrane, the boundary condition $p_f(H,t) = p_{f,0}$ is not set.

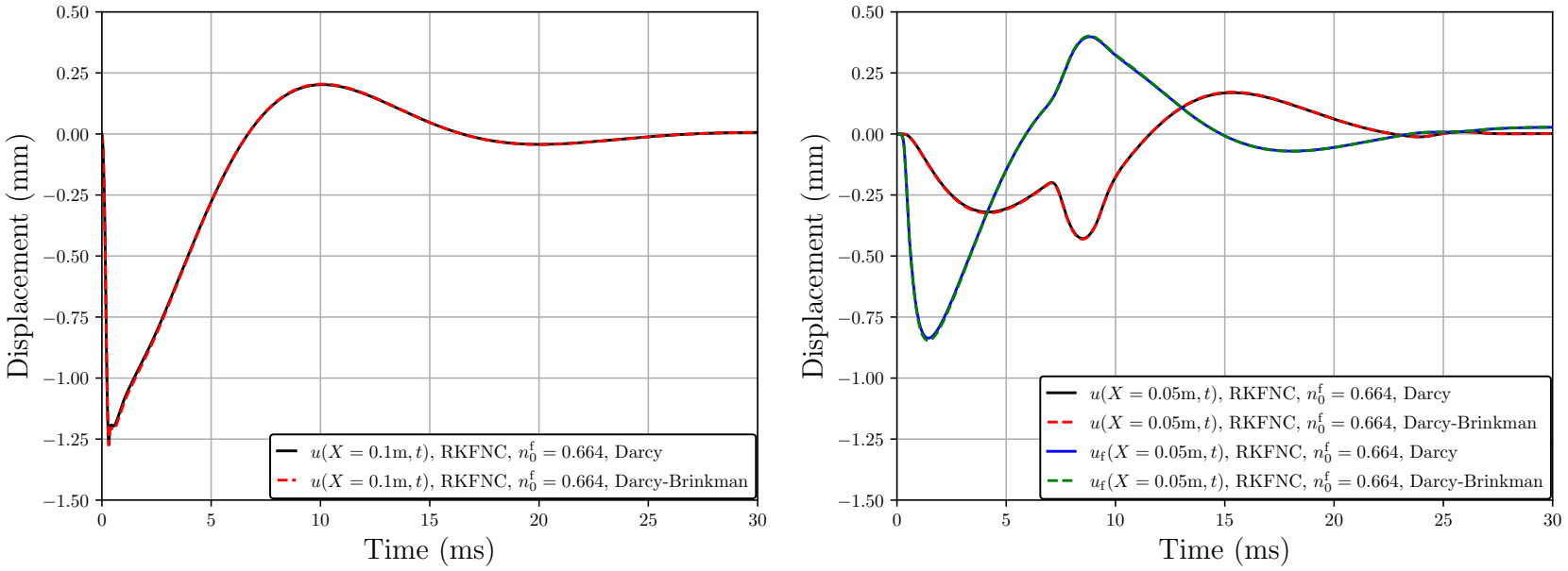

(a) (b)

Fig. 7 Displacement results from applying the Yen impulse (50 kPa) to the impermeable lung parenchyma for (a) solid skeleton displacement $u(X = H, t)$ (and by extension due to the no-slip/no-penetration condition, $u_{\text{f}}(X = H, t)$), and (b) solid skeleton displacement $u(X = H/2, t)$ and pore fluid displacement $u_{\text{f}}(X = H/2, t)$

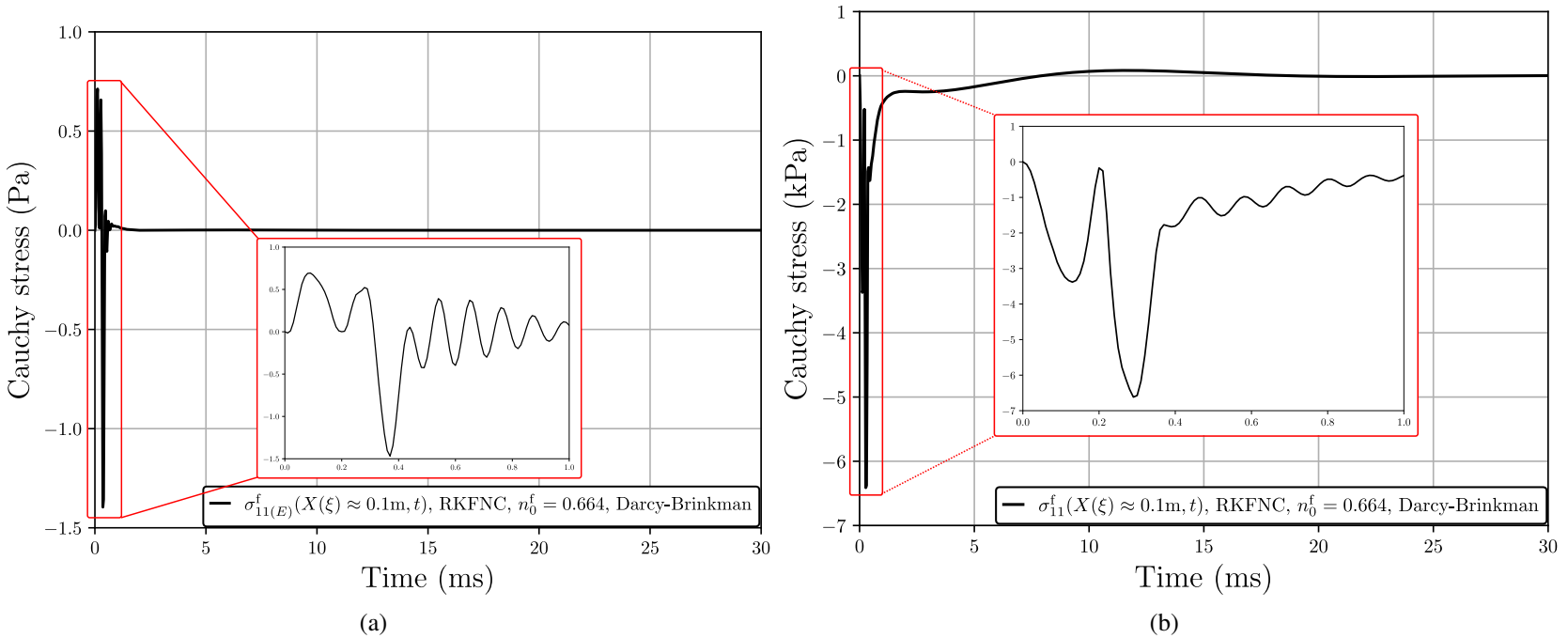

Fig. 8 Pore fluid stress results from applying the Yen impulse (50 kPa) to the impermeable lung parenchyma for (a) pore fluid extra stress at the Gauss point closest to $X = H$, and (b) total pore fluid stress $\sigma^{\mathrm{f}}_{11} \coloneqq \sigma^{\mathrm{f}}_{11(E)} - n^{\mathrm{f}} p_{\mathrm{f}}$ at the Gauss point closest to $X = H$

Next, we assume a permeable membrane (which might be more experimentally feasible), in other wrods, the pore air is allowed to escape from the top of the column. We note that the prescription of this pore fluid pressure boundary condition restricts the maximum overpressure we are able to apply to the mixture (i.e., the simulations fail for $t_0^\sigma = 50$ kPa; $\Delta t \to 0$ for RKFNC, NB does not converge). Again we see that the pore fluid extra stress has negligible effects on displacements (refer to Fig. 9) and total fluid stress (refer to Fig. 10). However, pore fluid extra stress is only one order of magnitude smaller than total pore fluid stress for the permeable membrane. In Fig. 11, we see how pore fluid extra stress "scales" with pore fluid velocity gradient—denoted by the slope of the velocity contour curve—and porosity, and how each evolve over time. Sampled times are (a) at maximum overpressure loading, (b) when overpressure loading stops, and (c) well after loading has ended. Peak overpressure loading occurs at $170\,\mu$s, but the effects of the shock loading are not observed until later, see, for example, Fig. 11(b) when the impulse ends. In Fig. 11(c) we see that the magnitude of the pore fluid extra stress has greatly dissipated well after load is removed.

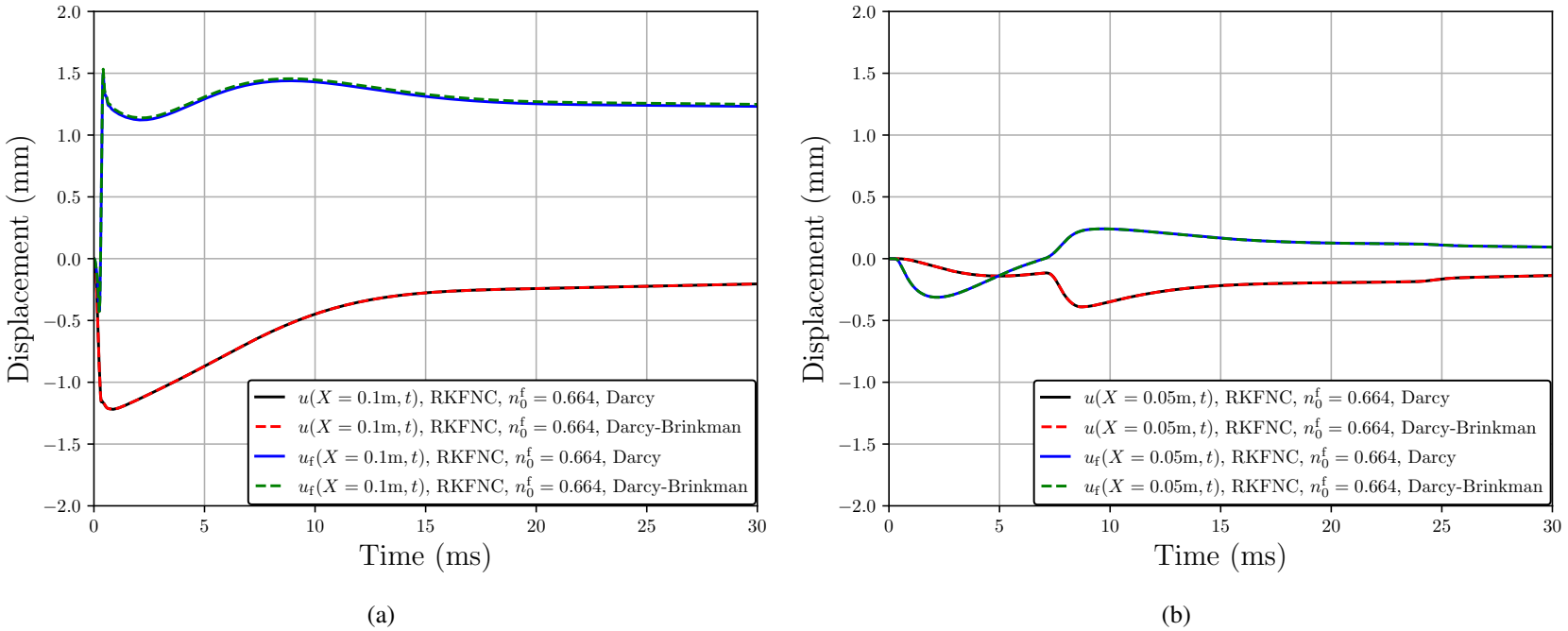

Fig. 9 Displacement results from applying the Yen impulse (25 kPa) to the permeable lung parenchyma for (a) solid skeleton displacement $u(X = H, t)$ and pore fluid displacement $u_{\text{f}}(X = H, t)$, and (b) solid skeleton displacement $u(X = H/2, t)$ and pore fluid displacement $u_{\text{f}}(X = H/2, t)$

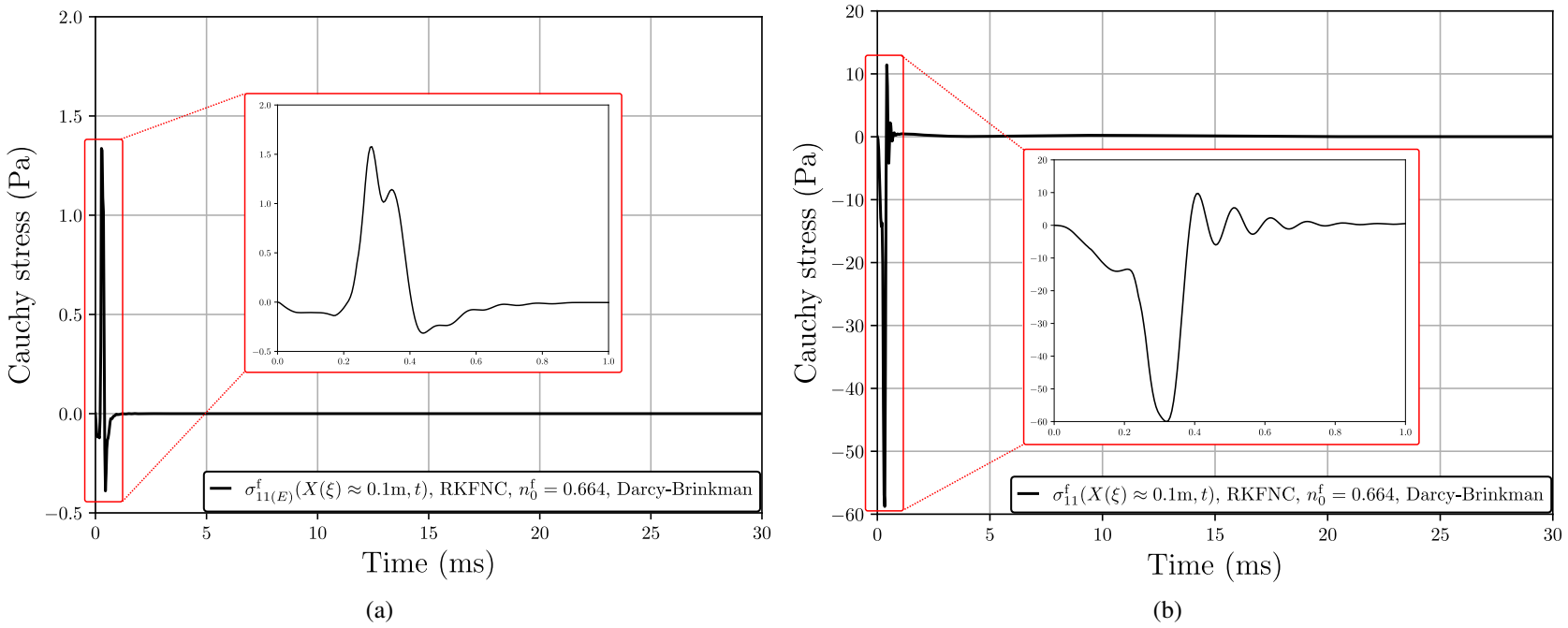

Fig. 10 Pore fluid stress results from applying the Yen impulse (25 kPa) to the permeable lung parenchyma for (a) pore fluid extra stress at the Gauss point closest to $X = H$, and (b) total pore fluid stress $\sigma^{\mathrm{f}}_{11} \coloneqq \sigma^{\mathrm{f}}_{11(E)} - n^{\mathrm{f}} p_{\mathrm{f}}$ at the Gauss point closest to $X = H$

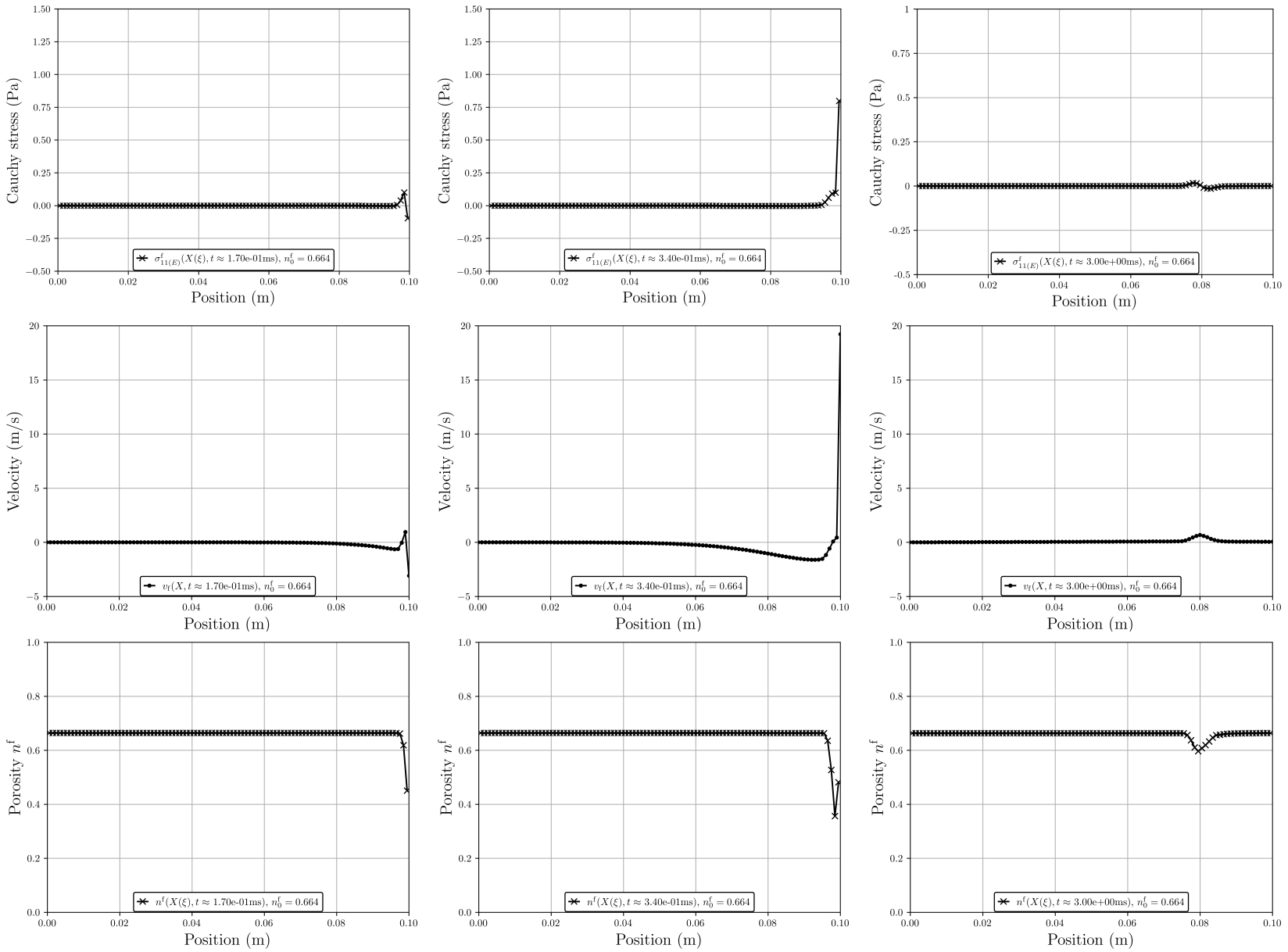

(a) $t = 0.17$ ms (b) $t = 0.34$ ms (c) $t = 3.00$ ms

Fig. 11 Contours along the length of the mesh for pore fluid extra stress $\sigma^{\mathrm{f}}_{11(E)}$, pore fluid velocity v_{f} and porosity n^{f} for permeable lung parenchyma after applying the Yen impulse with 25 kPa maximum overpressure

Since a permeable membrane induces higher pore fluid extra stress, we now swap the pore air for pore blood, in others words, we assume the lung is saturated with blood as the pore fluid, assuming blood can be modeled as a Newtonian fluid. We adjust the pore fluid density, bulk modulus, and viscosities appropriately (refer to Table 3). Initial porosity is also increased to $n_0^{\mathrm{f}} = 0.99$ (from 0.664), and maximum applied overpressure is increased to $t_0^{\sigma} = 50$ kPa (from 25 kPa). While the high initial porosity is not a physically realistic scenario, the magnitude of the pore fluid extra stress should increase as pore fluid extra stress scales with porosity and viscosity. This is what is observed in Fig. 12: the pore fluid extra stress accounts for some oscillations in the total pore fluid stress at the onset of the shock load. However, the solid extra stress (i.e., the material stress of the lung parenchyma tissue itself) is not affected by the inclusion of the pore fluid extra stress (as shown in Fig. 13). This may have to do with the fact that the motion of the lung parenchyma and the pore blood are not affected either (refer to Fig. 14).

In contrast to the example with pore air (refer to Fig. 9), pore fluid (blood) and solid skeleton (lung parenchyma) displacements are similar. When shear viscosity of the pore fluid is increased, the initial hydraulic conductivity $\hat{k}_0$ is reduced. Since seepage velocity $(n^{\mathrm{f}}\tilde{\boldsymbol{v}}_{\mathrm{f}})$ scales with hydraulic conductivity per Darcy's (and Darcy-Brinkman's) law, relative velocity between solid and fluid phases is reduced. Comparing now the contours of pore fluid extra stress, pore fluid velocity, and porosity (Fig. 15) for blood-saturated lung parenchyma to that of air-saturated lung parenchyma (Fig. 11), we see that in the latter the shock wave percolates more quickly through the mixture than in the former. Velocity of pore air is also greater in magnitude than for pore blood, even though the blood-saturated lung parenchyma was subjected to greater maximum overpressure (50 kPa versus 25 kPa). Furthermore, porosity gradients are small for high initial porosity in blood-saturated lung parenchyma compared to moderate initial porosity in air-saturated lung parenchyma. In fact, we see that porosity remains high for the duration of the simulation as compared to air-saturated lung parenchyma, where more fluctuations in porosity are observed.

In addition, because the density of the mixture is higher when pore air is swapped for pore blood, wave speed is thus also higher; correspondingly, the estimated stable time-step for explicit integrators (via CFL condition) is reduced by a factor of approximately 10^3. We found that the RKFNC integrator does not perform well

with this restriction on time-step, and often $\Delta t \to 0$, which is why the aforementioned results use the implict Newmark-beta scheme with constant acceleration ($\beta = 0.25, \gamma = 0.5$).

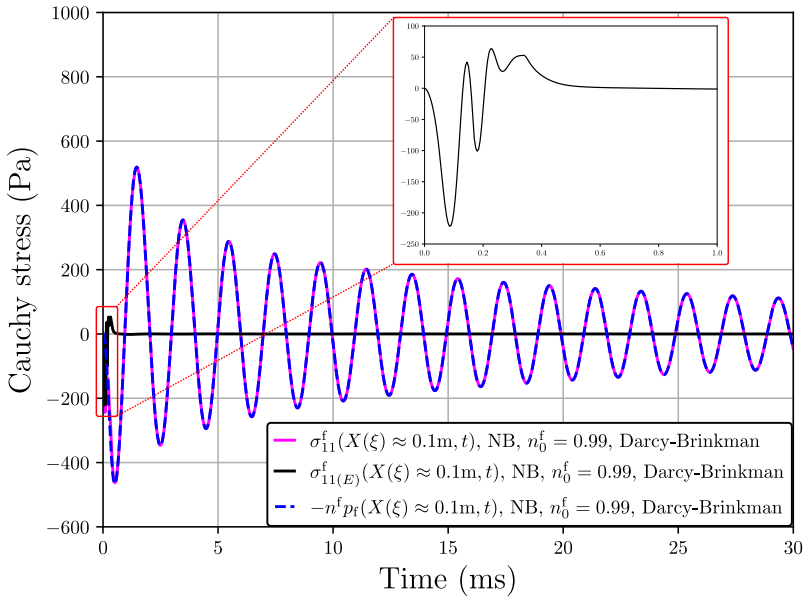

Fig. 12 Pore fluid stress results from applying the Yen impulse (50 kPa) to the permeable, blood-saturated lung parenchyma for the Gauss point closest to $X = H$

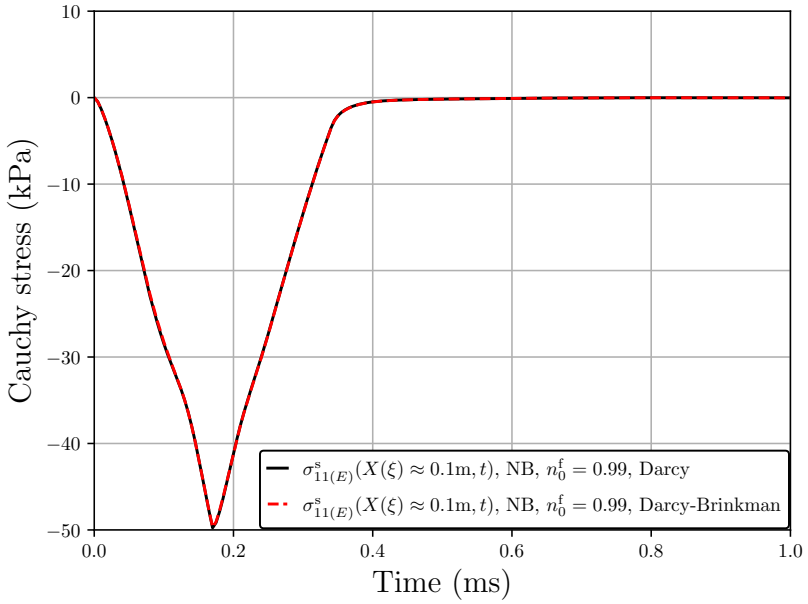

Fig. 13 Solid extra stress results from applying the Yen impulse (50 kPa) to the permeable, blood-saturated lung parenchyma for the Gauss point closest to $X = H$

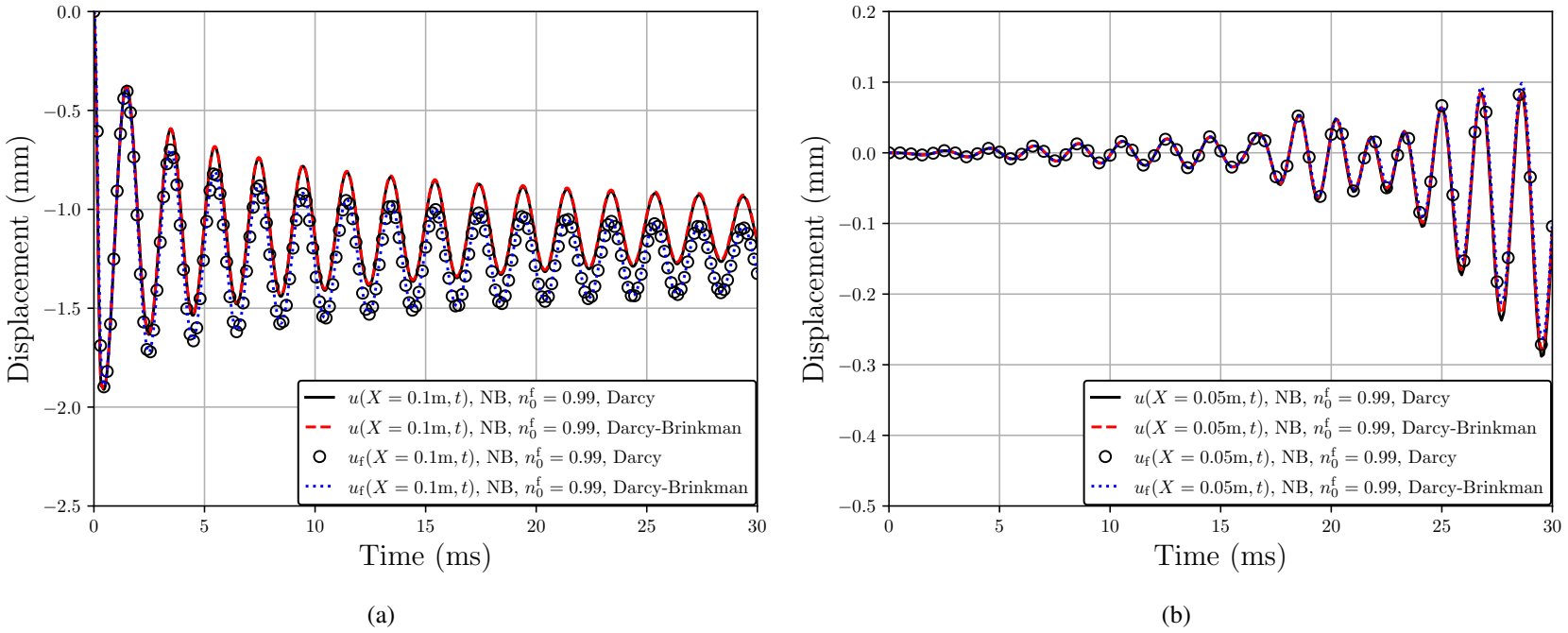

Fig. 14 Displacement results from applying the Yen impulse (50 kPa) to the permeable, blood-saturated lung parenchyma for (a) solid skeleton displacement $u(X = H, t)$ and pore fluid displacement $u_{\text{f}}(X = H, t)$, and (b) solid skeleton displacement $u(X = H/2, t)$ and pore fluid displacement $u_{\text{f}}(X = H/2, t)$

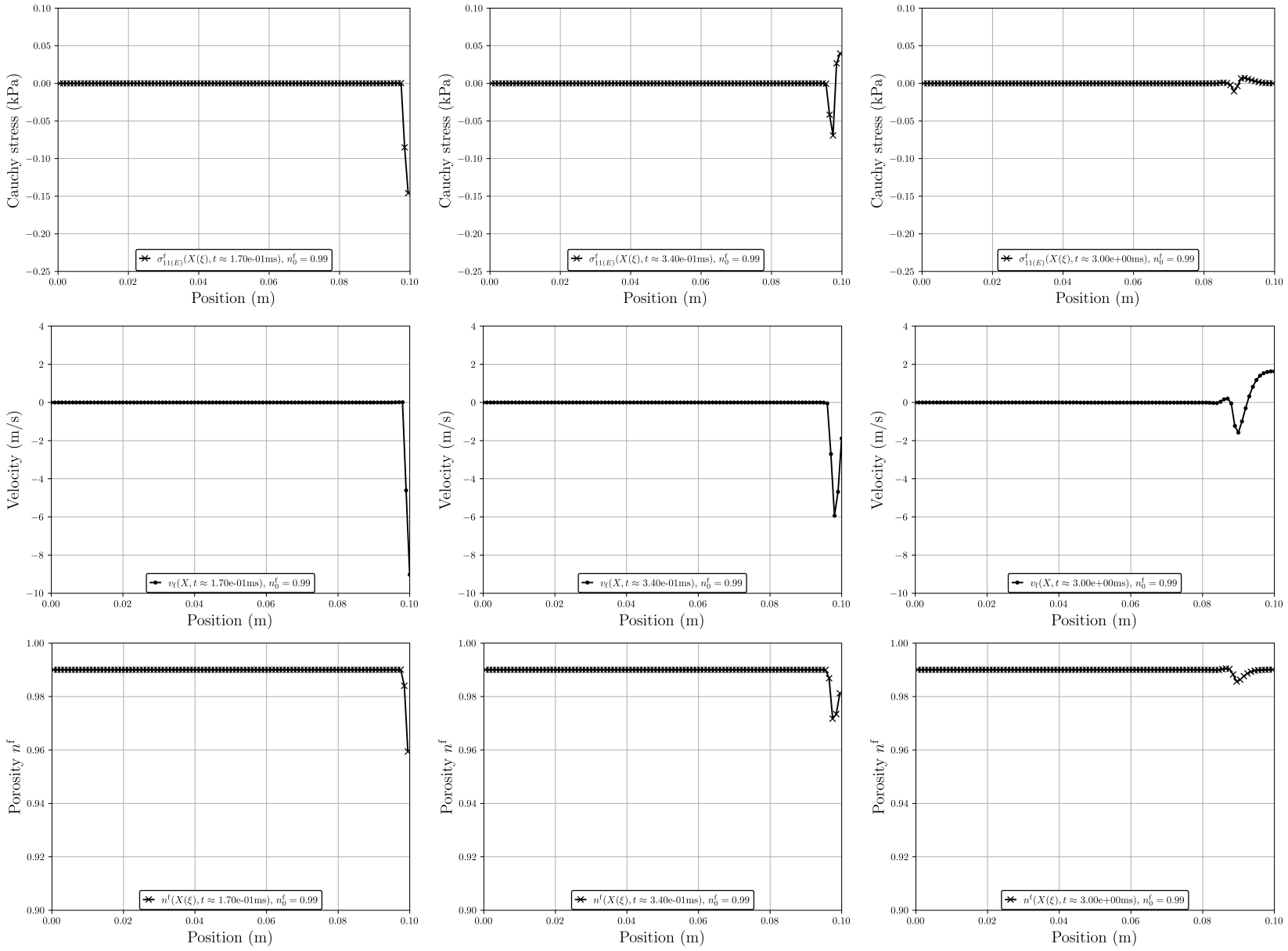

(a) $t = 0.17$ ms (b) $t = 0.34$ ms (c) $t = 3.00$ ms

Fig. 15 Contours along the length of the mesh for pore fluid extra stress $\sigma^{\mathrm{f}}_{11(E)}$, pore fluid velocity v_{f} and porosity n^{f} for permeable, blood-saturated lung parenchyma after applying the Yen impulse with 25 kPa maximum overpressure

We now present the results of the simulations using the Friedlander impulse loading[53] at maximum overpressure $t_0^\sigma = 25$ kPa (refer to Fig. 6(b)), which is more applicable for free-field shock loading (i.e., a shock wave resulting from a detonation of an explosive device).[54] Proceeding as before, we first assume an impermeable membrane of air-saturated lung parenchyma. Looking at Figs. 16 and 17, we see a similar trend: the pore fluid extra stress is small and does not account for any discrepancy between motions of solid and fluid, and total fluid stress, between nearly inviscid (Darcy) and viscous (Darcy-Brinkman) pore fluid flow.

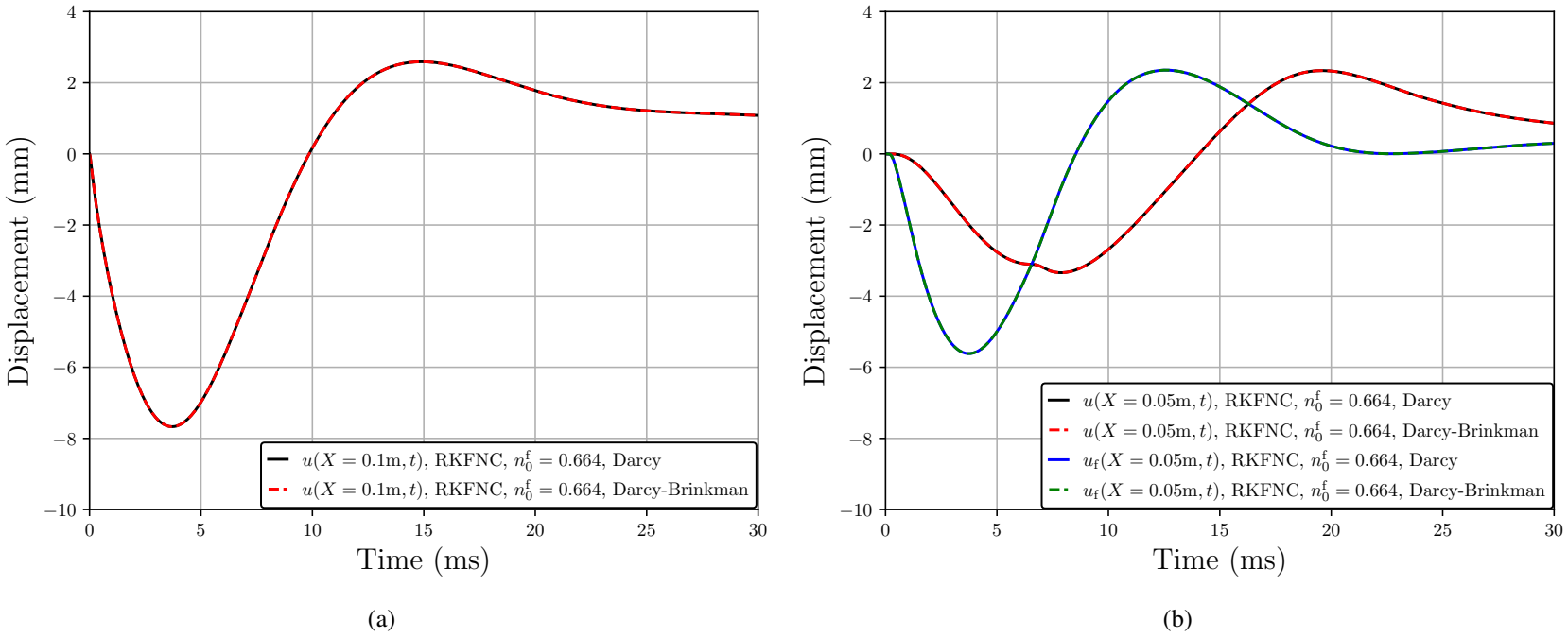

Fig. 16 Displacement results from applying the Friedlander impulse (25 kPa) to the impermeable lung parenchyma for (a) solid skeleton displacement $u(X = H, t)$ (and by extension due to the no-slip/no-penetration condition, $u_{\text{f}}(X = H, t)$), and (b) solid skeleton displacement $u(X = H/2, t)$ and pore fluid displacement $u_{\text{f}}(X = H/2, t)$

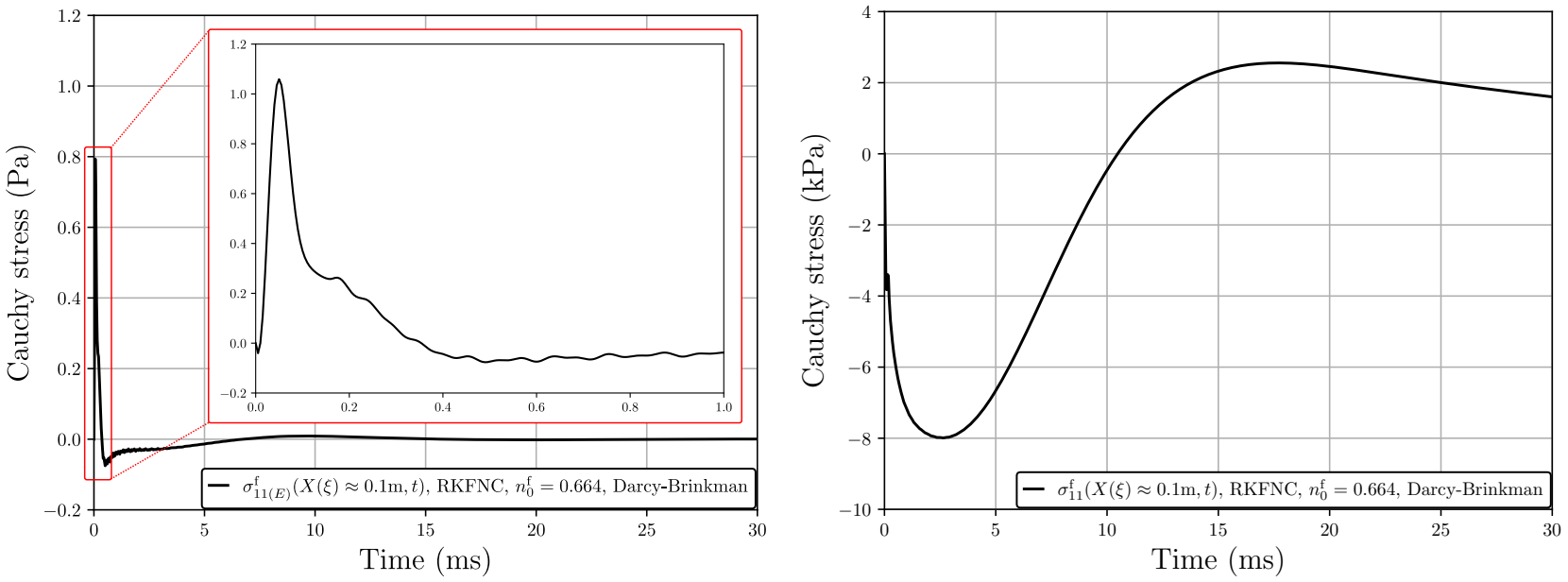

(a) (b)

Fig. 17 Pore fluid stress results from applying the Friedlander impulse (25 kPa) to the impermeable lung parenchyma for (a) pore fluid extra stress at the Gauss point closest to $X = H$, and (b) total pore fluid stress $\sigma^{\mathrm{f}}_{11} \coloneqq \sigma^{\mathrm{f}}_{11(E)} - n^{\mathrm{f}} p_{\mathrm{f}}$ at the Gauss point closest to $X = H$. Slightly higher amplitude of pore fluid extra stress when zoomed in is due to finer resolution of the data points in a second, shorter simulation.

When the top of the column allows fluid to escape (i.e., when we use the permeable boundary condition), we again see no difference between the nearly inviscid (Darcy) and viscous (Darcy-Brinkman) displacements (refer to Fig. 18), though we note that strains are much larger here than for the impermeable boundary. Total pore fluid stress is unaffected by the pore fluid extra stress (refer to Fig. 19). Furthermore, pore fluid extra stress begins to diminish as the shock wave moves along the mesh (where the time sampling locations in used for the contour stills are shown in by Fig. 20), as shown in Fig. 21. We again see how pore fluid extra stress is influenced by large gradients in pore fluid velocity (Figs. 21(a) and 21(b)). In contrast to the Yen impulse (shock-tube loading), we also see larger porosity gradients (Fig. 21(b)).

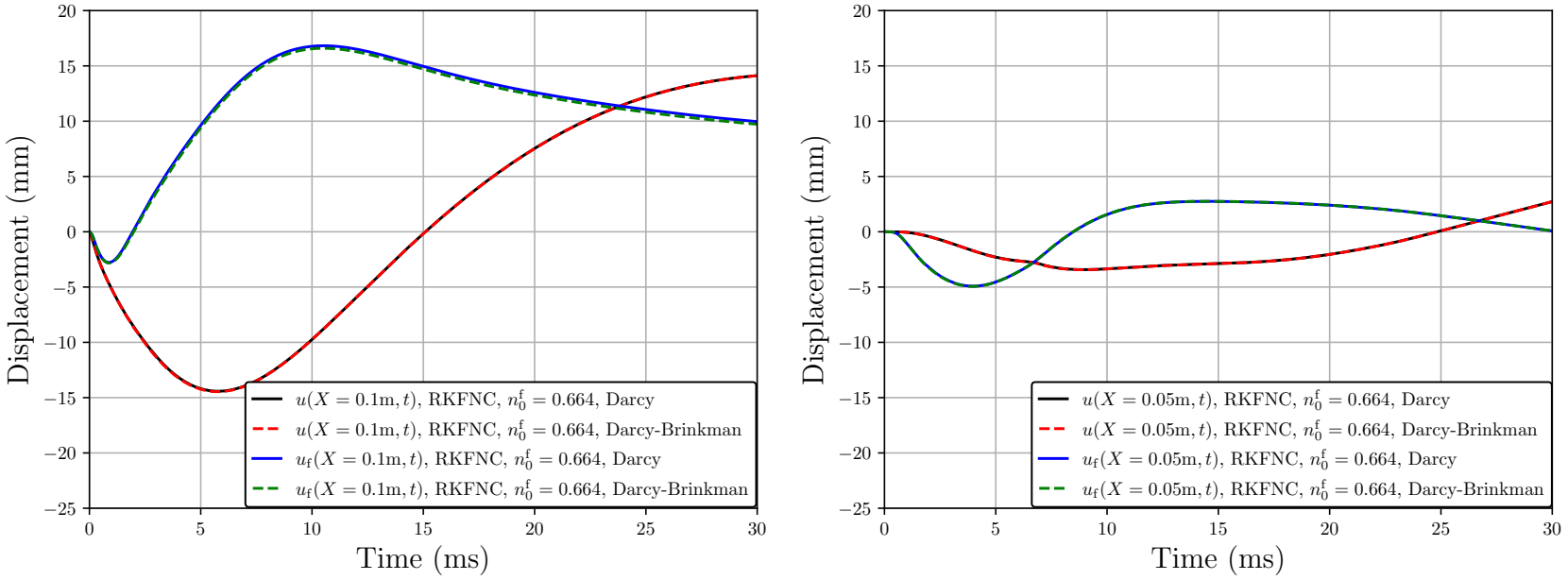

Fig. 18 Displacement results from applying the Friedlander impulse (25 kPa) to the permeable lung parenchyma for (a) solid skeleton displacement $u(X = H, t)$ and pore fluid displacement $u_{\text{f}}(X = H, t)$, and (b) solid skeleton displacement $u(X = H/2, t)$ and pore fluid displacement $u_{\text{f}}(X = H/2, t)$

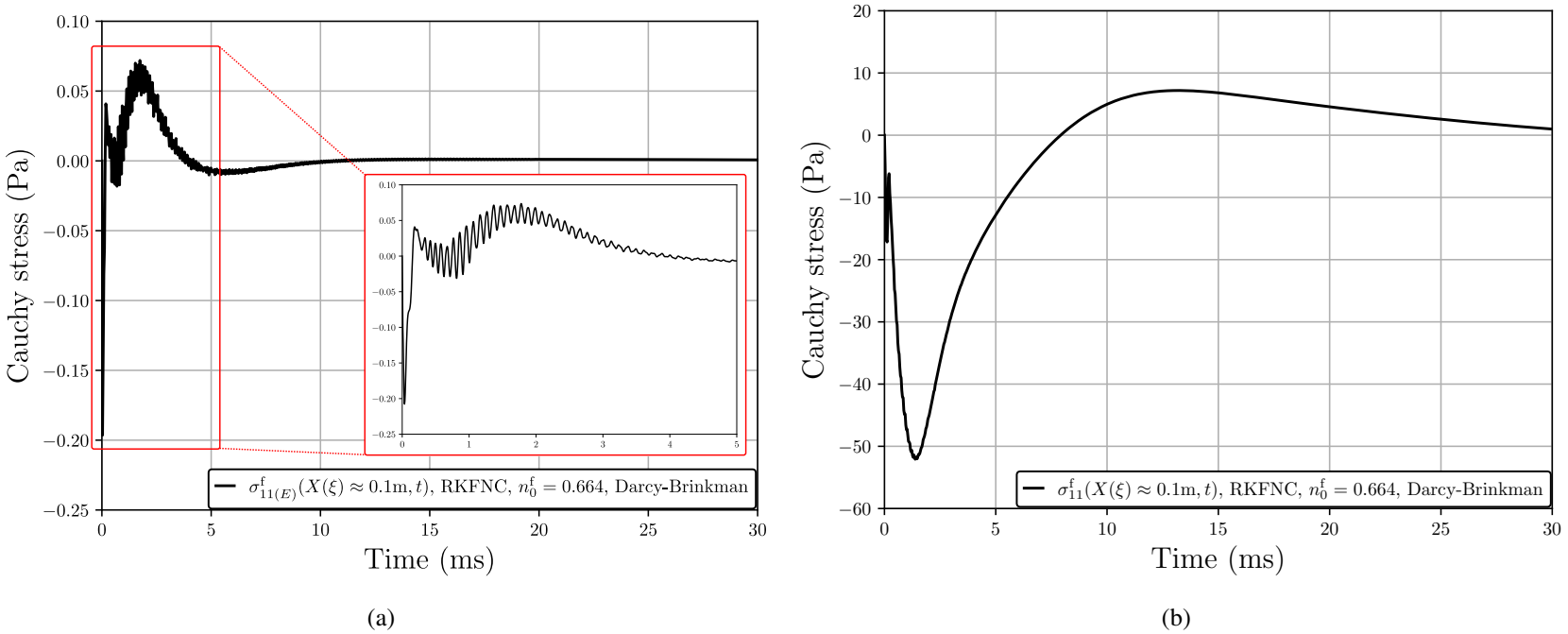

Fig. 19 Pore fluid stress results from applying the Friedlander impulse (25 kPa) to the permeable lung parenchyma for (a) pore fluid extra stress at the Gauss point closest to $X = H$, and (b) total pore fluid stress $\sigma^{\mathrm{f}}_{11} \coloneqq \sigma^{\mathrm{f}}_{11(E)} - n^{\mathrm{f}} p_{\mathrm{f}}$ at the Gauss point closest to $X = H$

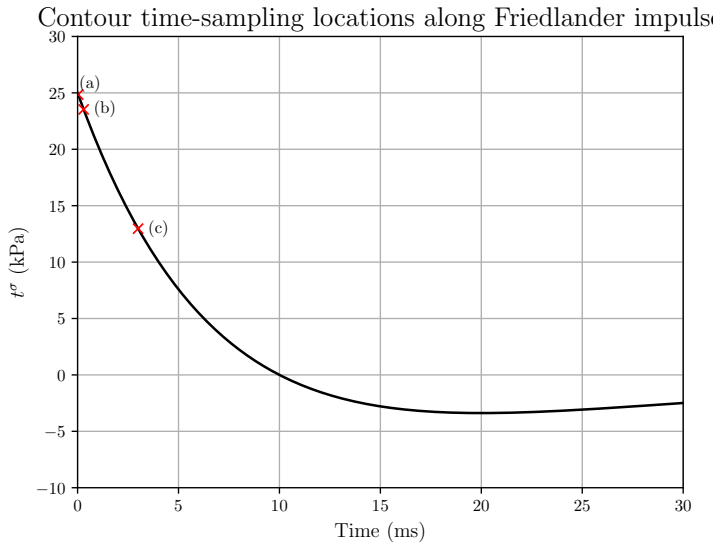

Fig. 20 Sampling locations along the Friedlander impulse for 25 kPa maximum overpressure used in the contour plots

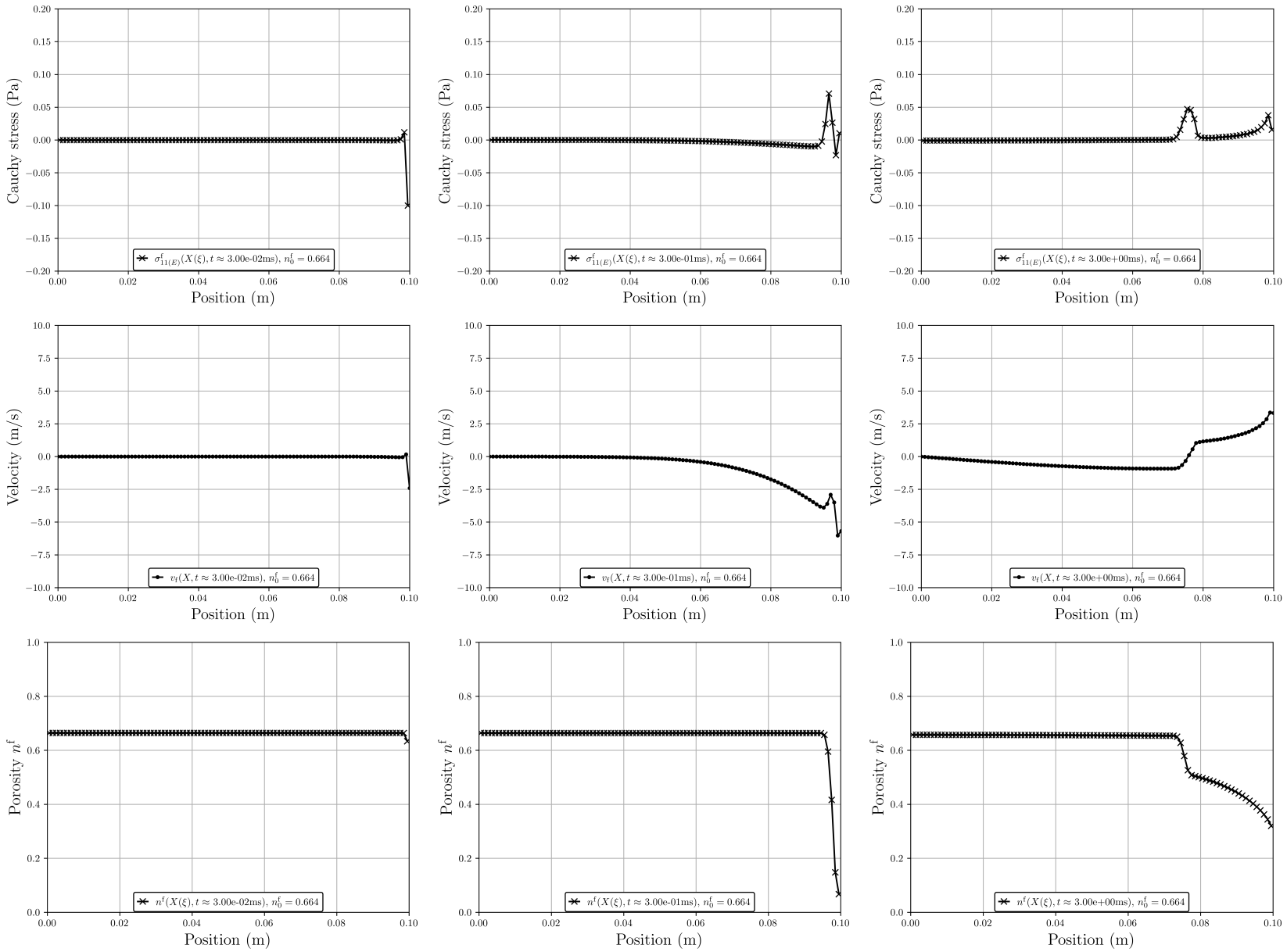

(a) $t = 0.03$ ms (b) $t = 0.30$ ms (c) $t = 3.00$ ms

Fig. 21 Contours along the length of the mesh for pore fluid extra stress $\sigma^{\mathrm{f}}_{11(E)}$, pore fluid velocity v_{f} and porosity n^{f} for permeable lung parenchyma after applying the Friedlander impulse with 25 kPa maximum overpressure

Continuing, the pore air is now swapped for pore blood; pore fluid density, bulk modulus and viscosities are adjusted accordingly. Initial porosity and load are increased to 0.99 and 50 kPa, respectively. We observe that the pore fluid extra stress has no impact on displacement (refer to Fig. 22), although its magnitude is on par with the total pore fluid stress, at least at the onset of the shock load before the pore fluid pressure response dominates (refer to Fig. 23). However, the pore fluid extra stress does not affect the solid extra stress, that is, no additional tensile forces indicative of potential damage in the lung parenchyma[55] are observed as compared to the nearly inviscid pore fluid (refer to Fig. 24). Similarly to the Yen impulse for blood-saturated lung parenchyma, we see (refer to Fig. 25) the shock wave percolating more slowly through the mixture than for air-saturated lung parenchyma, for either type of impulse loading.

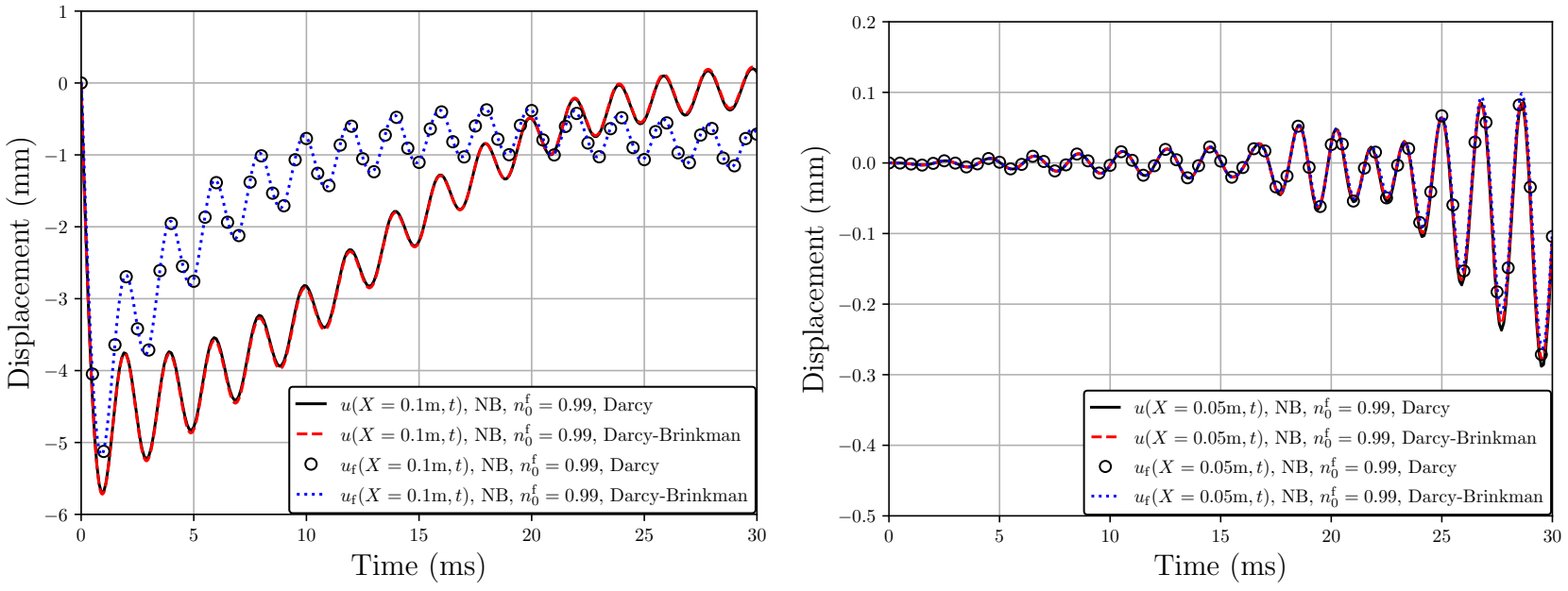

Fig. 22 Displacement results from applying the Friedlander impulse (50 kPa) to the permeable, blood-saturated lung parenchyma for (a) solid skeleton displacement $u(X = H, t)$ and pore fluid displacement $u_{\text{f}}(X = H, t)$, and (b) solid skeleton displacement $u(X = H/2, t)$ and pore fluid displacement $u_{\text{f}}(X = H/2, t)$

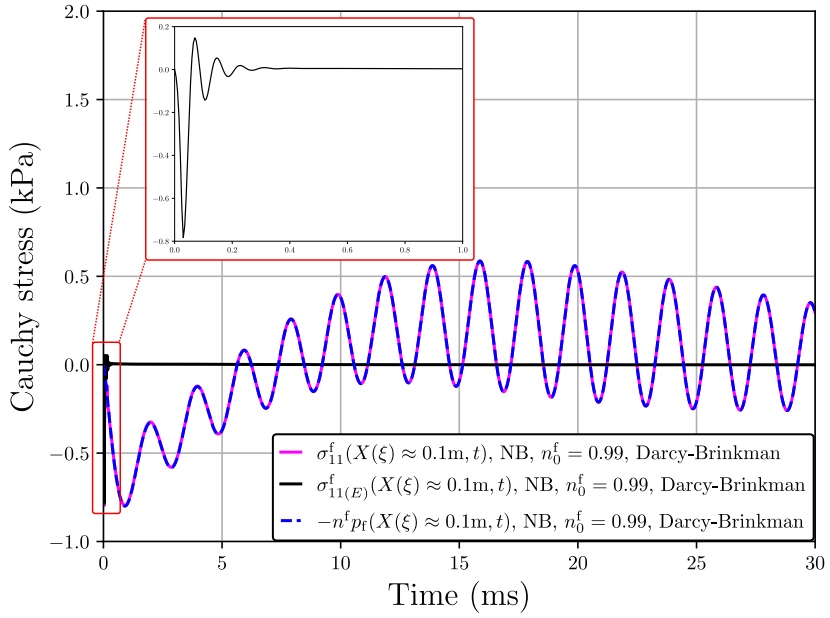

Fig. 23 Pore fluid stress results from applying the Friedlander impulse (50 kPa) to the permeable, blood-saturated lung parenchyma for the Gauss point closest to $X = H$

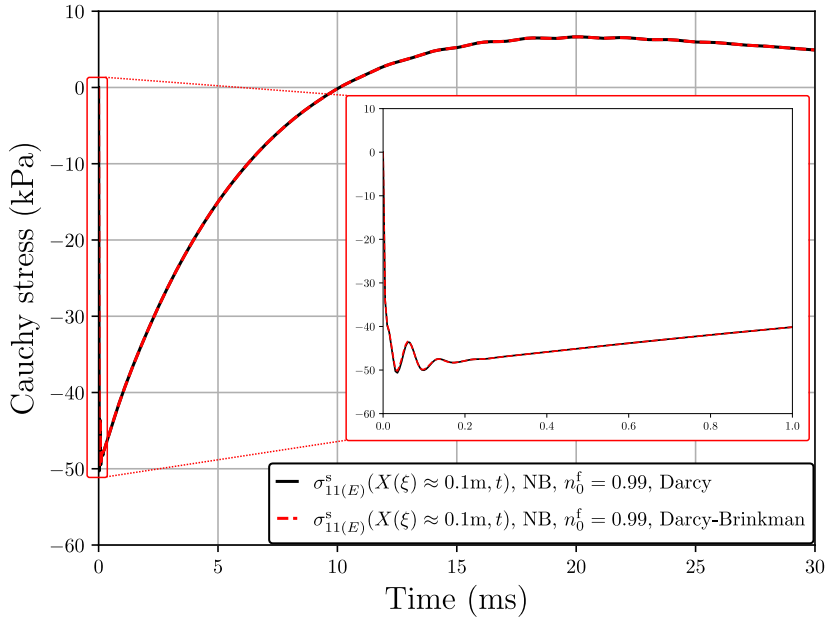

Fig. 24 Solid extra stress results from applying the Friedlander impulse (50 kPa) to the permeable, blood-saturated lung parenchyma for the Gauss point closest to $X = H$

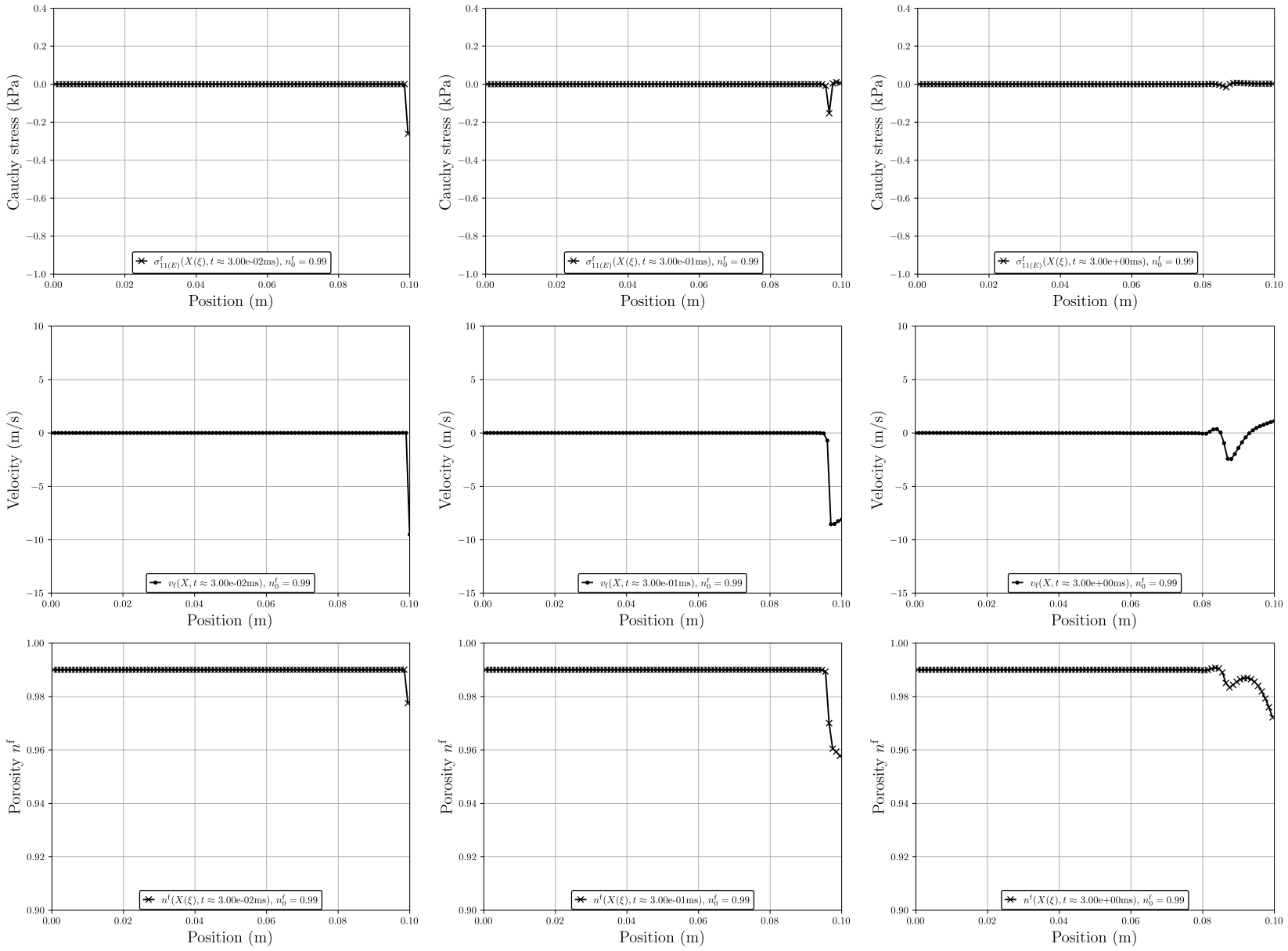

(a) $t = 0.03$ ms (b) $t = 0.30$ ms (c) $t = 3.00$ ms

Fig. 25 Contours along the length of the mesh for pore fluid extra stress $\sigma^{\mathrm{f}}_{11(E)}$, pore fluid velocity v_{f} and porosity n^{f} for permeable, blood-saturated lung parenchyma after applying the Friedlander impulse with 50 kPa maximum overpressure

5. Conclusion

We have expanded upon prior work[27–30] by assuming non-negligible contributions of pore fluid viscous stress to total pore fluid stress. It has been shown that inclusion of the pore fluid viscous stress (the pore fluid extra stress) led to higher-order continuity requirements in the variational forms of the governing equations for balance of mass of the mixture and balance of linear momentum of the pore fluid, via the porosity gradient and Laplacian of pore fluid velocity. A C^1 continuous finite-element, the Hermite cubic polynomial, has been employed to ensure global convergence of the weakened forms of the aforementioned equations. The implementation was verified for a small-strain analytical solution assuming finite strain numerical implementation.

Numerical simulations for shock loading of lung parenchyma then followed. It was shown that for impermeable (undrained) and permeable (drained) boundary conditions, with air as the pore fluid, inclusion of the pore fluid extra stress had negligible effects on deformations. For permeable boundary conditions, effect of pore fluid extra stress on total fluid stress is more noticeable, particularly when the saturating fluid is changed from air to blood, where the latter has viscosities two orders of magnitude larger than the former. However, inclusion of pore fluid extra stress does not affect the solid extra stress, that is, the material response of the lung tissue itself.

A limiting factor in the present simulations is the assumption of 1-D uniaxial strain. Indeed, pore fluid viscous stresses along the direction of flow are not expected to be as significant compared to shear stresses at the fluid-structure interface. The latter are responsible for development of boundary layers in the pore channels, which, though not necessary to model given the length scale of interest, could affect numerical results for 3-D simulations. Notwithstanding, we have demonstrated for 1-D uniaxial strain shock problems that pore fluid pressure is the dominant force compared to viscous effects, and that the pore fluid extra stress may be ignored in such scenarios.

Furthermore, overcoming the C^1 continuity requirement for solid skeleton displacement will allow for appropriate implementation of distinct phase temperatures via balances of energy of each phase. Recall from Irwin et al.[27] the dissipation inequal-

ity for distinct phase temperatures $\theta^{\mathrm{s}} \neq \theta^{\mathrm{f}}$:

$$\sum_{\alpha} \frac{1}{\theta^{\alpha}} \Big(\rho^{\alpha} \big[D_t^{\alpha} \psi^{\alpha} + \eta^{\alpha} D_t^{\alpha} \theta^{\alpha} \big] - \boldsymbol{\sigma}^{\alpha} : \boldsymbol{l}_{\alpha} - \hat{e}^{\alpha} + \hat{\rho}^{\alpha} \Big[\psi^{\alpha} - \frac{1}{2} \boldsymbol{v}_{\alpha} \cdot \boldsymbol{v}_{\alpha} \Big] + \boldsymbol{h}^{\alpha} \cdot \boldsymbol{v}_{\alpha} + \frac{1}{\theta^{\alpha}} \mathrm{grad}(\theta^{\alpha}) \cdot \boldsymbol{q}^{\alpha} \Big) \geq 0 \,. \tag{124}$$

With the assumption of negligible mass supplies (i.e., $\hat{\rho}^{\mathrm{s}} = \hat{\rho}^{\mathrm{f}} = 0$), the Clausius-Duhem inequality (dissipation inequality) for the mixture, now assuming thermally compressible solid (s) constituent, is written as

$$\begin{aligned} &\Big(\rho^{\mathrm{s}} D_t^{\mathrm{s}} \psi^{\mathrm{s}} + \frac{\theta^{\mathrm{s}}}{\theta^{\mathrm{f}}} \rho^{\mathrm{f}} D_t^{\mathrm{f}} \psi^{\mathrm{f}} \Big) + \Big(\Big[\rho^{\mathrm{s}} \eta^{\mathrm{s}} - \Lambda \frac{n^{\mathrm{s}}}{\rho^{\mathrm{sR}}} \frac{\partial \rho^{\mathrm{sR}}}{\partial \theta^{\mathrm{s}}} \Big] D_t^{\mathrm{s}} \theta^{\mathrm{s}} + \frac{\theta^{\mathrm{s}}}{\theta^{\mathrm{f}}} \rho^{\mathrm{f}} \eta^{\mathrm{f}} D_t^{\mathrm{f}} \theta^{\mathrm{f}} \Big) \\ &\qquad - \Big(\big[\boldsymbol{\sigma}^{\mathrm{s}} + \Lambda n^{\mathrm{s}} \mathbf{1} \big] : \boldsymbol{d}_{\mathrm{s}} + \Big[\frac{\theta^{\mathrm{s}}}{\theta^{\mathrm{f}}} \boldsymbol{\sigma}^{\mathrm{f}} + \Lambda n^{\mathrm{f}} \mathbf{1} \Big] : \boldsymbol{d}_{\mathrm{f}} \Big) \\ &\qquad + (\boldsymbol{h}^{\mathrm{f}} - \Lambda \mathrm{grad} n^{\mathrm{f}}) \cdot \tilde{\boldsymbol{v}}_{\mathrm{f}} - \Lambda \frac{n^{\mathrm{f}}}{\rho^{\mathrm{fR}}} D_t^{\mathrm{f}} \rho^{\mathrm{fR}} \\ &- \hat{\varepsilon}^{\mathrm{f}} \Big(\frac{\theta^{\mathrm{s}}}{\theta^{\mathrm{f}}} - 1 \Big) + \Big(\frac{1}{\theta^{\mathrm{s}}} \mathrm{grad}(\theta^{\mathrm{s}}) \cdot \boldsymbol{q}^{\mathrm{s}} + \frac{\theta^{\mathrm{s}}}{(\theta^{\mathrm{f}})^2} \mathrm{grad}(\theta^{\mathrm{f}}) \cdot \boldsymbol{q}^{\mathrm{f}} \Big) \geq 0 \,, \end{aligned} \tag{125}$$

where η^{α} is the phase entropy, $\hat{\varepsilon}^{\mathrm{f}}$ is the local interaction energy supply to the pore fluid (e.g., heat transfer), and Λ is a Lagrange multiplier satisfying the saturation constraint

$$\Lambda \Big(\frac{n^{\mathrm{s}}}{\rho^{\mathrm{sR}}} \frac{\partial \rho^{\mathrm{sR}}}{\partial \theta^{\mathrm{s}}} D_t^{\mathrm{s}} \theta^{\mathrm{s}} + n^{\mathrm{s}} \boldsymbol{d}_{\mathrm{s}} : \mathbf{1} + \frac{n^{\mathrm{f}}}{\rho^{\mathrm{fR}}} D_t^{\mathrm{f}} \rho^{\mathrm{fR}} + n^{\mathrm{f}} \boldsymbol{d}_{\mathrm{f}} : \mathbf{1} + \mathrm{grad}(n^{\mathrm{f}}) \cdot \tilde{\boldsymbol{v}}_{\mathrm{f}} \Big) = 0 \,. \tag{126}$$

Introducing the so-called "extra" terms,

$$\begin{aligned} \boldsymbol{\sigma}_E^{\mathrm{s}} &= \boldsymbol{\sigma}^{\mathrm{s}} + \Lambda n^{\mathrm{s}} \mathbf{1} \,, \\ \boldsymbol{\sigma}_E^{\mathrm{f}} &= \boldsymbol{\sigma}^{\mathrm{f}} + \Lambda \frac{\theta^{\mathrm{f}}}{\theta^{\mathrm{s}}} n^{\mathrm{f}} \mathbf{1} \,, \\ \eta_E^{\mathrm{s}} &= \eta^{\mathrm{s}} - \Lambda \frac{1}{(\rho^{\mathrm{sR}})^2} \frac{\partial \rho^{\mathrm{sR}}}{\partial \theta^{\mathrm{s}}} \,, \\ \boldsymbol{h}_E^{\mathrm{f}} &= \boldsymbol{h}^{\mathrm{f}} - \Lambda \mathrm{grad} n^{\mathrm{f}} \,, \end{aligned} \tag{127}$$

it can be shown that in order to satisfy the thermodynamic identity[56,57]

$$\frac{\partial \psi^{\mathrm{f}}}{\partial v^{\mathrm{f}}} = -p_{\mathrm{f}} \Rightarrow \frac{\partial \psi^{\mathrm{f}}}{\partial \rho^{\mathrm{fR}}} \frac{\partial \rho^{\mathrm{fR}}}{\partial v^{\mathrm{f}}} = -p_{\mathrm{f}} \Rightarrow (\rho^{\mathrm{fR}})^2 \frac{\partial \psi^{\mathrm{f}}}{\partial \rho^{\mathrm{fR}}} = p_{\mathrm{f}} \,, \tag{128}$$

the following must hold:

$$\Lambda = \frac{\theta^{\mathrm{s}}}{\theta^{\mathrm{f}}} p_{\mathrm{f}} \,. \tag{129}$$

This means that

$$\boldsymbol{h}^{\mathrm{f}}_{E} = \boldsymbol{h}^{\mathrm{f}} - \frac{\theta^{\mathrm{s}}}{\theta^{\mathrm{f}}} p_{\mathrm{f}} \mathrm{grad} n^{\mathrm{f}} \,, \tag{130}$$

such that the distinct phase temperature Darcy-Brinkman equation is written as

$$n^{\mathrm{f}} \tilde{\boldsymbol{v}}_{\mathrm{f}} = -\hat{k} \Big(\rho^{\mathrm{fR}} (\boldsymbol{a}_{\mathrm{f}} - \boldsymbol{b}) + \mathrm{grad} p_{\mathrm{f}} - \frac{1}{n^{\mathrm{f}}} \,\mathrm{div}\, \boldsymbol{\sigma}^{\mathrm{f}}_{E} + \frac{1}{n^{\mathrm{f}}} p_{\mathrm{f}} \mathrm{grad}(n^{\mathrm{f}}) \Big[1 - \frac{\theta^{\mathrm{s}}}{\theta^{\mathrm{f}}} \Big] \Big) \,. \tag{131}$$

Thus, the porosity gradient must be calculated when assuming distinct phase temperatures. Future work will include implementation of distinct phase temperatures in the numerical model, with the aim of formulating rate equations for phase entropies to enable a thermodynamically-consistent damage model for the solid (s) phase of lung parenchyma (similar to the one developed by Clayton et al.[9,10]) thus allowing us to quantify damage in lung tissue subjected to high-strain-rate loading.

6. References

1. Sobin S, Fung Y, Tremer H. Collagen and elastin fibers in human pulmonary alveolar walls. Journal of Applied Physiology. 1988;64:1659–1675.

2. Suki B, Ito S, Stamenović D, Lutchen K, Ingenito E. Biomechanics of the lung parenchyma: critical roles of collagen and mechanical forces. Journal of Applied Physiology. 2005;98:1892–1899.

3. Freed A, Zamana S, Paul S, Clayton J. A Dodecahedral Model for Alveoli. Part I. Theory and Numerical Methods. DEVCOM Army Research Laboratory (US); 2021. Report No.: ARL-TR-9148.

4. Suki B, Bates J. Lung tissue mechanics as an emergent phenomenon. Journal of Applied Physiology. 2011;110:1111–1118.

5. Brannen M, Kang G, Dutrisac S, Banton R, Clayton J, Petel O. The influence of the tertiary bronchi on dynamic lung deformation. Journal of the Mechanical Behavior of Biomedical Materials. 2022;130:105181.

6. Clayton J, Freed A. Viscoelastic-damage theory based on a QR decomposition of deformation gradient. DEVCOM Army Research Laboratory (US); 2019. Report No.: ARL-TR-8840.

7. Clayton J, Banton R, Freed A. A nonlinear thermoelastic-viscoelastic continuum model of lung mechanics for shock wave analysis. In: Shock Compression of Condensed Matter; Vol. 2272; Lane J, editor. Portland (OR): AIP Conference Proceedings; 2020; p. 040001.

8. Clayton J. Modeling lung tissue dynamics and injury under pressure and impact loading. Biomechanics and Modeling in Mechanobiology. 2020;19(6):2603–2626.

9. Clayton JD, Freed AD. A constitutive model for lung mechanics and injury applicable to static, dynamic, and shock loading. Mechanics of Soft Materials. 2020;2(3).

10. Clayton J, Banton R, Goertz A. A continuum model of the human lung: implementation and parameterization. DEVCOM Army Research Laboratory (US); 2021. Report No.: ARL-TR-9138.

11. Freed A, Clayton J. Coordinate indexing strategies for the laplace stretch in two and three dimensions. DEVCOM Army Research Laboratory (US); 2022. Report No.: ARL-TR-9530.

12. Truesdell C, Toupin R. The classical field theories. In: Principles of Classical Mechanics and Field Theory / Prinzipien der Klassischen Mechanik und Feldtheorie; Flügge S, editor. Berlin, Heidelberg: Springer Berlin Heidelberg; 1960; p. 226–858.

13. Bowen R. Theory of mixtures. In: Continuum Physics; Elsevier; 1976; p. 1–127.

14. Bowen R. Incompressible porous media models by use of the theory of mixture. International Journal of Engineering Science. 1980;18(9):1129–1148.

15. Bowen R. Compressible porous media models by use of the theory of mixtures. International Journal of Engineering Science. 1982;20(6):697–735.

16. Ehlers W. Foundations of multiphasic and porous materials. In: Porous Media: Theory, Experiments and Numerical Applications; Ehlers W, Bluhm J, editors. Berlin, Heidelberg: Springer Berlin Heidelberg; 2002; p. 3–86.

17. Coussy O. Poromechanics. John Wiley & Sons; 2004.

18. de Boer R. Trends in continuum mechanics of porous media: theory and applications of transport in porous media. Springer; 2005.

19. Bowen R, Chen P. Shock waves in a mixture of linear elastic materials. Rendiconti del Circolo Matematico di Palermo. 1972;21:267–283.

20. Bowen R, Wright T. On wave propagation in a mixture of linear elastic materials. Army Ballistic Research Laboratory; 1972. Report No.: BRL-TR-1581.

21. Bowen R, Chen P. Shock waves in ideal fluid mixtures with several temperatures. Archive for Rational Mechanics and Analysis. 1974;53:277–294.

22. Bowen R, Chen P, Nunziato J. Shock waves in a mixture of chemically reacting materials with memory. Acta Mechanica. 1975;21:1–11.

23. Clayton J. Analysis of shock waves in a mixture theory of a thermoelastic solid and fluid with distinct temperatures. International Journal of Engineering Science. 2022;175:103675.

24. Tsokos M, Paulsen F, Petri S, Madea B, Püschel K, Türk E. Histologic, immunohistochemical, and ultrastructural findings in human blast lung injury. American Journal of Respiratory and Critical Care Medicine. 2003;168(5):549–555; PMID: 12842857.

25. Cooper G, Townend D, Cater S, Pearce B. The role of stress waves in thoracic visceral injury from blast loading: Modification of stress transmission by foams and high-density materials. Journal of Biomechanics. 1991;24:273–285.

26. Cooper G. Protection of the lung from blast overpressure by thoracic stress wave decouplers. The Journal of Trauma: Injury, Infection, and Critical Care. 1996;40:105S–110S.

27. Irwin Z, Regueiro R, Clayton J. A Large Deformation Multiphase Continuum Mechanics Model for Shock Loading of Lung Parenchyma. Part I: Theory. DEVCOM Army Research Laboratory (US); 2023. Report No.: ARL-TR-9686.

28. Irwin Z, Regueiro R, Clayton J. A Large Deformation Multiphase Continuum Mechanics Model for Shock Loading of Lung Parenchyma. Part III: Numerical simulations. DEVCOM Army Research Laboratory (US); 2023. Report No.: ARL-TR-9688.

29. Irwin Z, Clayton J, Regueiro R. A large deformation multiphase continuum mechanics model for shock loading of soft porous materials. International Journal for Numerical Methods in Engineering. 2023; submitted.

30. Irwin Z, Regueiro R, Clayton J. A Large Deformation Multiphase Continuum Mechanics Model for Shock Loading of Lung Parenchyma. Part II: Numerical methods. DEVCOM Army Research Laboratory (US); 2023. Report No.: ARL-TR-9687.

31. Holzapfel G. Nonlinear solid mechanics: A continuum approach for engineering. John Wiley & Sons; 2000.

32. Vuong AT, Ager C, Wall W. Two finite element approaches for Darcy and Darcy–Brinkman flow through deformable porous media—mixed method vs. nurbs based (isogeometric) continuity. Computer Methods in Applied Mechanics and Engineering. 2016;305:634–657.

33. Vuong AT. A computational approach to coupled poroelastic media problems [thesis]. Technische Universität München (DEU); 2016.

34. Markert B. Porous Media Viscoelasticity with Application to Polymeric Foams [thesis]. Institut für Mechanik (Bauwesen) der Universität Stuttgart (DEU); 2005.

35. Ehlers W. Darcy, Forchheimer, Brinkman and Richards: classical hydromechanical equations and their significance in the light of the TPM. Archive of Applied Mechanics. 2022;92(2):619–639.

36. Ehlers W, Ellsiepen P, Blome P, Mahnkopf D, Markert B. Theoretische und numerische studien zur lösung von rand- und anfangswertproblemen in der theorie poröser medien, abschulußbericht zum dfg-forschungsvorhaben eh 107/6-2. Institut für Mechanick, Unversität Stuttgart (DEU); 1999. Report No.: 99-II-1.

37. Lande B, Mitzner W. Analysis of lung parenchyma as a parametric porous medium. Journal of Applied Physiology. 2006;101(3):926–933.

38. Nield D, Bejan A. Convection in Porous Media. Springer New York; 2013.

39. Bear J. Dynamics of fluids in porous media. Dover Publications, Inc.; 1972.

40. Winter R, Valsamidou A, Class H, Flemisch B. A study on Darcy versus Forchheimer models for flow through heterogeneous landfills including macropores. Water. 2022;14(4):546.

41. Sobieski W, Trykozko A. Darcy's and Forchheimer's laws in practice. Part 1. The experiment. Technical Sciences. 2014;17(14):321–355.

42. Hughes T, Cottrell J, Bazilevs Y. Isogeometric analysis: Cad, finite elements, nurbs, exact geometry and mesh refinement. Computer Methods in Applied Mechanics and Engineering. 2005;194(39-41):4135–4195.

43. Heider Y. Saturated Porous Media Dynamics with Application to Earthquake Engineering [thesis]. [Stuttgart, Germany]: Institut für Mechanik (Bauwesen) Lehrstuhl für Kontinuumsmechanik; 2012 OCLC: 824646288.

44. Hughes T. The finite element method: Linear static and dynamic finite element analysis. Dover Publications, Inc.; 2000.

45. Newmark N. A method of computation for structural dynamics. Journal of the Engineering Mechanics Divison. 1959;85(3):67–94.

46. Cash JR, Karp A. A variable order runge-kutta method for initial value problems with rapidly varying right-hand sides. ACM Translations on Mathematical Software. 1990;16(3):201–222.

47. Bogacki P, Shampine L. A 3(2) pair of runge - kutta formulas. Applied Mathematics Letters. 1989;2(4):321–325.

48. de Boer R, Ehlers W, Liu Z. One-dimensional transient wave propagation in fluid-saturated incompressible porous media. Archive of Applied Mechanics. 1993;63(1):59–72.

49. Holmes M, Parker N, Povey M. Temperature dependence of bulk viscosity in water using acoustic spectroscopy. Journal of Physics: Conference Series. 2011;269(1).

50. Yen R, Fung Y, Liu S. Trauma of lung due to impact load. Journal of Biomechanics. 1988;21(9):745–753.

51. Rand P, Lacombe E, Hunt H, Austin W. Viscosity of normal human blood under normothermic and hypothermic conditions. Journal of Applied Physiology. 1964;19(1):117–122.

52. Shang J, Wu T, Wang H, Yang C, Ye C, Hu R, Tao J, He X. Measurement of temperature-dependent bulk viscosities of nitrogen, oxygen and air from spontaneous rayleigh-brillouin scattering. IEEE Access. 2019;7:136439–136451.

53. Friedlander F. The diffraction of sound pulses. I. Diffraction by a semi-infinite plane. The Royal Society. 1946;186(1006).

54. Dewey J. The Friedlander equations. In: Blast Effects: Physical Properties of Shock Waves; Sochet I, editor. Springer International Publishing; 2018; p. 37–55.

55. Fung Y. Biomechanics. Motion, flow, stress, and growth. Springer; 1990.

56. Davison L. Fundamentals of shock wave propagation in solids. Springer; 2008.

57. Clayton J. Differential geometry and kinematics of continua. Singapore: World Scientific; 2014.

List of Symbols, Abbreviations, and Acronyms

TERMS:

1-D	one-dimensional
2-D	two-dimensional
3-D	three-dimensional
ARL	Army Research Laboratory
CFD	computational fluid dynamics
CFL	Courant-Friedrichs-Lewy
DEVCOM	US Army Combat Capabilities Development Command
DOF	degree(s) of freedom
FE	finite element
FSI	fluid-structure interaction
NB	Newmark-beta integrator
NURBS	Non-uniform rational B-spline
ODE	ordinary differential equation
RKFNC	Runge-Kutta Cash-Karp integrator
SF	safety factor
TPM	theory of porous media

MATHEMATICAL SYMBOLS:

t	time
$\boldsymbol{x}, x_k$	Cartesian spatial coordinates
$\boldsymbol{X}, X_K$	Cartesian reference coordinates
$\boldsymbol{u}_\alpha, u_{i(\alpha)}$	displacement of phase α
n^α	volume fraction of phase α
m_α	mass of phase α
$\rho^{\alpha\mathrm{R}}$	real mass density of phase α [Mass/Length^3]
ρ^α	partial mass density of phase α [Mass/Length^3]
$\hat{\rho}^\alpha$	mass supply to phase α
J_α	Jacobian of deformation of phase α
$\boldsymbol{F}_\alpha, F_{iI(\alpha)}$	deformation gradient of phase α
p_α	Cauchy pressure of phase α [Force/Length^2]
$\boldsymbol{v}_\alpha, v_{i(\alpha)}$	velocity of phase α [Length/Time]
$\boldsymbol{d}_\alpha, d_{ij(\alpha)}$	velocity gradient of phase α [Time^{-1}]
$\boldsymbol{a}_\alpha, a_{i(\alpha)}$	acceleration of phase α [Length/Time^2]
$\boldsymbol{h}^\alpha, h_i^\alpha$	interaction force of phase α with other phases
$\boldsymbol{\sigma}^\alpha, \sigma_{ij}^\alpha$	partial Cauchy stress of phase α [Force/Length^2]
$\boldsymbol{P}^\alpha, P_{iI}^\alpha$	first Piola-Kirchhoff stress of phase α [Force/Length^2]
η^α	entropy per unit mass of phase α [Length^2/Time^2·Temperature]
ψ^α	free energy per unit mass of phase α [Length^2/Time^2]
θ^α	temperature of phase α
ε^α	energy supply per unit mass to phase α [Length^2/Time^2]
$\boldsymbol{q}^\alpha, q_i^\alpha$	heat flux vector of phase α [Length^2·Mass/Time^2]
$\hat{k}$	hydraulic conductivity [Length^3·Time/Mass]
η_α	shear viscosity of phase α [Force·Time]
κ_α	bulk viscosity of phase α [Force·Time]

$\varkappa$	solid skeleton intrinsic permeability [Length^2]
K_α^η	isentropic bulk modulus of phase α [Force/Length^2]

1 (PDF) DEFENSE TECHNICAL INFORMATION CTR
DTIC OCA

1 (PDF) DEVCOM ARL
FCDD RLB CI
TECH LIB

36 (PDF) DEVCOM ARL
FCDD RLA B
R BECKER
C HOPPEL
P GILLICH
A TONGE
FCDD RLA HC
J CRONE
J KNAP
FCDD RLA MB
G GAZONAS
FCDD RLA T
B LOVE
M FERMEN-COKER
S SCHOENFELD
FCDD RLA TA
S TURNAGE
C WILLIAMS
FCDD RLA TB
S ALEXANDER
R BANTON
T BAUMER
D CASEM
J CLAYTON
B FAGAN
A GOERTZ
C HAMPTON
R KARGUS
M KLEINBERGER
D KRAYTERMAN
J MCDONALD
C MEREDITH
T PLAISTED
K RAFAELS
R REGUEIRO
S SATAPATHY
T WEERASOORIYA
C WEAVER
S WOZNIAK
T ZHANG
FCDD RLA TE
J LLOYD
T SCHARF
FCDD RLA TF
J CAZAMIAS